



POLITECNICO DI TORINO

DIPARTIMENTO DI INGEGNERIA MECCANICA  
E AEROSPAZIALE (DIMEAS)

Master's Degree Thesis

Master's Degree in Biomedical Engineering

**Feasibility Study of  
Average Threshold Crossing (ATC)  
Technique Application in  
Muscle Synergies Analysis**

**Relatori**

Prof. Danilo DEMARCHI  
Dr. P. MOTTO ROS

**Candidato**

Marco CASTAGNA

Torino, March 2019

# Abstract

In the last few decades, the concept of “Muscle Synergies” has been investigated as a way to better grasp the strategies used by the Central Nervous System (CNS) to simplify the control of body’s muscles. Behind this theory, in the fulfillment of a particular motor task that involves the recruitment of a certain number of muscles, the brain acts managing few temporal activation patterns that correspond to few muscles modules. In this way, the associated computational burden on the CNS is reduced to the control of a few modules instead of a higher number of individual muscles.

The aim of this study is to verify the feasibility of the Average Threshold Crossing (ATC) approach in examining muscle synergies. More specifically, the ATC is an event-driven transmission technique that consists of an event generated each time the Surface Electromyography (sEMG) signal exceeds a fixed threshold. The number of threshold crossing events related to a particular time window is correlated to the force produced by the muscle. ATC offers a drastic reduction of data and the simple hardware schemes, its wireless suitability and low power consumption, are all advantages which have piqued the interest of its application in muscle synergies analysis.

To extract muscle synergies, the most common procedure described in literature was followed. Starting from the sEMG envelopes matrix, it is based on the Non-negative Matrix Factorization (NNMF) decomposition algorithm. Since the ATC depends on two parameters (threshold level and time window), in order to find the best combination that extracts ATC signals which are very similar to the sEMG envelopes, it has been considered to use a simulated approach based on sEMG signals. The results of the simulations have shown that the ATC technique, with the particular combination of time window = 50 ms and threshold level 2.8, is able to extract a signal which is very similar ( $R^2 \geq 85\%$ ) to the sEMG traditional envelope only when it is computed averaging across multiple realizations. The latter is valid when the sEMG signal is characterized by a Signal to Noise Ratio (SNR) at least of 10dB and for activations with temporal support at least of 150 ms.

As a final step, using real sEMG signals collected from the lower limbs of 8 healthy subjects during gait, it has been possible to compare the outputs of the extraction, i.e. synergies weights  $W$  and temporal coefficients  $H$ , between the two methods: traditional and ATC. Specifically, the results have been extracted from the average sEMG envelope (both traditional and ATC) within a subgroup, which

is made by 10 gait cycles, and for 10 consecutive subgroups to characterize the intra-variability during the locomotion. Referring to both methods, the results of the muscle synergy analysis have found that the mean number of synergies across the subjects is  $5 \pm 0.5$ . Relative to the similarity of the weights  $W$  and the temporal coefficients  $H$ , the Cosine Similarity (CS) and the Zero-lag Cross Correlation (CC) have been used respectively. In all subjects, both indexes have shown a very high similarity, reaching average values always higher than 95% and characterized by very low standard deviations across the subgroups.

# Contents

<b>Abstract</b>	II
<b>List of Figures</b>	VI
<b>List of Acronyms</b>	VIII
<b>1 Introduction</b>	1
<b>2 Muscular System Physiology and sEMG Recording</b>	3
2.1 The Muscular System: Basic Principles . . . . .	3
2.1.1 The Skeletal Muscle . . . . .	5
2.2 Surface Electromyography (sEMG) . . . . .	14
2.2.1 sEMG Signal Principles . . . . .	18
2.2.2 Noise Sources in Surface ElectroMyoGraphy (sEMG) Signal	19
2.2.3 sEMG Signal Acquisition Chain: General Model . . . . .	21
2.2.4 sEMG Signal Time and Frequency Descriptors . . . . .	22
<b>3 Average Threshold Crossing</b>	25
3.1 ATC Approach . . . . .	25
3.2 Previous Studies . . . . .	28
<b>4 Muscle Synergies</b>	30
4.1 Motor Control Model . . . . .	31
4.2 Muscle Synergies Analysis . . . . .	32
4.3 Previous Studies . . . . .	39
<b>5 sEMG Signal Simulation and ATC Testing</b>	43
5.1 Approach and Parameters . . . . .	43
5.1.1 Simulate sEMG Signal Generation . . . . .	44
5.1.2 ATC Parameters . . . . .	47
5.2 Methods . . . . .	51
5.2.1 Output Similarity Index . . . . .	51
5.2.2 Simulation Setup . . . . .	52

5.3	Simulations Results . . . . .	54
<b>6</b>	<b>ATC-based Muscle Synergies Analysis</b>	<b>61</b>
6.1	Materials and Methods . . . . .	63
6.2	Muscle Synergies Extraction . . . . .	66
6.2.1	Gait Cycle Bases . . . . .	66
6.2.2	Muscle Synergies Extraction Setup . . . . .	68
6.3	Results . . . . .	72
<b>7</b>	<b>Conclusions</b>	<b>81</b>
	<b>Bibliography</b>	<b>88</b>
	<b>Acknowledgements</b>	<b>89</b>

# List of Figures

2.1	View of the Skeletal muscle. . . . .	4
2.2	View of the Smooth muscle. . . . .	4
2.3	View of the Cardiac muscle. . . . .	5
2.4	Skeletal muscle structure with an enlargement to showing muscle fiber. . . . .	6
2.5	Sarcomere structure with photomicrograph view. . . . .	7
2.6	Sarcomere structure: myosin and actin filaments enlargement. . .	8
2.7	Excitation-contraction coupling of skeletal muscle. . . . .	9
2.8	Schematic view of changes in striation pattern due to the sliding-filament model of muscle contraction. . . . .	10
2.9	Single muscle twitch. . . . .	12
2.10	Muscle stimulation. . . . .	12
2.11	Types of Muscle Actions. . . . .	13
2.12	Intramuscular ElectroMyoGraphy (iEMG). . . . .	15
2.13	Surface ElectroMyoGraphy (sEMG) Signal. . . . .	16
2.14	Electrodes configuration. . . . .	17
2.15	Example of the frequency spectrum of the sEMG signal. . . . .	19
2.16	Example of the Cross talk. . . . .	20
2.17	Simplified Model of sEMG Signal Acquisition Chain. . . . .	22
3.1	Comparison between standard sEMG and Average Threshold Crossing (ATC) sampling . . . . .	26
3.2	TC signal and comparator output. . . . .	27
3.3	ATC, Force, ARV signals in time domain. . . . .	28
4.1	Muscle Synergies Hypothesis . . . . .	32
4.2	Muscle Synergies Blocks Chain Analysis. . . . .	33
4.3	Step 2. General processing of sEMG signal. . . . .	34
4.4	Example of Matrix $\mathbf{M}$ factorization in two smaller matrices $\mathbf{W}$ and $\mathbf{H}$ . . . . .	35
4.5	NNMF Decomposition Example . . . . .	36
4.6	VAF/ $R^2$ as function of number of muscle synergies. . . . .	37
4.7	Example of Muscle synergies in lower limb. . . . .	42
5.1	sEMG signal simulation overall process. . . . .	44
5.2	Step 1: Colored noise signal extraction. . . . .	45

5.3	Step 2: Pure noise and pure signal components generation. . . . .	46
5.4	Step 3: Example: Final sEMG signal generation, 10dB. . . . .	47
5.5	ATC Threshold effect . . . . .	48
5.6	ATC Time Window effect . . . . .	50
5.7	$R^2$ formula. . . . .	51
5.8	Single repetition, ATC signal. . . . .	52
5.9	Multi repetitions, ATC signals and average ATC curve in black. . . . .	53
5.10	Results: Single repetition, $R^2_{\mu}$ , Signal to Noise ratio (SNR) = 10dB. . . . .	55
5.11	Results: Single repetition, $R^2$ distribution. . . . .	56
5.12	Results: Multi repetitions, $R^2_{\mu}$ , SNR = 10dB. . . . .	57
5.13	Results: Multiple repetitions, $R^2$ distribution, SNR = 10dB. . . . .	58
6.1	ATC-based synergies extraction blocks diagram. . . . .	63
6.2	Traditional synergies extraction blocks diagram. . . . .	64
6.3	Traditional synergies extraction blocks diagram. . . . .	64
6.4	ATC envelope calculation. . . . .	65
6.5	Gait Cycle Phases. . . . .	66
6.6	Gait muscles timing. . . . .	68
6.7	Schematic representation of the walking path . . . . .	69
6.8	Average envelope (10 reps). . . . .	71
6.9	sEMG envelopes comparison. . . . .	73
6.10	$R^2_{\text{overall}}$ curve. . . . .	74
6.11	Traditional Envelope over ATC threshold. . . . .	75
6.12	Traditional synergies extraction blocks diagram, traditional envelope above ATC threshold. . . . .	75
6.13	Subject 2. Plot of the traditional synergies weights $W$ . . . . .	78
6.14	Subject 2. Plot of the ATC synergies weights $W$ . . . . .	78
6.15	Subject 2. Plot of the traditional temporal coefficients $H$ . . . . .	79
6.16	Subject 2. Plot of the ATC temporal coefficients $H$ . . . . .	79
6.17	Subject 2. Cosine similarity and Zero-lag Cross Correlation. . . . .	80
6.18	Shared Muscle Synergies . . . . .	80

# List of Acronyms

**CNS** Central Nervous System

**RS** Sarcoplasmatic Reticulum

**AP** Action Potential

**EMG** ElectroMyoGraphy

**iEMG** Intramuscular ElectroMyoGraphy

**sEMG** Surface ElectroMyoGraphy

**MUAP** Motor Unit Action Potential

**ECG** ElectroCardioGraphic

**ARV** Averaged Rectified Value

**RMS** Root Mean Square

**MNF** Mean Frequency

**MDF** Median Frequency

**ATC** Average Threshold Crossing

**WBAN** Wireless Body Area Networks

**IR-UWB** Impulse-Radio Ultra-Wide Band

**CPGs** Central Pattern Generators

**SNR** Signal to Noise ratio

**NNMF** Non-negative Matrix Factorization

**HFPS** Heel contact (H), flat foot contact (F), push off (P) and limb swing (S)

**CMRR** Common-mode Rejection Ratio

# Chapter 1

## Introduction

The main target of the thesis consists in the feasibility assessment of the ATC technique application in the muscle synergies analysis environment. The study has been organized in two main parts. The first one aims to extract the best combination of ATC parameters that allows to calculate an ATC signal, called “ATC envelope”, that is as similar as possible to the traditional sEMG envelope ( $f_{low}=10\text{Hz}$ ). This part has involved the sEMG signal simulation in order to have the total control and better choice of the proper sEMG characteristics to test and understand the ATC applicability field. In the second part, exploiting the combination just found, starting from real sEMG signals, the ATC-based method of muscle synergies extraction will be compared to the traditional one based on the standard sEMG envelope. More specifically, will be compared the final outputs of the muscle synergies extraction, i.e. the synergies weights  $W$  and the temporal coefficients  $H$ , allowing to understand the performance of the ATC-based approach.

After this briefly introduction, the work is structured in other six main chapters.

The second chapter, which is called *Muscular System Physiology and sEMG Recording*, is divided in two main sections and has the aim to instruct and guide the reader to better grasp the basic principles that regard the muscular system, mostly focusing on the skeletal muscle physiology, and of the surface electromyography (sEMG) signal. More particularly, have been provided some information about its main functions and characteristics, acquisition, noise sources and time and frequency descriptors that are generally used to describe it.

In the third chapter *Average Threshold Crossing* have been described and introduced the fundamental concepts behind the event-driven technique that will play a main role during the whole thesis. Its theoretic definitions, principal characteristics and advantages have been discussed and compared with respect to the standard sEMG sampling and transmission technique. Finally, in the last section,

have been reported and cited the main important ATC-based previous works.

The fourth chapter, named *Muscle Synergies*, is structured in three sections. The first one provides a global overview on the traditional approach that is generally pursued in literature to face with the muscle synergies topic. In the second section, beginning from a quickly introduction on the historical precedents, are then expressed the muscle synergies-based motor control model, the main steps in the muscle synergies analysis and the quality results assessment. In the last section, finally, is provided a brief report of the main works about muscle synergies that are strictly related to the goal of this thesis.

In the fifth chapter *sEMG Signal Simulation and ATC Testing*, in order to test the ATC technique in different conditions of sEMG signal characteristics and to find the best combination of ATC parameters (time window and threshold level) to reach the final goal, it has been considered to simulate the sEMG signal with a model based on a Gaussian modulation function. It will be discussed about the generation of the simulate sEMG signal, the methods used to run the simulations and the output used to assess the similarity between the Gaussian function, that models the burst of activity, and the ATC signal. Finally, the results have been discussed and shown.

The sixth chapter, called *ATC-based Muscle Synergies Analysis*, compares and analyzes the outputs of the muscle synergies extraction computed with the two different approaches, i.e. ATC and traditional, starting now from real sEMG signals collected from the lower limb during gait. The chapter is divided in three main sections that regard respectively the extraction methods, the extraction conditions and the final results.

The last chapter, *Conclusions*, shows the conclusions and introduces some future works.

## Chapter 2

# Muscular System Physiology and sEMG Recording

### 2.1 The Muscular System: Basic Principles

The muscular system represents one of the main human body organ systems, composed by several organs that work together to permit the main aim: body movement. It is involved in most physiological processes and among its principals functions are the movement of body parts, stability and posture control, heat production, blood circulation and help in digestion.

After receiving an electrical stimulus from the nervous system, called an action potential (AP), the muscle cells generate contraction force determining (voluntary or involuntary) movements. Due to the role of the nervous system, the muscular system is often called the *neuromuscular system*.

Muscle tissue is classified into three types according to structure and function: skeletal, cardiac and smooth.

- **The Skeletal Muscle:** This muscle is linked through tendons to bones and its contraction determines possible locomotion, facial expressions, posture, and other voluntary movements of the body. Histologically, skeletal muscle is composed by long cylindrical fibers and observing it using an optical microscope, muscle cells appear striated with many nuclei squeezed along the membranes. It constitutes two-fifths of the total body mass. Moreover, skeletal muscle plays a role in the heat generation as a byproduct of contraction action and offers protection to internal organs and structures [1].

This muscle type is more described in the section 2.1.1.

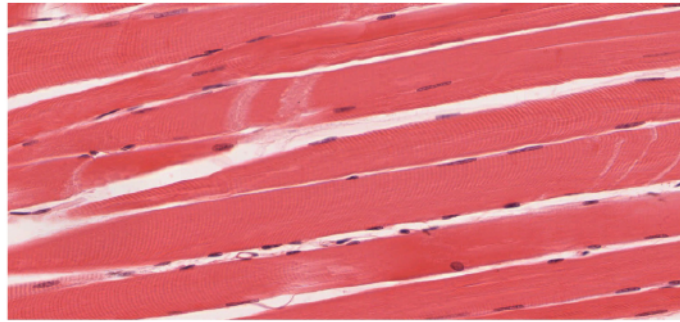


Figure 2.1: View of the Skeletal muscle. [1].

- **The Cardiac Muscle:** Heart muscle or myocardium is a type of muscle that makes up the walls of the heart. Unlike skeletal muscle, the heart muscle works autonomously and rhythmically, thanks to the presence of the sinoatrial node and atrioventricular node conduction system. Its rhythm of contraction is regulated by the autonomic nervous system and, specifically, the sympathetic nervous system increases the rhythm of the beat, while the parasympathetic nervous system decreases it [2]. Despite being an involuntary muscle, it has a striped appearance under microscopy. And cardiac cells, called *cardiomyocytes*, are single cells with their own nucleus.

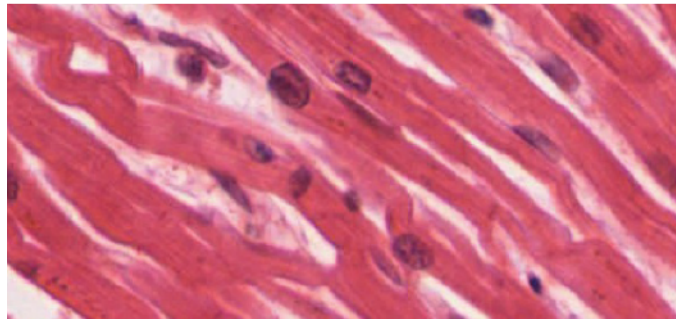


Figure 2.2: View of the Smooth muscle. [1].

- **The Smooth Muscle:** The term 'smooth' muscle derives from the fact that it lacks the striations typical of skeletal and cardiac muscle and, therefore, appears uniformly bright under the light microscope (Figure 2.2)—is the type of muscle found in internal organs, blood vessels, and other structures that are subjected to involuntary control [2]. The smooth muscle is characterized by spindle-shaped cells with a single nucleus and, like cardiac muscle, its contractions are totally controlled by the autonomic nervous system.

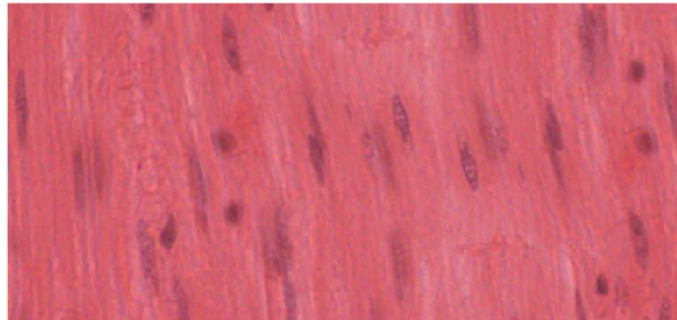


Figure 2.3: View of the Cardiac muscle. [1].

### 2.1.1 The Skeletal Muscle

This study touches on several arguments, like muscle synergies and the Average Threshold Crossing (ATC) technique, that are closely related to ElectroMyoGraphy (EMG). EMG signals represent the skeletal muscles' electric activity, the principal anatomical and physiological aspect of the skeletal muscle that will be discussed in this study. Generally, when people are thinking about muscles, such as biceps or triceps, they are thinking about skeletal muscles. These are representative of motor, or voluntary body movements, powered by voluntary stimuli provided by the somatic part of the peripheral nervous system, known as *Somatic Nervous System*. Differently, smooth and cardiac muscle tissues are effector organs of the autonomic nervous system.

About two fifths of the body is skeletal muscle, and approximately another 10% is smooth and cardiac muscle. An high percentage of proteins, about 50–75%, is used in the body to form the skeletal muscle and that percentage represents the 30–50% of total-body protein turnover. The main bases muscle components are: water (75%), protein (20%), and other substances including inorganic salts, minerals, fat, and carbohydrates (5%). As previously mentioned, skeletal muscle acts in multiple functions of the body. From a mechanical perspective, the role played by skeletal muscle is manifold: the conversion from chemical energy to mechanical energy to produce force and power represents the main goal; secondly, it acts in maintaining posture, producing movement that influences activity, allowing for participation in social and occupational settings, maintaining or increasing health, and contributing to functional independence. Moreover, from a metabolic point of view, skeletal muscle is involved in making a contribution to the metabolism of basal energy, used as a deposit for important substrates such as amino acids and carbohydrates, the generation of heat to maintain the internal temperature, and the consumption of more oxygen and nutrients consumed during physical activity and exercise [3].

## Physiologic Anatomy of Skeletal Muscle

In this section, the fundamentals of muscle structure will be described beginning from the whole of a gross muscle down to individual muscle fibers.

The contraction force is produced by the “body” of a muscle, which is almost always connected to bones through cords of inelastic connective tissue, called tendons. Figure 2.4 is a representation of a skeletal muscle structure.

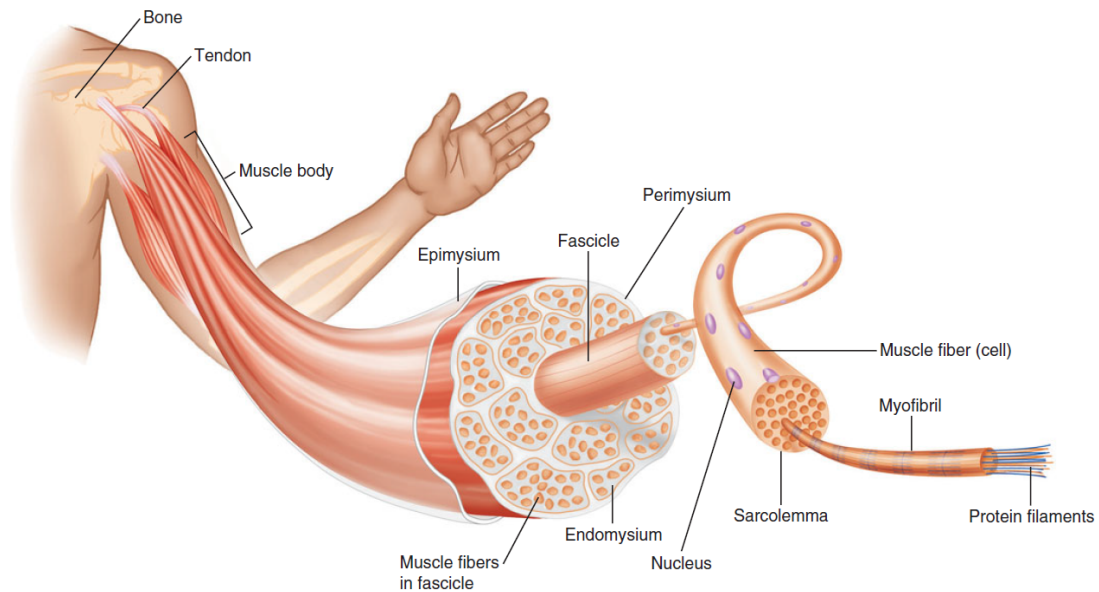


Figure 2.4: Skeletal muscle structure with an enlargement to showing muscle fiber [2].

Skeletal muscles are surrounded by a connective tissue layer called *epimysium*, which is continuous with the connective tissue of the tendons. Inside the muscle, there is another connective tissue layer, the *perimysium*, which determines the internal organization of the muscle fibers groups (called *fascicles*). A fascicle contains up to one hundred and fifty individual muscle fibers (muscle cells) and each muscle fiber generally extends over the entire length of the muscle, each sheathed in a thin sheath of connective tissue called *endomysium*. Under the superficial plasma membrane of muscle fiber, called *sarcolemma*, unlike other cells, there are many nuclei. This, since each muscle fiber formed during embryonic development from the fusion of several cells. Typical fiber dimensions are approximately 100  $\mu\text{m}$  in diameter and 1 cm in length. Isolating a single muscle fiber, the internal cytosol, called *sarcoplasm*, is full of mitochondria (ATP producing organelles) and hundreds of particular elements, elongated contractile units, called *myofibrils*. Myofibrils are made up of two types of protein strands or myofilaments, which are actin and myosin; which form thin and thick filaments, respectively. The intracellular arrangement of myofibrils determines the type

of fibrocell: smooth or striated. All muscle fibers are surrounded by a network membrane, *the sarcoplasmic reticulum*, which is also closely related with other structures called transverse tubules (T tubules), these are continuous with the sarcolemma and penetrate the cell's interior. Both play an important role in the activation of muscle contractions, since they collaborate in the transmission of neural signal inputs from the sarcolemma to the myofibrils [2].

### Structure at the Molecular Level

Each bundle of myofilaments and their necessary proteins, troponin and tropomyosin, titin, nebulin (together with other proteins) is called a *sarcomere*. The sarcomere represents the repetitive-contraction functional unit of skeletal muscle fiber and its structure is shown in Figure 2.5.

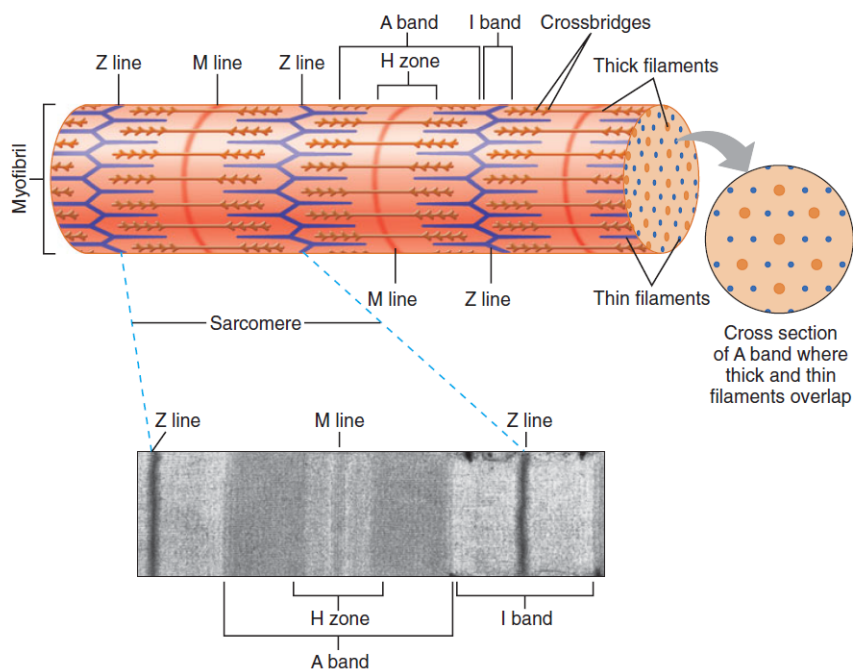


Figure 2.5: Sarcomere structure with photomicrograph view [2].

The structure of the sarcomere can be explained looking it through a microscope that shows the alternation of light and dark: the I-band consists only of actin filaments, the A-band represents the effective thick filament extension and the zone called H-zone (or H-band) which includes the non overlapping piece of actin and myosin filaments. Finally, inside I-band, there is the Z-line, which runs perpendicularly respect to the long axis and each segment included between two

Z-line corresponds to a sarcomere. Because the myosin forms thicker strands with respect to the complex made by actin plus troponin-tropomyosin block, the latter is generally the “thin filament” of the sarcomere. For the same reason, since the myosin filaments and their multiple heads are characterized by more mass and are thicker, these are nicknamed the “thick filament” of the sarcomere. Actin and myosin myofilaments interaction is the basis of the muscle force generation mechanism. These protein filaments during muscle contraction, slide on each other and, overlapping, determine the shortening of myofibrils and, consequently, of the muscle fiber. So at the base of muscle contraction there is the sliding of actin filaments on those of myosin [4].

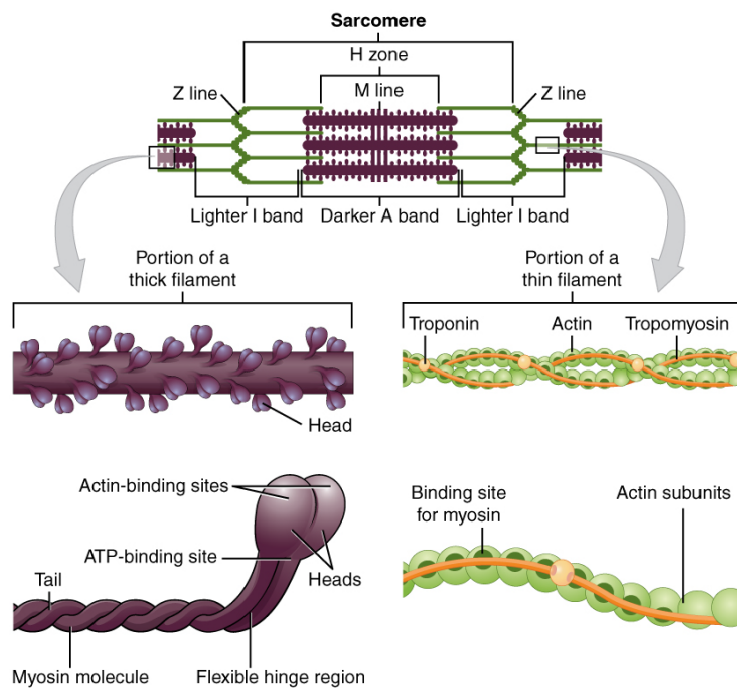


Figure 2.6: Sarcomere structure: myosin and actin filaments enlargement [1].

### Physiology of Muscle Activation: Excitation–Contraction Coupling

“Excitation–Contraction Coupling” refers to the two-step process composed of the muscle fibers excitation by impulses provided by the Central Nervous System (CNS) and the fibers’ contraction and force generation step.

Figure 2.7 shows the main phases of the process.

When a contraction occurs, a nerve impulse from the spinal cords reaches the neuromuscular junction through a motor neuron. The latter represents the neuron whose axons interface directly with the various muscle fibers and all, together

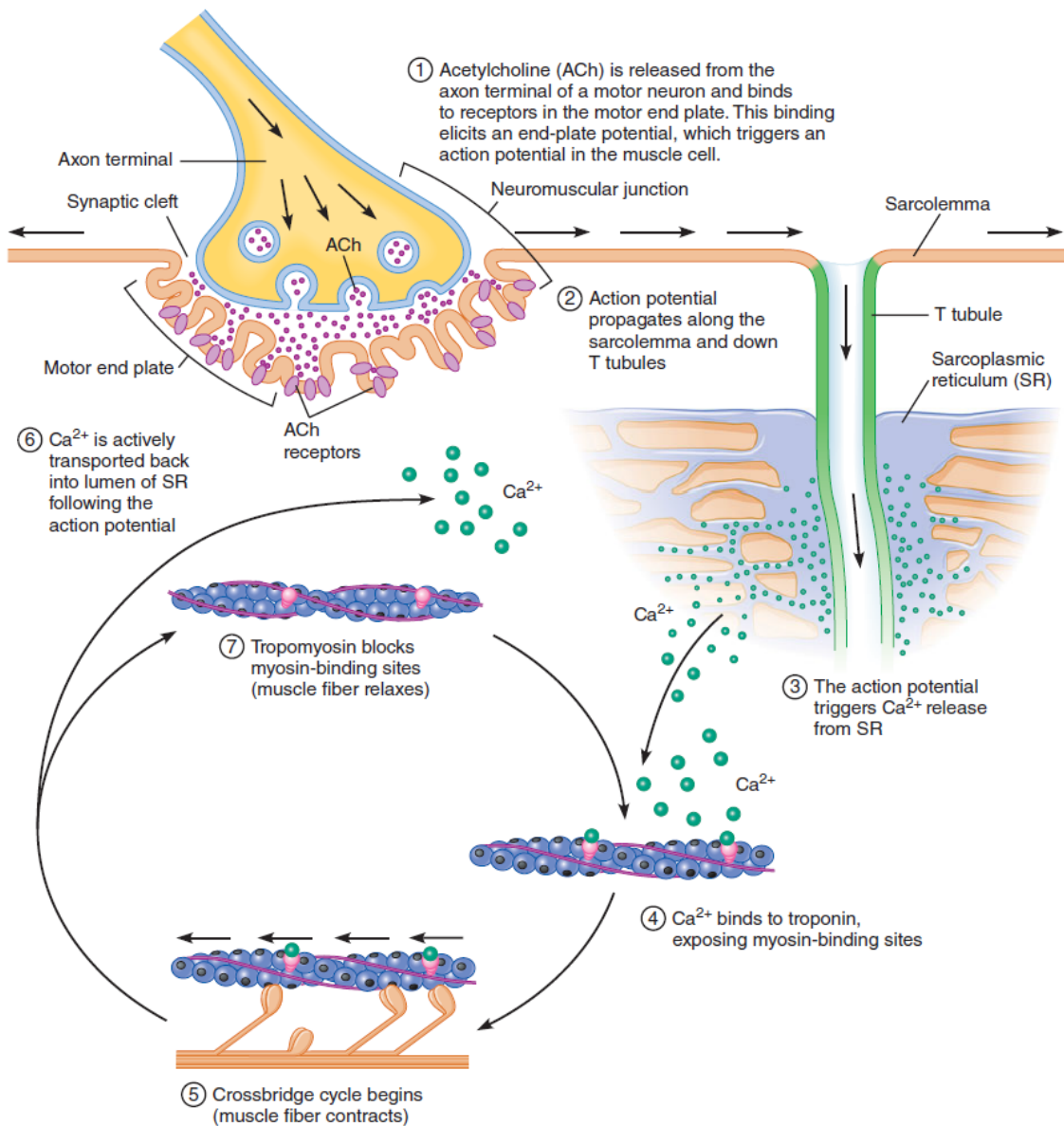


Figure 2.7: Excitation-contraction coupling of skeletal muscle [2].

with the neuromuscular junction, form the *motor unit*. The nerve impulse's arrival at the neuromuscular junction determines the release of *Acetylcholine* neurotransmitters from the axon terminal, which diffuse to a specific region of the sarcolemma, named *motor end plate*. Here, they link with specific ACh receptors triggering a change in ion permeability that results in a depolarization, i.e. AP. Once born, the AP in the muscle fiber propagates through the whole sarcolemma and down across the T tubules. It passes through these structures, the AP triggering calcium release from the nearby Sarcoplasmic Reticulum (SR). Due

to adjacent T tubules, SR membranes are physically connected by two proteins named dihydropyridine receptors, or DHP receptors, and ryanodine receptors. The opening of calcium channels is prompted by the activation of *ryanodine* receptors after a conformational change of DHP receptors, due to the passage of AP down the T tubules. Calcium then moves out of the RS and into the cytosol. This calcium then is used as the input signal that begins the crossbridge cycle and, therefore, muscle fiber contraction [2]. According with Figure 2.8, during

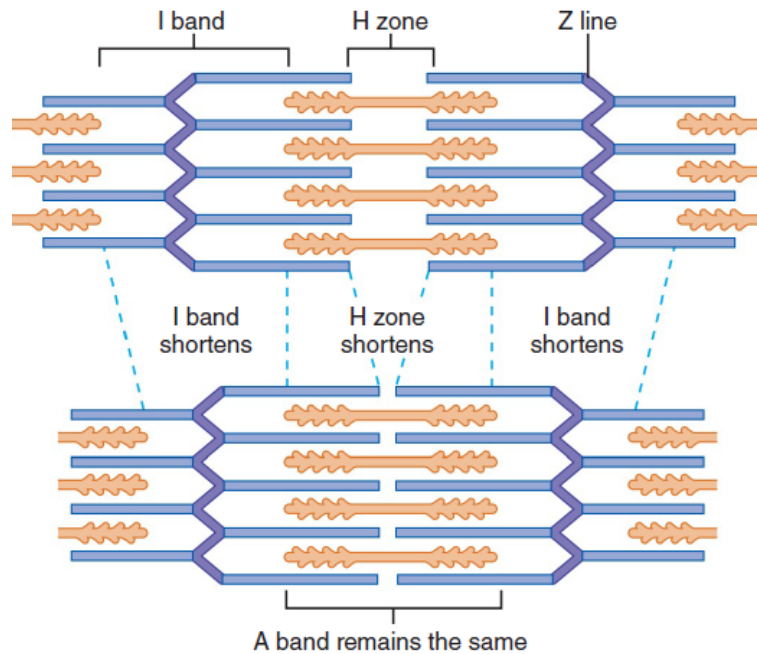


Figure 2.8: Schematic view of changes in striation pattern due to the sliding-filament model of muscle contraction [2].

the contraction, the A-band remains constant, while the I-band and H-zone are reduced, and the Z-lines come near the M-line.

### Muscle fibers types

Skeletal muscle fibers are the largest cells in the body. Within each muscle one can recognize different types of fibers, classified according to their resistance and contraction speed.

The muscle fibers are usually classified into three categories:

- *Type I*: The type I fibers, called “slow twitch” or red fibers, are recruited in low intensity but long-lasting muscle actions. Type I fibers are thinner and smaller than white fibers and are characterized by using oxygen as an energy source (aerobic metabolism). Different to types IIa and IIb, red fibers

are characterized by a lower contraction speed. The name “red” is due to the high number of capillaries that perfuse this fiber type. They are mostly located in muscles responsible for maintaining posture and in the muscles used for slow and repetitive movements.

- *Type IIb*: Also called “rapid contraction” or “white fibers”, are involved in intense and high intensity muscle actions. Type IIb produce energy consuming mainly phosphocreatine and glucose; and, thus, are based primarily on anaerobic metabolism. IIb white fibers are bigger and more connected to the Central Nervous System (CNS) than red fibers and are characterized by higher force and speed contraction. These fibers are recruited during short exercises that require a large neuromuscular commitment and are activated only with the maximum of slow-twitch fibers has been recruited.
- *Type IIa*: Always white fibers, type IIa are slightly smaller and slower than IIb fibers and are recruited first according to the Henneman theory. With greater resistance, for the intermediate characteristics these fibers are also called intermediate contraction white fibers. Thanks to their middling, intermediate, position, they are adaptable in different situations and can specialize to particular responses [3].

### **Skeletal Muscle Contraction Mechanics**

Through the countless activities that people do every day, muscle contractions can be very different from each other in terms of force and duration. The muscle contraction is achieved thanks to two different mechanisms: the recruitment of new motor units with increasing effort and the increase in the discharge frequency of a single motor unit. What is clear is that each of them, whether strong, weak, short, or long, is built on a simple muscle *twitch*. As previously mentioned, a motor unit is composed of the motor neuron, the neuromuscular junction and all the muscle fibers that it innervates. It is not possible to control each fiber alone, but an AP that travels on a motor neuron triggers the stimulation of all the motor unit fibers. A twitch, shown in Figure 2.9, is the mechanical answer of a single muscle cell, a motor unit, or a whole muscle to an individual AP. A twitch can be simulated only in the laboratory since it can never happen in nature. It can be classified in three main phases: the latent period, a contraction phase and a relaxation phase. The latent period consists of a few milliseconds delay which takes place between the AP in the muscle fiber and the beginning of fiber contraction. The following phase represents the real contraction that generates force and, finally, the relaxation phase occurs between the peak tension and the moment when the contraction returns to zero.

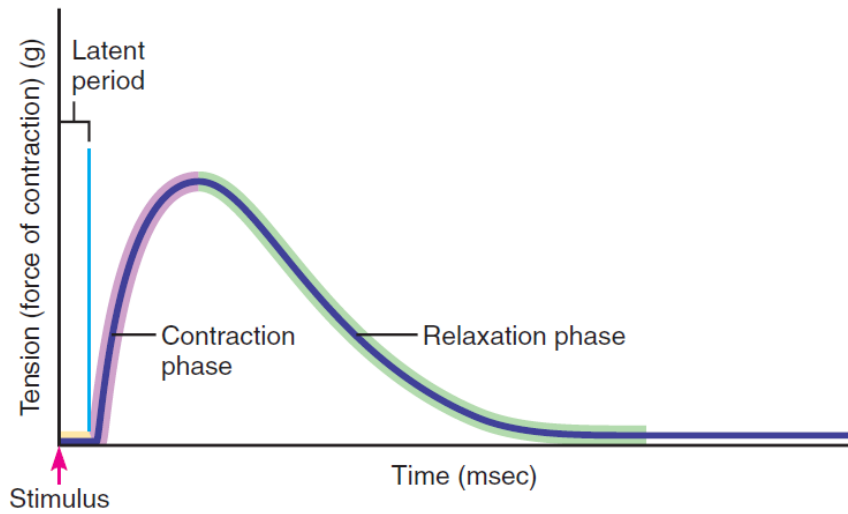


Figure 2.9: Single muscle twitch [2].

When a muscle is stimulated with a certain frequency that does not permit the relaxation of the previous twitch, a superimposition of the twitch on the other determining *the summation process*. The latter is characterized by a greater force level produced respective to a single twitch and, if the stimulation frequency reaches high enough values such as 20 Hz, a *tetanus* occurs. This corresponds to the maximum force that the muscle can generate [2] [3].

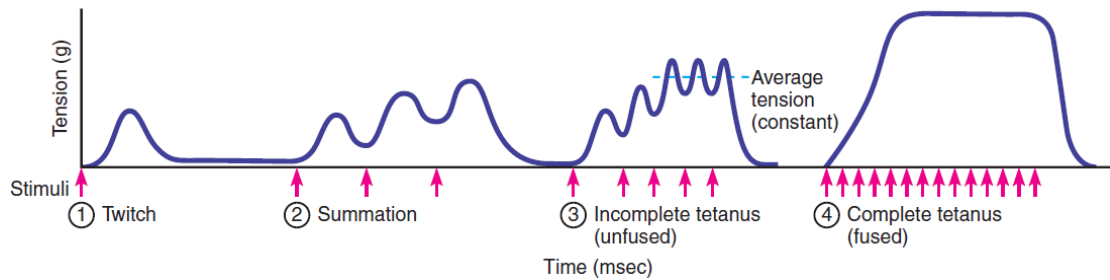


Figure 2.10: Muscle stimulation [2].

### Types of Muscle Actions

A muscle contraction can be classified into three main types: *static*, *dynamic concentric* and *dynamic eccentric*.

The static contraction, also called an *isometric* contraction, occurs when the muscle contracts without changing its length and without moving the load. This situation occurs when the muscle shortening is due to a load equal to the muscular tension, or when a load is backed in a fixed position by muscle tension.

Dynamic actions, also defined as an *isotonic* contraction, occurs when a muscle is shortened by shifting a load that remains constant for the entire duration of the shortening period. Dynamic actions are divided into concentric or eccentric actions. Concentric (or positive phase) is related to when the muscle is shortened by developing tension (e.g. lifting a weight). As opposed to eccentric (or negative phase) occurs when the muscle stretches and develops tension (e.g. slowly lowering the same weight) [4].

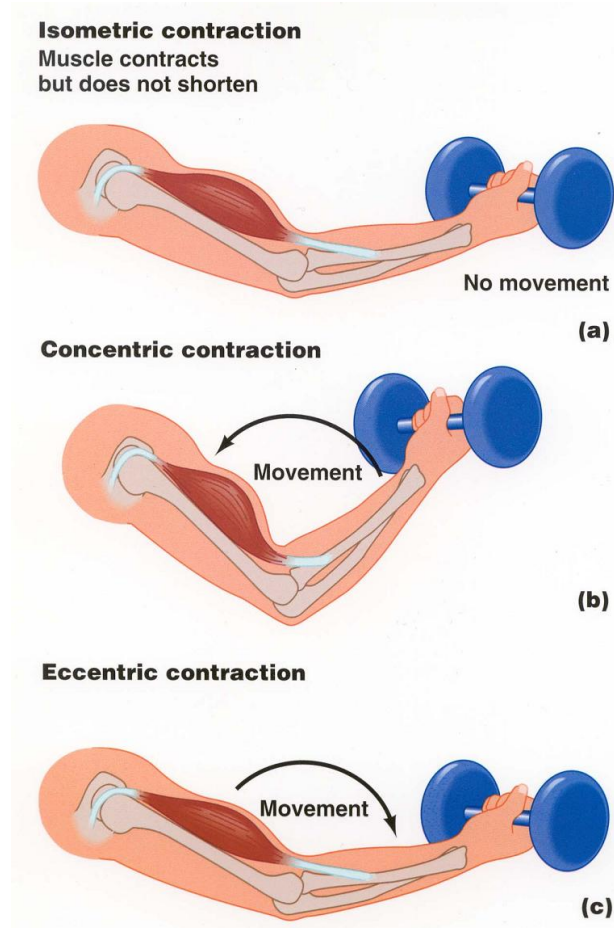


Figure 2.11: Types of Muscle Actions [5].

## 2.2 Surface Electromyography (sEMG)

Carlo J. De Luca, in his publication "*The use of surface electromyography in biomechanics*", claimed:

Electromyography is a seductive muse because it provides an easy access to physiological processes that cause the muscle to generate force, produce movement and accomplish the countless functions which allow us to interact with the world around us. The current state of Surface Electromyography is enigmatic. It provides many important and useful applications, but it has many limitations which must be understood, considered and eventually removed so that the discipline is more scientifically based and less reliant on the art of use. To its detriment, electromyography is too easy to use and consequently too easy to abuse [6].

ElectroMyoGraphy (EMG) represents a medical registration technique which allows the recording of the electric signals produced by the skeletal muscles during its contraction. The source of EMG signals are the AP, which is generated on muscle fibers at the neuromuscular junction and propagates up to the tendons, where it disappears. Since the smallest aspect of the muscle that can be individually controlled by the CNS is the motor unit, it is reasonable to think that the EMG signal is the summation of all electrical contribution of each motor unit involved in the muscle contraction. Referring to a single motor unit, the signal obtained by summation of all AP of all motor unit fibers is called Motor Unit Action Potential (MUAP).

EMG involves the use of electrodes applied directly to the patient. The complex biosignals acquired summarize all the information related to the anatomical and physiological aspects of the activated muscles, the neural control associated, and the instrumentation used for the recording. EMG is obtained through the use of an instrument called an *electromyograph* to produce a record called an *electromyogram* [7].

There are two types of EMG: *Surface ElectroMyoGraphy (sEMG)* and *Intramuscular ElectroMyoGraphy (iEMG)*.

**Intramuscular ElectroMyoGraphy:** This technique represents the "classic" way to record and evaluate an EMG signal. It is based on the insertion of a needle electrodes into the skin and directly into the studied muscle. Differently to non-invasive techniques, iEMG is suitable for single MUAP analysis, thanks to its high volume selectivity determined by the short distance between the electrodes and the source. The extracted electric signal, is an interference signal (Figure 2.12) in which there is the possibility to distinguish singular motor unit contributors, such as signal morphology or activations instants. The decomposition process of iEMG is composed of detection and classification steps.

Despite its importance as an instrument for physiological investigations, iEMG is seldom used in clinical applications. The current clinical uses, by a neurophysiologist, of iEMG signals are related to the diagnosis of myopathies (neuropathologies), motor neuron dysfunctions and the neuromuscular junction issues through the analysis of interference signals or of the shape of some motor units' AP, usually without signal decomposition [8].

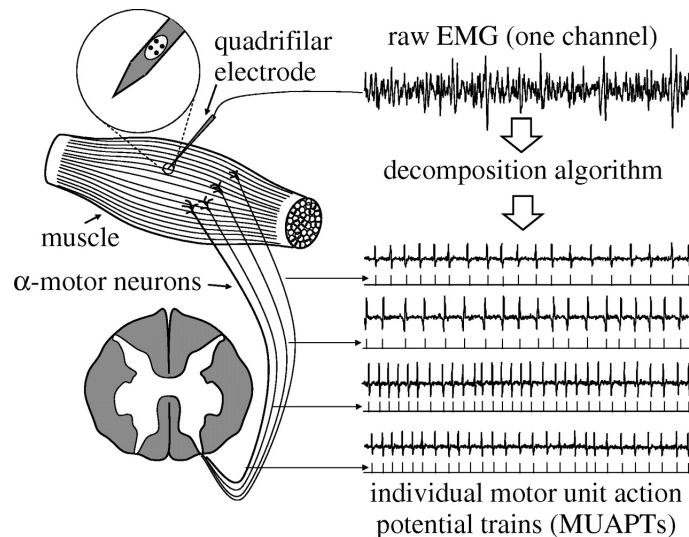


Figure 2.12: Intramuscular ElectroMyoGraphy (iEMG) [8].

Another advantage of this technique is the absence of any tissues filter effect, due to the tissue layers interposed between the source and surface electrodes. Despite its peculiarities, the iEMG is characterized by several limitations, among are: the invasive electrode placement and their sterilization, the unsuitability to carry out long-term examinations, and the its unsuitability for dynamic motor tasks.

**Surface ElectroMyoGraphy:** sEMG assesses the electrical activity of muscle contraction by opportunely positioning electrodes directly on the skin. A non-invasive technique, the electrodes are placed on the surface of the skin (not into) above the muscle of interest. As such, this technique is not as localized in terms of withdrawal volume but is suitable for superficial muscles. The biosignal acquired is an interference signal which algebraically adds all the motor unit AP of all recruited motor units. The number of electrodes can vary from two to more complex arrays of multiple electrodes, as necessary to capture the overall muscle activity information. The positioning of the electrodes needs a high level of attention. An appropriate location on the muscle, interface stability with the skin and an appropriate preparation of the skin itself are all factors in capturing data using sEMG. In comparison to the iEMG, this alternative has lower selective in the MUAP extraction and recognition, but is easier to implement and less

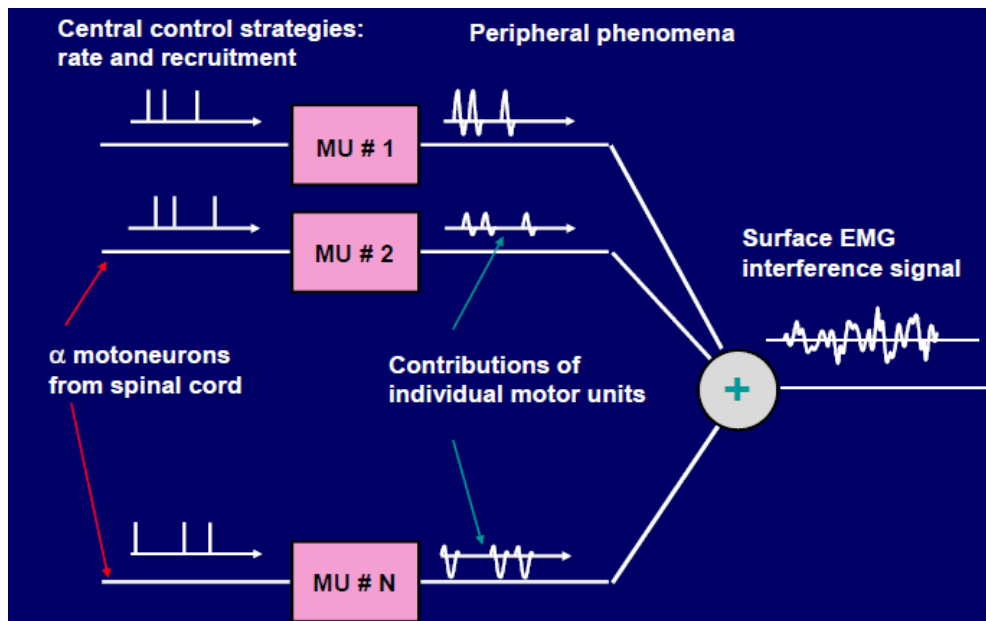


Figure 2.13: Surface ElectroMyoGraphy (sEMG) Signal.

stressful on the subject. It also allows dynamic and long-lasting tests. In this case, however, a singular MUAP can be identified from sEMG recorded using indwelling electrodes by a decomposition process.

Generally, the main advantages of sEMG are:

- Information on the moment, on duration, on the entity of the activation of a muscle during a movement;
- Indications regarding the overall activity of a muscle or muscle group;
- Informs the patient of the degree of contraction or relaxation of one of their own muscles or muscle groups (Bio-feedback);
- The myoelectric signal can be used to control an external device;
- Analysis of patients unwilling to undergo the more invasive techniques;
- Possibility of dynamic and long-lasting test;
- Easy to perform and painless;

For all these reasons this type of electromyography has become more used in clinical and in rehabilitation's applications [9, 10].

### Electrodes material, size, montage and positioning

Currently, there are several set-up types to record sEMG signals, which differ in materials, dimensions and detection configurations. The most used electrodes are made of silver/silver chloride (Ag/AgCl), silver chloride (AgCl), silver (Ag) or gold (Au). Ag/AgCl electrodes, in particular, have the ability to not be polarized, and reduce surface potential sensitivity to sliding movements at the electrode-skin interface and, when a conductive gel layer is interposed, they increase the electrode-skin interface stability. Concerning the dimension of the surface electrodes, they range from millimeters to a few centimeters in diameter or length; and, together with the inter-electrodes distance, vary primarily on the aim of the given study, the dimensions of the study muscle, the muscle architecture and on the desired spatial resolution [11].

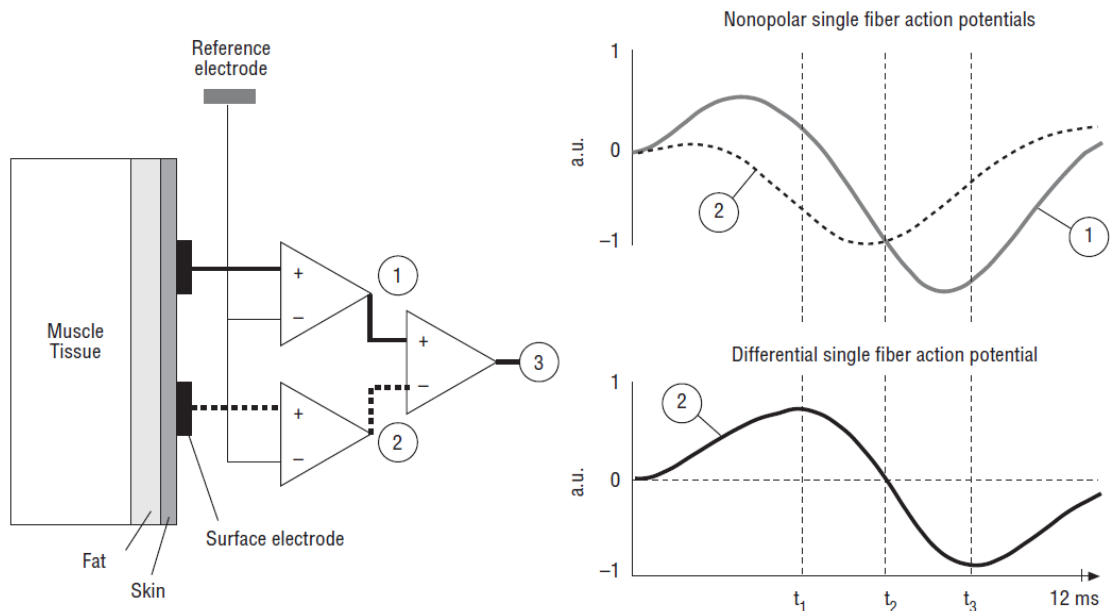


Figure 2.14: Electrodes configuration [11].

Another fundamental aspect in the sEMG recording is the electrode montage. There are two principal configurations: monopolar and bipolar. The first gives information about the surface potential on the skin and is measured directly above muscle tissue, as compared to a reference electrode placed above a bony region. Its main characteristics are: large volumes of sampling (which makes it susceptible to disturbances), and it preserves all information contained in the signal without spatial filtering. The second is the result of the differences between two monopolar sEMG. It is characterized by a reduced sampling volume (which

makes it less susceptible to disturbances), and it removes some signal components according to signal propagation speed, inter-electrode distance and spectral content [11].

### 2.2.1 sEMG Signal Principles

The sEMG signal amplitude, according to its interference aspect, represents a random signal which can be represented by a Gaussian distribution function. The sEMG signal amplitude is found in a range comprised between 0 and 10 mV (peak-to-peak) or between 0 and 1.5 mV (RMS). The frequency content of the signal is limited to the 0 to 500 Hz range and the most of the power is in the 50-150 Hz range [12].

Currently, the main applications of sEMG are related to the following fields:

1. *Biomechanics and movement analysis:*  
Recognition of muscle activation intervals and intensity, muscle coordination;
2. *Muscle fatigue and non-invasive fiber typing:*  
Myoelectric fatigue manifestations observation;
3. *Rehabilitation and sport medicine:*  
Assessment of effectiveness of rehabilitation treatments;
4. *Occupational medicine:*  
Monitoring the “Cinderellas”<sup>1</sup>, postural type problems, muscle hyperactivity;
5. *Biofeedback:*  
Tension headache, muscle retraining, coordination retraining.

Two very important aspects to know when detecting and recording sEMG signal are the following: the *signal-to-noise ratio* and the distortion of the signal. The first one consists of the ratio between the energy in the sEMG signal divided by the energy in the noise signal, It is an indicator of the signal quality.

---

<sup>1</sup>“The Cinderella Hypothesis” proposed by Hägg (1991), explained that the trapezius motor units recruitment is characterized by a fixed order. Firstly, until the complete muscle relaxation and for low-intensity contractions, are recruited small and low-threshold motor units. Secondly, larger motor units are activated. A long-time activation of these units may cause degenerative processes, damage and pain [13].

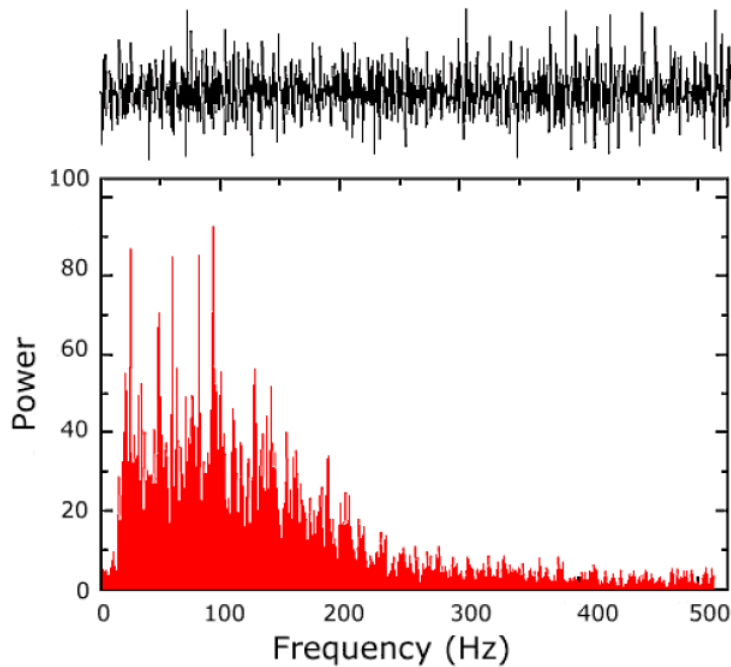


Figure 2.15: Example of the frequency spectrum of the sEMG signal [12].

The second refers to the fact that the relative contribution of any frequency element in the sEMG signal should not be altered [12].

### 2.2.2 Noise Sources in sEMG Signal

“Noise” are all the signals that are not part of the sEMG signal, such as movement artifacts, detection of the ElectroCardioGraphic (ECG) signal, ambient noise from other machinery, and the inherent noise in the recording equipment. The aim is to maximize the signal-to-noise ratio as much as possible in order to increment the signal fidelity. There are different types of noise sources to keep under control [14] [12]:

- **Inherent Noise in the Electrode:** “Inherent noise” refers to general electric disturbance given off by all electronic instruments. These cover a frequency range which extends from 0 Hz to several thousands Hz and this noise source can not be completely eliminated. A good practice to keep it at low levels is to use only high-quality electronic equipment, intelligent circuit design and construction techniques.
- **Motion Artifact:** Signal disturbance due to electrode cable motion and instability of the electrode-skin interface. During a muscle contraction, one

might observe sliding between the electrode and skin due to a change in muscle length. Two solutions to reduce these artifacts consist of the use of a conductive gel layer placed at the electrode-skin interface and the realization of suitable circuitry design. Moreover, another source of movement artifacts is represented by the virtual movement of the muscle innervation zone during dynamic contractions. This noise usually covers frequencies under 10 Hz and sometimes causes narrow and wide peaks in the signal.

- **Electromagnetic Noise:** The sources of this noise are represented by all electric and magnetic environmental radiation, such as radio and television transmission, electrical-power wires, light bulbs, fluorescent lamps, etc. These disturbances can both overlap the sEMG signal and kill it. They are generally characterized by an amplitude that is about three times larger than the sEMG signal. The principal cause for the environmental noise derives from the 60 Hz in USA (or 50 Hz in UE) radiation from power sources (this is also called Power-Line Interference (PLI)). Through off-line processes (e.g. filters) it is possible to reduce noise in the reordered signals.
- **Cross Talk:** “Cross talk” is defined as the reading, through the sEMG signal collection system, of muscle activity that does not correspond to what one would like to observe. This noise is mainly due to signals generated at the extinction of the potentials at the tendons. It can cause an incorrect signal interpretation. Presently, there are no methods that can eliminate cross talk efficiently after the signal recording. Cross talk needs particular attention in the signal collection phase and correctly choosing electrodes-size and inter-electrode distances. Using a spatial filter approach, it is possible to control it.

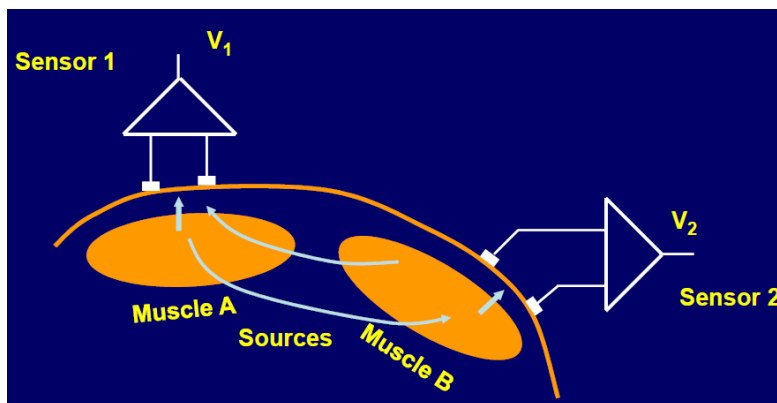


Figure 2.16: Example of the Cross talk.

- **Inherent Instability of the Signal:** This name relates to the behavior of the signal amplitude or frequency content which is naturally unstable and

stochastic. The spectral contributes, between 0 Hz and 20 Hz, are mainly unstable because they are affected by the firing rate of the motor units, which are naturally almost-random. Information in the sEMG continually change due to the numbers of active motor units, motor firing rate and mechanical interaction between muscle fibers.

- **ElectroCardioGraphic (ECG) Artifacts:** The electrical activity of the heart is the most important interference component for sEMG in the scapular girdle and, in general, causes disturbances in the EMG signals mainly taken at trunk-level muscles. There are no methods that can eliminate ECG artifacts efficiently after the signal recording. A way to reduce its acquisition is get an high common mode rejection ratio (CMMR) withdrawal system and by the careful placement of bipolar recording electrodes along the heart's axis if possible. Moreover, an high-pass filter at 100 Hz represents a good way to remove ECG disturbs.

### 2.2.3 sEMG Signal Acquisition Chain: General Model

As previously explained, for sEMG acquisition, the interested frequencies are mainly in the band between 20 Hz to 400 Hz and the signal amplitude oscillates from 0 to 10 mV (peak-to-peak), depending on muscle contraction intensity. Given sEMG's time and frequency characteristics, it's clear that a very sensitive and specific analogue to digital acquisition set-up is required. A simplified model is shown in Figure 2.17.

The acquisition chain is made on several principal blocks, including *detection*, *amplification*, *conditioning* and *digitalization* of sEMG.

The first block, the amplification, consists of a differential amplifier and its role is to multiply the difference between two voltage signals by a fixed gain. It is useful as it permits the amplification of low amplitude sEMG levels; and it is necessary for the regulation of the amplitude itself to match the dynamic range of the A/D converter. This is the only way to be sensitive and to digitize small sEMG fluctuations. This differential amplifier generally is an instrumentation amplifier and has a very high Common-mode Rejection Ratio (CMRR) in order to attenuate common mode components.

The second block, the filtering, removes the aliasing disturbances due to the existence of some higher frequency components than the maximum theoretical band of the signal. The filtering is made by a low-pass filter at about 400 Hz.

Finally, the digitalization, is carried out by an A/D converter. The most important aspect related to A/D converter is its *resolution*, as it decides what analogical variation the detection system is able to sense and, hence, to digitalize. The resolution of A/D converters are defined by dividing its dynamic range by its number

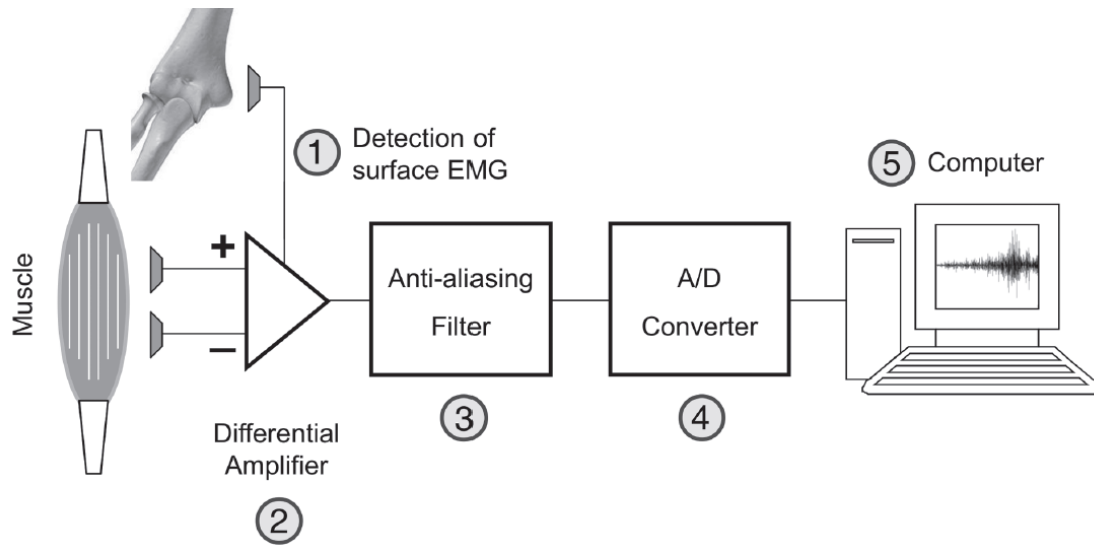


Figure 2.17: Simplified Model of sEMG Signal Acquisition Chain [11].

of levels. The role of A/D converters are to sample and convert analogue to digital data with a specific sampling frequency according to the Nyquist-Shannon theorem. The removal of frequency components is an operation that can be carried out at a later time through the implementation of digital filters [11].

## 2.2.4 sEMG Signal Time and Frequency Descriptors

With the aim of easily summarizing the principal information of sEMG, some physiological parameters have been extracted. There exists some which derive from the time analysis (ARV and RMS) and others that derive from spectrum analysis (MDF and MNF).

### Time Descriptors

These are indicative of muscle contraction intensity. Usually, amplitude descriptors are calculated on processed signals, i.e. after rectified or squared samples obtained during the motor task recording. The most important amplitude descriptors are:

- **Averaged Rectified Value (ARV):** Parameter which consists of a single value obtained from several samples of sEMG. It is calculated as the average of absolute values and it is indicative of temporal amplitude variation of sEMG, regarding directly to the degree of myoelectric activity. Generally the entire

sEMG recording is separated into many epochs, usually of 250 ms to 500 ms, and for each of them the ARV value is calculated, allowing its time trend observation.

$$ARV = 1/N \sum_{n=1}^N |EMG[n]|$$

- **Root Mean Square (RMS):** Is calculated as the arithmetic mean of the squares of a set of samples and explains the power of sEMG. The entire sEMG recording is generally separated into many epochs, usually of 250 ms to 500 ms, and for each of them it is calculated the RMS value.

$$RMS = \sqrt{1/N * \sum_{n=1}^N x_n^2}$$

The square root operator in the formula, despite RMS is always an amplitude describer, makes this last different from the previous one. In fact, the RMS value weights the different sEMG samples otherwise, attenuating the amplitudes of the smaller ones and amplifying the amplitudes of the higher ones. In this way epochs of high myoelectric activity are more evident with respect to epochs of low activity. This is the reason why RMS is usually preferred with respect to ARV, being a transporter that contains a physical meaning [11].

Considering *constant force isometric contractions*, both in the case of voluntary and electrically stimulated cases, the trend of these two descriptors is to increase over time is increasing. This is due to the decrease in the speed of conduction of the AP on the muscle fibers during prolonged activities, thus determining the slowest passage of AP in the electrode detection zone (i.e. the shape of the potential detected on the surface with the greater area) [11].

### Frequency Descriptors

Frequency descriptors are indicative of how fast the muscle contraction activity changes intensity. The calculation of *the power spectral density function* allows to obtain a description of how sEMG power is spread on all the spectral components, giving a spectrum. The sEMG spectrum is an important tool because its changes are in accordance to many factor that affect the signal, such as conductive velocity.

The latter is primarily responsible for changes in the form of the AP taken on the surface and closely related to the concept of muscle fatigue.

Generally two principal frequency descriptors are extracted from the sEMG power spectrum: Mean Frequency (MNF) and Median Frequency (MDF). As amplitude descriptors, they are always estimated over shorts epochs in order to observe time variations of spectral contributors [11].

- **Mean Frequency (MNF):** The mean frequency is the statistical moment of order one. Looking at the formula, the numerator is composed by the summation of products between frequencies and its correspondence power spectrum and this for all frequencies between 0 to half of the sampling frequency used; at the denominator, instead, there is the signal power (total area under power spectral density function).

$$MNF = \frac{\sum_{f=0}^{f_s/2} fP(f)}{\sum_{f=0}^{f_s/2} P(f)}$$

- **Median Frequency (MDF):** It represents the frequency value that divides the power spectral density function  $P(f)$  exactly in half.

$$\sum_{f=0}^{MDF} P(f) = 0.5$$

The importance of calculating both these position descriptors is due to the “colored” nature of sEMG signals and the calculation of both can give a more precise interpretation of spectrum variations.

In this case, considering *constant force isometric contractions*, both in the case of voluntary and electrically stimulated contractions, the trend of these two descriptors over time is decreasing. This is due to the same precedent motivations.

MNF is usually higher than MDF due to the skewed shape of sEMG power spectrum, but MDF is less affected by random noise [11].

## Chapter 3

# Average Threshold Crossing

### 3.1 ATC Approach

The reduction in the amount of data to be managed, the reduction of the power consumption and the reduction of the size and circuitry complexity are becoming increasingly necessary to keep up with today's technological progress.

Starting from the classic blocks structure of an amplification chain of a standard sEMG signal acquisition system, as shown in Figure 2.17, a new approach which satisfies the requirements just mentioned will be introduced.

The Average Threshold Crossing (ATC) is an event-driven transmission technique that consists of an event generated each time the sEMG signal exceeds a fixed threshold. Recently studied, it is different from other techniques present in literature [15] [16] [17].

Figure [15] shows a comparison between the operating scheme of the ATC event-driven transmission and the operating scheme of a standard sEMG signal transmission. What can be noted is that, while the standard approach (blue blocks [S1...S17]) involves to acquire and transmit all samples with a specific sampling rate of  $1/T_s$  and independently of the signal amplitude, the event-driven approach (red blocks [E1..E4]) generates a single event only when the sEMG amplitude overcomes a precise threshold  $V_{th}$ . It has been demonstrated that the counting of TC events in a precise time window is closely related to force exerted by the muscle activity [15]. Considering the possibility of transfer these generated packets using Impulse-Radio Ultra-Wide Band (IR-UWB) technology, which is becoming increasingly popular in Wireless Body Area Networks (WBAN) and in bio applications thanks to its qualities of low power consumption, robustness against interferences and usefulness to measure distance, it is possible to reduce the quantity of signal data sent over-the-air [16]. Indeed, an approach of this kind is based on simply triggering a wireless pulse every time the sEMG signal

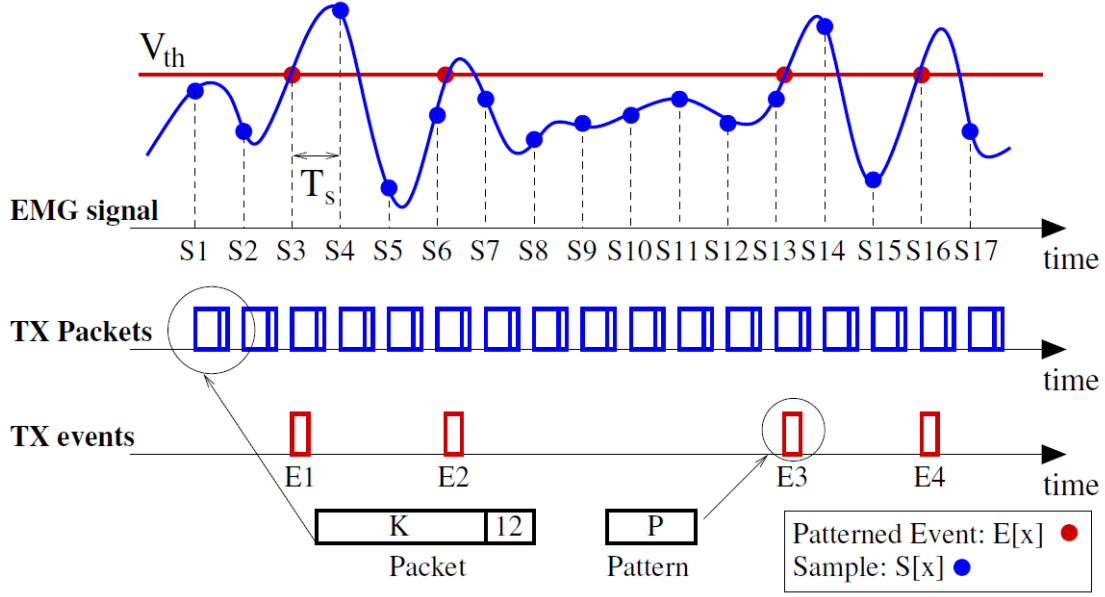


Figure 3.1: Comparison between standard sEMG sampling and Average Threshold Crossing (ATC) sampling technique [15].

overcomes a given threshold and, therefore, consists in a reduction of transmitted information and reduction of power consumption [15].

Another important aspect to highlight is that, while standard sEMG signal acquisition and transmission involve to quantize and digitize the analogical input (ADC conversion), strongly influencing circuitry area necessary, power consumption and data transmission, the ATC wireless system does not requires this step. ATC allows the size reduction of the silicon circuit area, since it doesn't need the analog to digital converter component, clock generator and complex logic to manage the data [16]. Consequently, the ATC system acquisition unit is composed by three blocks: the differential amplifier, the comparator and the UWB transmitter. The fundamental element of the system is the threshold comparator, which receives two signals at the input: a constant signal and the sEMG signal. The first one represents the threshold voltage  $V_{th}$  with which the comparison is made, the second one is the sEMG signal, previously subjected to an analog conditioning.

$$V_o = \begin{cases} 1, & \text{if } V_{emg} > V_{th} \\ 0, & \text{if } V_{emg} < V_{th} \end{cases}$$

The comparator output consists of a quasi-digital signal, the TC signal, whose aspect is digital but information content is contained in its the temporal features, as shown in figure 3.2.

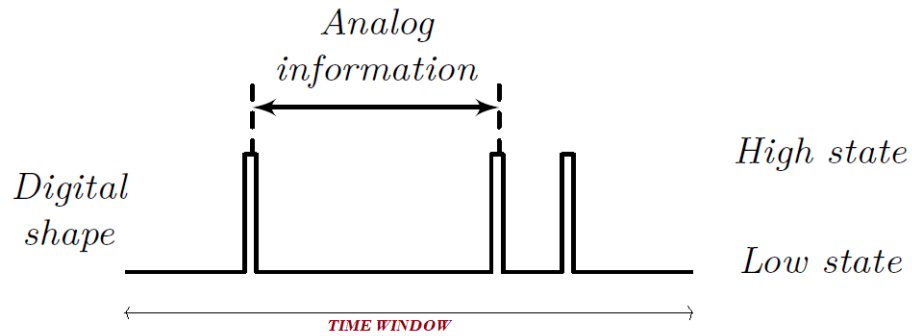


Figure 3.2: TC signal and comparator output.

“ATC” parameter is calculated as:

$$ATC = \frac{TCevents}{TimeWindow}$$

Through the concatenation of successive ATC values it is possible to extract a signal with a similar behavior respective to the sEMG envelope, but made by an extremely lower number of samples.

In the formula: “TCevents” is the number of TC events in the specific window and “TimeWindow” is the time window length. This value has shown increase with the force applied in an isometric and isotonic contraction [16].

After this briefly introduction it is possible to summarize the ATC principal advantages:

- very low power consumption;
- limited area circuitry and size;
- reduced amount of data to be elaborated and transmitted;
- suitable for WBAN applications;
- Robust to loss of events.

Despite the main advantages specific of the simplification basis on which this technique is founded, it includes also few disadvantages in comparison to the features extracted from integer sEMG signal [15] [16] [17]:

- loss of several time and frequency features;
- loss of all morphological information;
- difficulty in the suitable comparator threshold;

## 3.2 Previous Studies

The ATC approach has been investigated during the last few years at the *Istituto Italiano di Tecnologia (IIT)* as a way to merge the most important requirements that should characterize a wearable, portable, low power consumption, wireless and multi channels acquisition system. The main results of this research based on ATC, has been the development of a low-complexity radio system for portable biomedical application [15]. The system, through the use of IR-UWB wireless technology, is able to communicate the muscle force information bidirectionally with a receiver, without requiring an ADC for the data digitization. In particular, the work has focused on the demonstration of the correlation between the performance of the system in terms of ATC events (digital pulses) and the performance of the system looking at the ARV values calculated on the raw sEMG signal. Merging this information with a force signal recorded through a dynamometer during a maximum voluntary contraction, it has been possible to find a large correlation between the precedent signal and show the validity of the wireless-ATC based system.

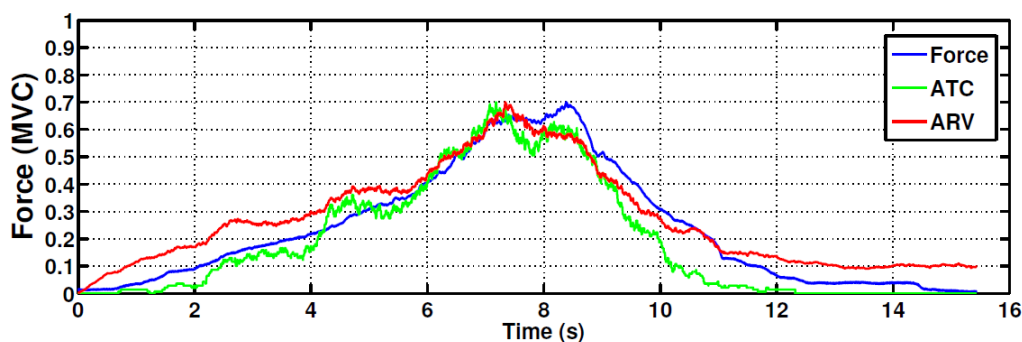


Figure 3.3: ATC, Force, ARV signals in time domain [15].

The study has demonstrated that the IR-UWB technology combined with the ATC technique allows the reduction of the size and power consumption of the EMG acquisition system and to monitor muscles activation through the reduced

amount of data managed and transmitted by the hardware.

A second study published by the same research group in [17], regards the extension of the previous ATC based wireless system to a more complex multi-channel acquisition version. The data is conveyed by exploiting the Address-Event Representation (AER) approach. The previous scheme is maintained, starting from the raw sEMG which is extracted from the quasi-digital signal, i.e. the TC signal, which gives impulses to the IR-UVB transmitter that accordingly sends data. The work has determined a confirmation in the reduction of both the power consumption in both board dimensions.

Between the most recent studies we can also mention the dynamic threshold version, or D-ATC [18]. The comparison with the standard ATC has shown improvements in robustness and larger correlation with respect to force level. Exploiting the same theory [19], there is the validation of a prototype for ATC/sEMG multichannel acquisition board and the validation of the ATC parameters, i.e. threshold and time window. The value of the *threshold* should be set neither too high, in order to avoid the lost of important parts of the sEMG activation, but neither too low in order to avoid the catching noise. Typically the threshold level is set to 100 mV higher with respect to the baseline noise. Regarding the choice of the *time window*, it should have enough length to modulate the muscle activity, but a value that is not too high to compromise the time resolution and the real-time applicability. Generally values are between 50 ms and 200 ms [20]. Another use of the previous system has been investigated in the pattern recognition field [21].

In the work carried out by S. Bianca described in [22] has been finally designed a prototype based on the previous work in [19] for multi-channel acquisition of sEMG signals using ATC approach. Finally, F. Rossi in his study explained in [23], expanded this new board in order to real time control a Functional Electrical Stimulation (FES), as therapy used in neuromuscular rehabilitation. Through the use of ATC event-driven technique applied to sEMG is possible to drive a FES stimulator that stimulate muscle contractions and body movements in the patient in order to restore some basic voluntary muscle functions.

## Chapter 4

# Muscle Synergies

The study of the strategies actuated by the Central Nervous System (CNS) to generate a movement are still a subject of research. Despite the seeming simplicity which characterizes repetitive movements execution like reaching for an object, walking or running, it hides an high control complexity level. The CNS, considering and elaborating the inputs generated by the environment, performs any movements managing and coordinating multiple limbs having several degrees of freedom and redundant muscles activations. In fact the musculoskeletal system presents an higher number of muscles compared to joints and the same movements can be reached from different muscles activations.

How the CNS faces this approach is one of the main issues that science is trying to answer, maybe opening a new clinical scenario in the CNS diseases treatment [24].

Beginning from *Bernstein* in 1967 and then several investigators in the last decades, it has been tried to understand how the CNS can reduce the computational burden associated to movement generation through the use of a lower number of discrete elements, muscle primitives or modules, which have been defined *Muscle Synergies*. More specifically, muscle synergies can be defined as muscles blocks in which muscles are co-activated with a specific level and, considering a generic movement, they allow to lighten up the CNS load making sure that the control of each single muscle is reduced to the control of blocks of them [25].

In support of this, principally in the last two decades, have been conducted many experimental researches that have demonstrated the validity of this modular approach in humans and animals and also its possible alteration caused by neural injuries, determining pathological behavior and altered movements [24].

In this scenario, the analysis and the extraction of muscle synergies can represent a diagnostic tool in the assessment and rehabilitation of neuromotor diseases.

## 4.1 Motor Control Model

As previously explained, the synergistic hypothesis states that the CNS recruits a small number of muscle synergies to generate motor control. One important aspect, which is intrinsic in the definition of muscle synergies, is that the number of muscle synergies need to be lower respect to the number of muscles. Otherwise, the synergistic hypothesis lose meaning and the muscles are not clustered together in single functional units [24].

Another important aspect regards the fact that muscle synergies do not give information only about which muscles are grouped, but also show “how” they work together [24]. This is shown in the figure 4.1 under the term *weights*.

Among the several motor control theory existing today, the most approved is the hierarchic control theory which consists of a complex circuitry that extends from motor cortex to spinal interneurons. More specifically, the realization of voluntary movements is due to the correct time activation of spinal interneuronal muscle synergies by the motor cortex, which handles the modules through specific time activation pattern in order to realize a precise motor task. This scenario is also resumed in Figure 4.1. Furthermore, a movement realization involve a combination of several muscle synergies each one with its specific time activation pattern. The single muscle synergy vector  $W_i$  containing muscle weights is constant over time and what changes is its activation in the time.

In according to what expressed, it is possible to represent the muscular activity through a model that linearly combines muscle synergies:

$$M(t) = \sum_{i=0}^N c(i) * W(i)$$

where  $M(t)$  is the muscular activity,  $c(i)$  the time activation pattern of the specific muscle synergy and  $W(i)$  represent the  $i$  synergy vector.  $N$  is the number of muscle synergies.

For what concern the rhythmic activities like walking, running, chewing etc, exists a specific theory named Central Pattern Generators (CPGs). The CPGs provides for the existence of spinal circuits where are memorized rhythmic motor patterns used for rhythmic activities. More precisely, it is possible to distinguish two main control levels: the first level, defined *high*, is represented by the motor cortex, the cerebellum and basal ganglia, all in the CNS, and covers the master role of selecting, initiating and modulating the motor programs in according to environmental inputs. The second level, defined *low*, is represented by the spinal cords and has the aim to generates the basics rhythmic motor patterns of the motor tasks [26].

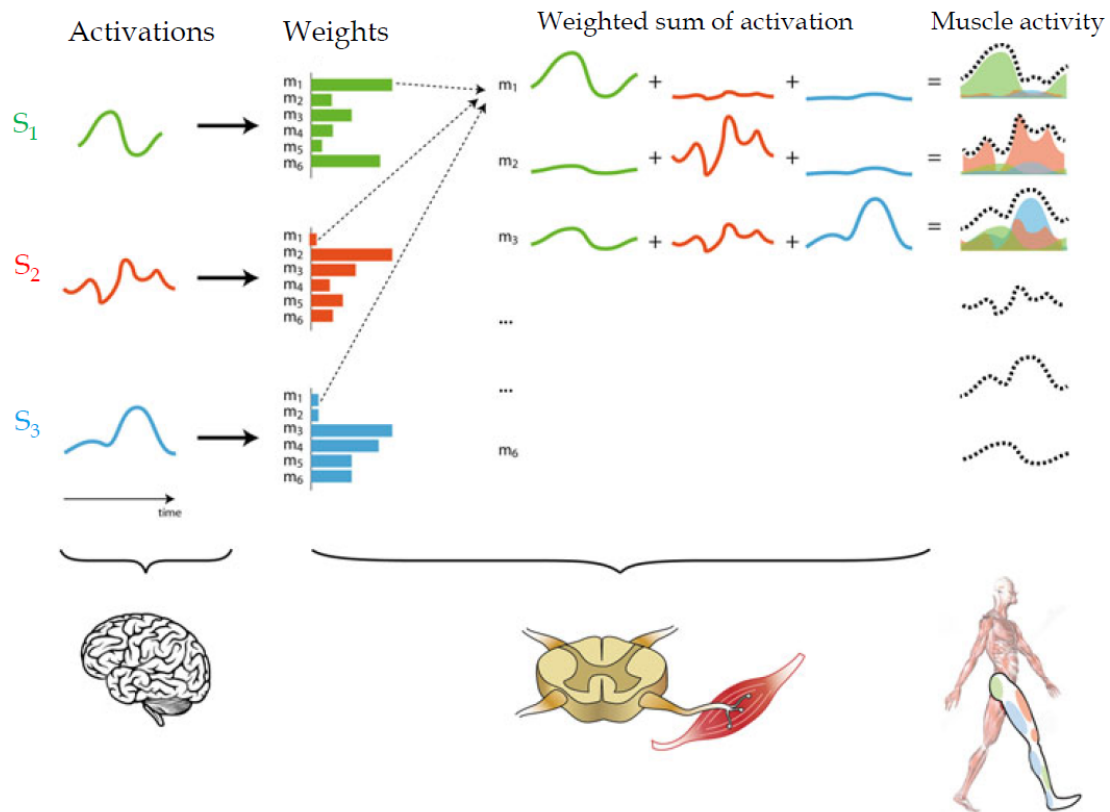


Figure 4.1: Muscle Synergies Hypothesis: the summation of products between time activations signals and muscle synergies weights defines the muscular activity [24].

## 4.2 Muscle Synergies Analysis

The study of muscular synergies is a very hot research topic thanks to the potentialities that could offer. On one side, the extraction of muscle synergies from sEMG recordings can be used to reduce the number of features needed to describe the complex muscular activation structure employed during a movement and this approach could be exploited, for example, in the bio-robotic prosthesis control. On the other side, the analysis of muscle synergies, together with taking other measures (e.g behavioral or biomechanical), represents a supplementary diagnostic tool to highlight and better understanding the impairments that characterize a person with neurologic pathologies, such as stroke, spinal cord injuries (SCI), Cerebral Palsy (CP), multiple sclerosis etc. which are all CNS disorders causing motor control alterations [24].

The 'traditional' blocks chain followed in the analysis of muscular synergies is shown in the figure 4.2.

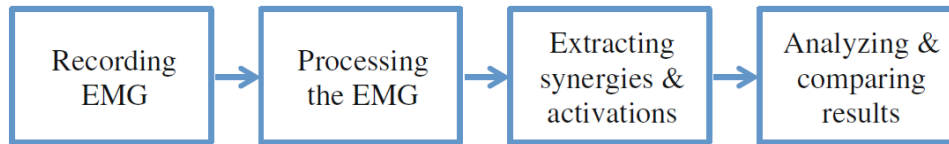


Figure 4.2: Muscle Synergies Blocks Chain Analysis [24].

Firstly, the synergies analysis requires the muscular activity expressed by a higher number of muscles involved in a specific movement, generally done through Surface ElectroMyoGraphy (sEMG) analysis, using non-invasive electrodes. After the appropriate processing of these acquired signals, they are used as input for specific factorization algorithms able to extract the *weights synergies vectors* and their corresponding *time activations*. The last step consists in the results analysis and interpretation [24].

### 1. Recording ElectroMyoGraphy Signal

As previously explained, since the aim is the extraction of some strategic muscle co-activations, higher is the number of acquired muscle, higher is the solution quality found.

The quality of sEMG signals and consequently that of extracted synergies is highly influenced by the electrodes positioning, in according to what expressed in the previously paragraph 2.2 about *electrodes material, size, and positiong* and to what contained in SENIAM project [27], which includes a list of good practice rules related to surface electrodes positions on different muscle types.

The data need to be stored to permit for further offline processing [28] [24].

### 2. Processing the EMG

This step is fundamental to make suitable the several EMG registrations for the next step of synergies extraction, since a correct acquisition phase is not enough to allow it. The processing consists of the sEMG signal cleaning from everything that is not related to muscle activation and here are included all the disturbs explained in the previous paragraph 2.2.2 [25] [24].

Generally this consists of a *Filtering* operation of the signal, through appropriate instrument called *filters*. Looking at figure 4.3, reports an example of vastus lateralis muscle sEMG cycling activity through the principal phases of processing. The graph (a) shows the raw sEMG signal that is band pass filtered between 20

Hz and 400 Hz in order to limit the correct band of the signal under the 400 Hz and to eliminate the low frequencies disturbs such as motion artifacts, shown in graph (b). Finally, the filtered signal is rectified (c, blue line) and low pass filtered at 10-12 Hz obtaining the envelope shown in graph (c, red line), which represents a smooth and slow curve that delineates the trend of the rectified sEMG signal [24].

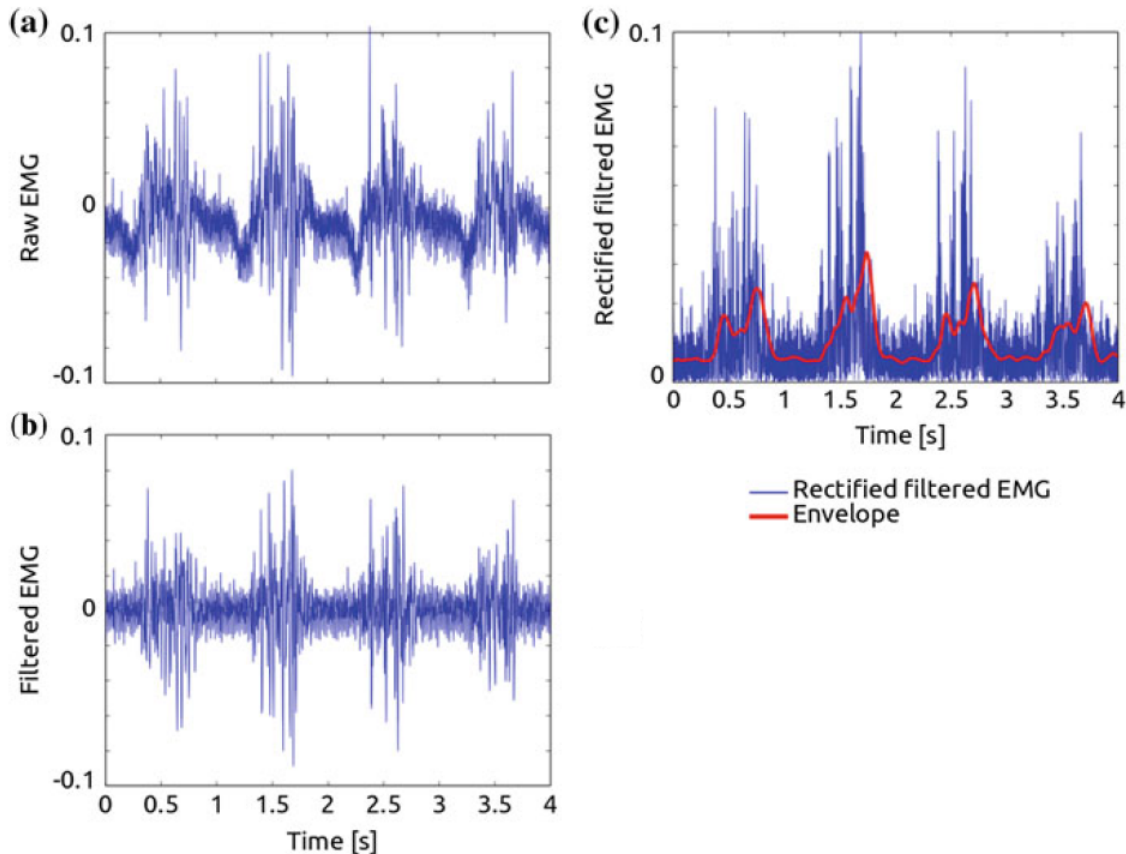


Figure 4.3: Step 2. General processing of sEMG signal. The graph (a) shows the raw sEMG signal that in graph (b) is band pass filtered between 20 Hz and 400 Hz and finally rectified and low pass filtered at 10 Hz obtaining the envelope (c) [24].

### 3. Extraction of Muscle Synergies

The synergies identification is generally attributed to specific algorithms called *Matrix Factorization Algorithms*. Mathematically, the “matrix factorization” is defined as a factorization of a matrix into a product of matrices and in this scope it is used as an assessment tool to verify the hypothesis of representing a complex motor task through a reduced number of muscular co-activations modules named muscle synergies. The number  $n$  of muscle synergies involved in a particular

movement is unknown and it is supposed and it is verified later, it can not be calculated uniquely. Within this category of algorithms there are many that differ for initial assumptions returning various results difficult to integrate. Nevertheless, the best performing algorithms like Factor Analysis (FA), the Independent Component Analysis (ICA), the Non-Negative Matrix Factorization (NNMF), the Principal Component Analysis (PCA) and the Probabilistic Independent Component Analysis (pICA), they return results very similar to one another. All the several methods, despite different assumptions, consider the input data using this model:

$$\vec{x} = \sum_{i=1}^K c_i \vec{w}_i + \vec{\epsilon}$$

where  $\vec{x}$  is a matrix of M-dimensional data vector,  $\vec{w}_i$  is the  $i$ th of K basis vectors also of M dimensions,  $c_i$  represent the scalar activation coefficients for the considered basis vector and  $\vec{\epsilon}$  M-dimensional vector is used to model the noise contribute. From a physiological point of view,  $\vec{x}$  represents the M muscles sEMG signals activity,  $\vec{w}_i$  are the several muscle synergies activated in time by the specific coefficients  $c_i$ . In the following analysis will be used the Non-Negative Matrix Factorization (NNMF) approach [29].

### Non-Negative Matrix Factorization (NNMF)

Once the envelopes are obtained from sEMG signals, they need to be adapted in term of *time samples* obtaining a matrix  $\mathbf{M}$  of  $m$  rows and  $t$  columns, within each single row corresponds to a muscle observation during an activity long  $t$  time samples. The NNMF algorithm factors the  $m$ -by- $t$  matrix  $\mathbf{M}$  into non-negative factors  $\mathbf{W}$  ( $m$ -by- $n$ ) and  $\mathbf{H}$  ( $n$ -by- $t$ ), where  $n$  is the number of muscle synergies. The algorithm proceeds in an iterative way starting from random values for  $\mathbf{W}$  and  $\mathbf{H}$  and minimizing the objective function that is defined as the root mean squared residual between  $\mathbf{M}$  and the obtained approximation  $\mathbf{WH}$  [30]. For a more complete view on mathematical aspects of the algorithm, read [30] or [29]. Matrix  $\mathbf{W}$  contains on its rows the muscle synergies vectors in which each single muscle contribute activity is expressed. Matrix  $\mathbf{H}$  explains information about how the specific synergy is time activated.

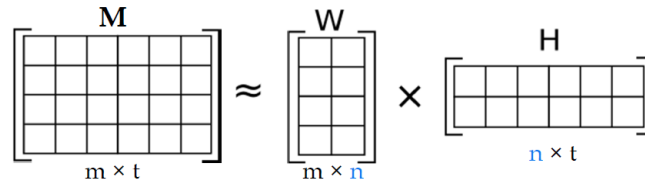


Figure 4.4: Example of Matrix  $\mathbf{M}$  factorization in two smaller matrices  $\mathbf{W}$  and  $\mathbf{H}$ .

The overall process can be resumed in the Figure 4.5.

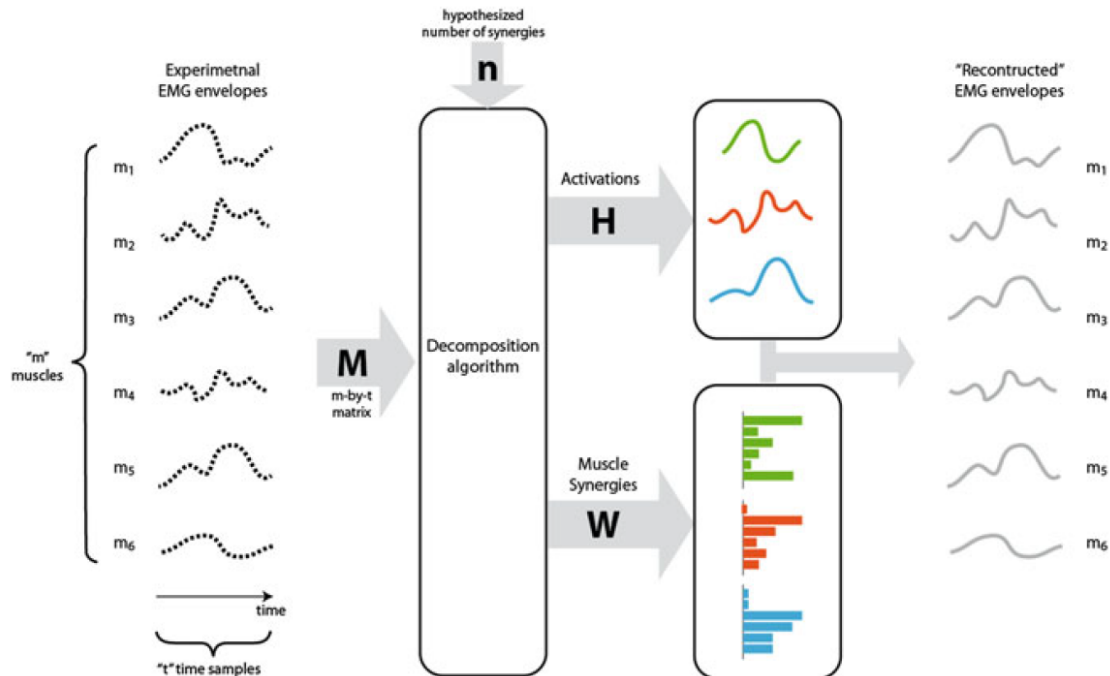


Figure 4.5: Example of Matrix  $M$  composed of six muscle activity envelopes that is factored into two smaller matrices  $W$  and  $H$ , which product can rebuild the original  $M$  matrix [24].

#### 4. Muscle Synergies: Quality Assessment, Results Interpretation and Comparison

As mentioned before, the correct number " $n$ " of synergies can not be found automatically from none of the existent extraction methods. What is carried out to find the better configuration, consists on doing different iterations, each of them with a distinct supposed number  $n$  of synergies and selecting at the end the one that respects a certain selection quality criterion. The most widespread selection criterion is based on calculating the VAF or  $R^2$  value correspondent to each value of  $n$  synergies and choosing the first that satisfy the fixed quality requirements. The two indexes give information about the variance that is accounted for in the reconstructed signals with respect to the original variance. Both VAF or  $R^2$  are limited between 0 and 1 and the extremities respectively mean that the extracted synergies do not represent the most part of the Surface ElectroMyoGraphy (sEMG) variance and that the extracted synergies instead represent the most part of the Surface ElectroMyoGraphy (sEMG) variance [24].

An example of this situation is generally represented on a graph, as shown in Figure 4.6, that is constituted by the number of muscle synergies on its abscissa axis and the percentage value of the chosen indicator on the axis of the ordinates. The selection criterion generally consists of choosing the lower number of synergies that allow to overcome the 90% of VAF or the 85% of  $R^2$  [31].

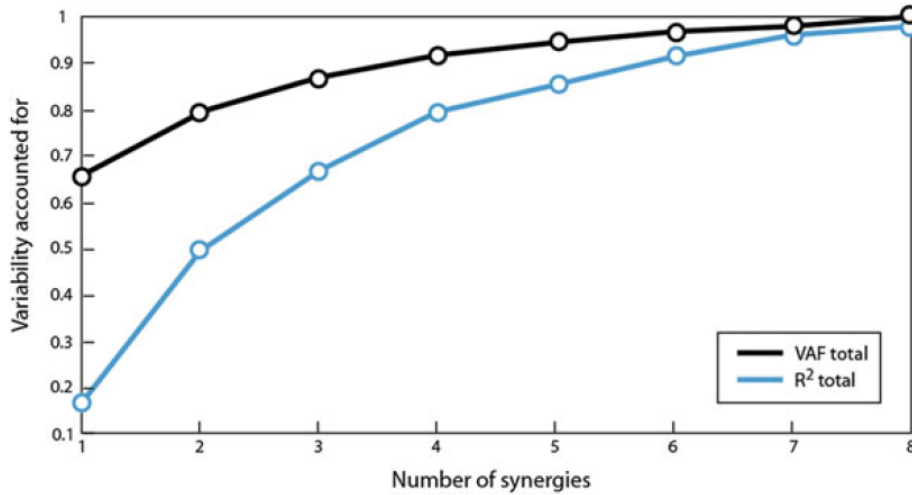


Figure 4.6: VAF/ $R^2$  as a function of the number of extracted muscle synergies [24].

In order to exploit synergies in the diagnostic, rehabilitative or prosthetic control field, it is very important to be able to assess, in terms of quality, the goodness and reliability of the extraction. Even before observing the final extracted synergies, it may be useful to observe and study carefully the envelopes from which synergies are obtained. Referring to envelopes of a generic healthy subject during a particular motor task, this operation can be very useful both in pathologic cases detection and in the interpretation of different movement conditions. The analysis is usually done by visual inspection and the features that are important to check are: the presence of activation peaks, their position and their number, the appearance of abnormalities and the deviation from the average trend. If the interest is to have an higher precision level of time profile shapes correspondence, several mathematical and statistical methods can be used.

After the EMG envelopes analysis, in order to focus on the two main aspects to which the synergies analysis replies, the muscle synergies vectors  $W$  and the associated time activation coefficients profiles  $H$  need to be analyzed.

Referring to a particular motor task, for instance the gait, in order to make an accurate analysis of synergies results, the integration of information and knowledges from other fields like physiology and biomechanics is extremely important. Given

the number  $n$  of computed synergies, it is very important to identify which muscles are mainly activated for each of them and their correspondent time-activation during the motor task, that are respectively expressed by weight vectors in the matrix  $W$  and coefficients in the matrix  $H$ . Starting from these evaluations, the next step requires to contextualize the movement in a physiologic and biomechanic context in order to understand if the extraction is how expected and if the movement conditions are according to what requested.

The operation just described represents the first approach used to evaluate the results goodness and can be defined as visual inspection. A second approach that can be used for quality and quantity assessment is offered by mathematical tools. The operator *Cosine Similarity* allows to compare the similarity between two synergies vectors and the index varies in the range between 0 and 1 respectively for absence of similarity and maximum similarity [32, 33, 34].

$$CS = \frac{W_i * W'_i}{\|W_i\| * \|W'_i\|}$$

The *Cross-Correlation* instead represents the operator par excellence used to evaluate the similarity between two profiles and is used for the activation coefficients, computed with zero lag; in addition it can give information about the delay between two profiles. The index range extends from 0 to 1 respectively for absence of similarity and total similarity [33, 34].

$$CC = \frac{R_{xy}[0]}{\sqrt{R_{xx}[0] * R_{yy}[0]}}$$

### 4.3 Previous Studies

The amount of studies and works regarding the muscle synergies is vast and manifold. Despite it is not an aim of this thesis, a good part of the literature research about the muscle synergies is related to the comparison between different factorization algorithms, in order to compare the performances and highlight the defects between them. In the work called “Matrix Factorization Algorithms for the Identification of Muscle Synergies: Evaluation on Simulated and Experimental Data Sets” published by Matthew C. Tresch, Vincent C. K. Cheung and Andrea d’Avella, the aim was to test the various factorization algorithms both on real and simulated data [29]. The study demonstrated that there were no evident differences, both in terms of number of synergies and identified synergies, between the best main performing algorithms, such as factorization algorithm (FA), Independent Component Analysis (IPA) and Non-negative Matrix Factorization (NNMF). Despite this evidence, the Non-negative Matrix Factorization (NNMF) decomposition algorithm [35] is the most widespread one and it has been followed in the analysis of this thesis.

In [36] there is an important review that summarizes and reports a general overview on the muscle synergies theory application in the specific research fields of clinics, robotics and sport.

While the muscle synergies extraction method has been chosen according to the most used one in literature, i.e. the NNMF, the main aspects, with particular interest on the gait, that have been useful to investigate for the specific application of the thesis are:

- Effect of EMG pre-processing;
- Choice of the number of synergies;
- Muscle synergies during locomotion;

#### **Influence of sEMG Pre-processing**

The several techniques that can be followed during the sEMG pre-processing can determine variability in the muscle synergies extraction.

D. Rimini’s research team, in the publication “Influence of pre-processing in the extraction of muscle synergies during human locomotion” [28], has studied the effect of a new approach of pre-processing, based on CIMAP (Clustering for Identification of Muscle Activation Patterns) algorithm [37], on the muscle synergies extraction. The CIMAP algorithm has the aim to extract, looking at different gait cycles, only the principal activations of the muscles, where with “principals” it refers to activations that are proper requested by the biomechanical functions.

The synergies extraction results provided 5 instead of 6 synergies, which were characterized by purer and stabler synergies weights  $W$  and temporal coefficients  $H$ , maintaining a great reconstruction quality of the original EMG matrix.

Another work by Paulina Kieliba's team [38], has recently investigated how changes in the normalization techniques (maximum voluntary contraction – MVC – or maximum amplitude of the signal - SELF), in the initial band-pass filtering ([20 – 500 Hz] or [50 – 500 Hz]) and in the low-pass filter cut-off frequencies (0.5Hz, 4Hz, 10Hz, 20Hz) influence the muscle synergies extraction. The results have shown that neither the normalization mode, nor the band-pass filtering determine appreciable changes in the synergies extraction, while the low-pass cut off frequency represents the main source of differences in the number of synergies and in the synergies weights muscle contributions. More specifically, the value of the variance accounted for is strongly dependent by it and, generally, have been identified two extremes conditions: very low cut-off frequency, such as 0.5 Hz, determines the signal over-smooth, that causes the false synergies weight increase and the inter-variability rise; conversely, too high low cut-off frequencies, like 20 Hz, provide a signal that is too noise sensible, decreasing, for the same number of synergies, the variance accounted for. This is the reason why, generally, the best solution is represented by a compromise choice between the two extremes; the choice can be moved toward one of them for specific case and with particular aims.

### Number of Muscle Synergies

Generally, the number of muscle synergies is decided by picking the first condition in which the variance index, i.e. Variance Accounted For (VAF) or the Determination Coefficient  $R^2$ , is higher than a certain threshold value, that, usually, consists in 90-95% for the VAF and 80-85% for the  $R^2$  or when the curve slope is approximately flat.

This is what generally happens, but it is not a rule and every research team makes its own choices giving proper and specific justifications.

In the work of Gelsy Torres-Oviedo and Lena H. Ting, named "Muscle Synergies Characterizing Human Postural Responses" [39], the criterion chose to select the number of synergies is made by the application of a double VAF threshold. In particular, it is firstly checked that the  $VAF_{\text{muscle}}$  is higher than 75% and secondly that the  $VAF_{\text{overall}}$  is higher than 90%. With this safer second condition, they assure to be able to represent the original activation of each single muscle.

Another study by D. Rimini, V. Agostini and M. Knaflitz, named "Evaluation of Muscle Synergies Stability in Human Locomotion: A comparison between normal and fast walking speed", the suitable number of synergies is assessed by the calculation of the overall Uncentered Pearson correlation coefficient, i.e.

the  $VAF_{overall}$ , and selecting the first number of synergies that fulfill the condition  $VAF_{overall} \geq 90\%$  [34].

In the work published by Vincent C. K. Cheung's team in [31], the number of synergies is selected when the reconstruction quality of the EMG matrix reaches the condition of  $R^2 \geq 80\%$ .

Finally, another different approach is always proposed by Vincent C. K. Cheung, in which the number of synergies is chosen according to the  $R^2$  curve slope. More particularly, when the curve reaches a *plateau*, i.e. a flat condition, it means that an additional increase in the number of synergies would be useless in terms of variance content [40].

### **Muscle Synergies During Gait**

Thanks to several years of researches trying to assess the best representation of muscles modules during locomotion, today it has been arrived to a common version. It has been demonstrated that, mainly according to the number of recorded muscles and in order to explain all the basic biomechanical functions, are needed and shared across subjects 4, 5 or 6 muscle synergies [33, 34] [42-47]. Generally, the precise number depends on whether the back muscles are included or not in the acquisition.

In the study by Y. P. Ivanenko and R. E. Poppele and F. Lacquaniti "Five basic muscle activation patterns account for muscle activity during human locomotion", it has been considered to extract the muscle synergies during gait for differing speeds and gravitational loads. The results have been extracted from the sEMG signals recording of 12-16 ipsilateral/trunk muscles using factor analysis (FA). It has been possible to demonstrate that 5 muscles modules were enough to account for at least 90% of the variance and this was valid across all the speeds and the gravitational loads. This important result has allowed to confirm that the gait, for different conditions, is always managed by few oscillating circuits [41].

Another analysis has been provided by Evelyn Morin in [42]. Through Non-negative Matrix Factorization decomposition algorithm have been extracted the muscle synergies from 6 lower limbs muscles, i.e. tibialis anterior (TA), medial gastrocnemius (GA), rectus femoris (RF), biceps femoris (BF), adductor longus (AL), gluteus medius (GM) and erector spinae (ES). The analysis has shown that 4 muscle synergies account for a percentage of at least 70% and 5 muscle synergies account for at least 90%. More specifically, considering the case of 5 muscle synergies for the right limb, the first module shows strong activation of the GA, which acts to plantarflex the ankle; the second module is composed by RF and AL and they act in order to stabilize the hip and knee extension. Chronologically, module 1 starts after the activation of module 2. In the third module the actor is the TA together with the RF, which allows both ankle dorsiflexion and the knee

extension in initial swing phase. Module four is mainly represented by BF that act to decelerate the leg at final swing. Finally, in the fifth module the main actors are the TA and the GM that act during the initial stance [42].



Figure 4.7: Example of muscle synergies decomposition computed on 6 lower limbs muscles: TA, GA, RF, BF, AL and GM [42].

Finally, D.Rimini, V.Agostini and M.Knaflitz, in the work described in [33], characterize the gait muscle synergies analysis across more than 180 gait cycles and for 12 healthy subjects. Considering a data set of 12 sEMG signals from dominant lower limb and trunk, they found that all the 12 subjects are characterized by 5-7 muscle synergies. Looking at the synergies weights  $W$  and the temporal coefficients  $H$ , have been calculated both the single subject intra-similarity and the consistency across different subjects. Trough the use of two similarity indexes, i.e. Cosine Similarity (CS) and Zero-lag Cross Correlation (CC), respectively across synergies weights  $W$  and the temporal coefficients  $H$ , has been possible to evidence that 5 muscle synergies are shared across all the subject and that, for each single subject, the average CC and CS show very high similarity and very low standard deviation across all gait cycles subgroups (1 subgroup = 10 gait strides). The 5 muscle synergies correspond to the principals locomotion biomechanical functions.

## Chapter 5

# sEMG Signal Simulation and ATC Testing

Once understood the basis of ATC technique and Muscle Synergies, the ATC role will be now better discussed.

The main target of this chapter consists in the extraction of an ATC signal that is very similar with respect to the traditional sEMG signal envelope. Seeing that the muscle synergies extraction algorithm works receiving in input a matrix made by traditional sEMG signal envelopes, if the similarity between them and the ATC ones is verified, consequently the synergies output should be expected to be very similar as well. Since the last one is obtained after a low pass filter step with generally  $f_c = 10\text{Hz}$ , the traditional sEMG signal envelope has the role of representing the average and smooth muscle behavior during a particular time period. Time support and activation shape are the two most importance features that the ATC signal should reconstruct.

As long as the ATC technique is based on two different parameter, i.e. time window and threshold level, let's now investigate which is the perfect subset of ATC parameters that allows to reach the target.

### 5.1 Approach and Parameters

The answer lies intrinsically in the sEMG content. It has been needed to understand which is the best way to test the ATC parameters as a function of the different sEMG signal characteristics.

The use of simulation is the way that has been considered to assess the applicability of the ATC technique. Indeed, the use of simulate sEMG signals allows to have the total control of all the parameters combinations (SNR, Frequency Range,

Burst Activity etc.) that can be used to study and test the ATC technique. In order to assess and quantitatively evaluate the similarity of the ATC output with respect to the traditional one, a proper indicator will be exploited. As a last step, a sensitivity analysis will be carried out that explains how the similarity indicator value changes according to the simulation parameters modifications.

### 5.1.1 Simulate sEMG Signal Generation

The following procedure will be explained with the aim of generating a simulated version of sEMG signal that allows to test the ATC technique for different conditions of signal to noise ratio (SNR), frequency content, shape and temporal support of the burst of activity [43].

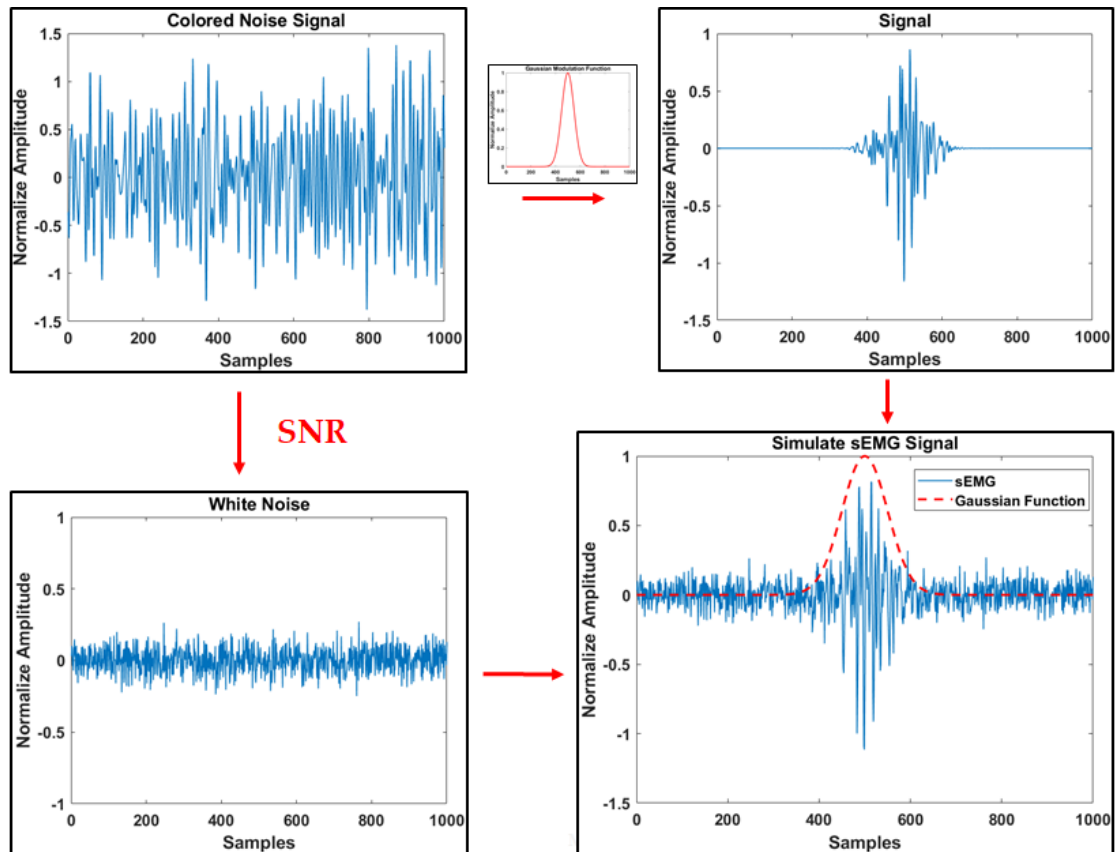


Figure 5.1: sEMG signal simulation overall process: starting from the colored noise in the top left subplot, in the bottom left is obtained the white noise signal, while in the top right is obtained the pure signal by multiplying the colored noise for a Gaussian function. Finally, in the bottom right the summation brings to the final simulate sEMG signal.

The first step is represented by the creation of a white noise signal of a certain power. In accordance with the frequency content of interest for simulating the sEMG signal, the white noise signal is filtered using a 4th order Butterworth band-pass filter. This type of filter is particularly suitable for the sEMG signal since it is characterized by a maximally flat response in the transmission band and minimum ripple in passband, i.e. amplitude linearity in passband [44].

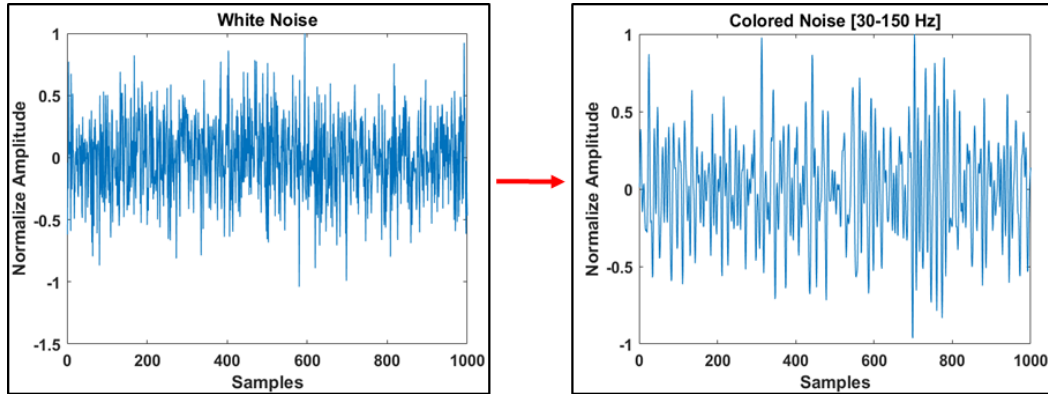


Figure 5.2: Step 1: Colored noise signal extraction.

The frequency content has been set within the lower limit of 30 Hz and the higher limit of 150 Hz, considering that band as informative of the most of the power of the Surface ElectroMyoGraphy [6]. In the Figure 5.2 is reported an example of the current step.

In the second step, according to a desired SNR value, starting from the power of the colored noise signal is generated a new white noise signal that will represent the noise part in the final sEMG.

The calculation of the noise power is obtained reversing the following formula:

$$SNR_{dB} = 10 * \log (P_s / P_n)$$

The choice of the SNR values has been done trying to account both for very bad and very good acquisition conditions and the values considered are 0 dB, 5 dB, 10 dB, 15 dB and 20 dB. Generally, the acceptability level is to have a level that is higher than 10-15 dB.

On the other hand, the colored noise is multiplied by a Gaussian modulation function that allows to model the burst of activity [45]. Through the use of that specific function is possible to simulate the gradual sEMG activation due to the successive recruitment of different motor units and the dimension of the temporal

support of the activation.

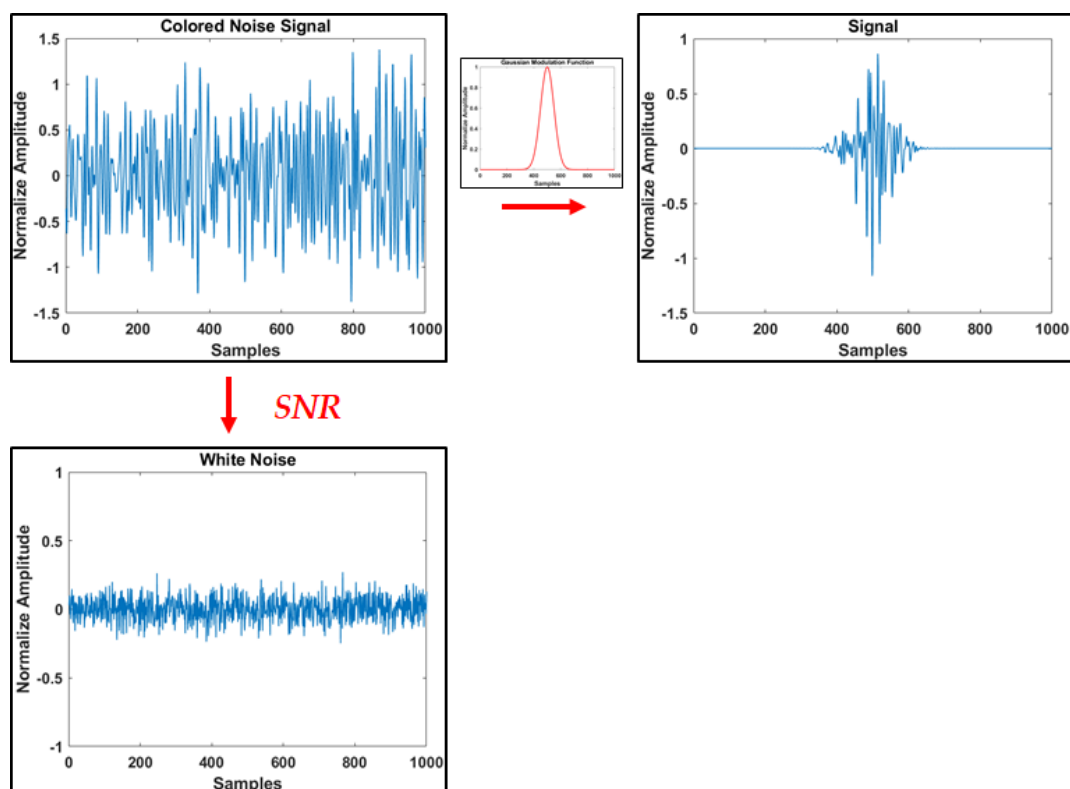


Figure 5.3: Step 2: Pure noise and pure signal components generation.

Particularly, the shape is controlled by a specific parameter of the Gaussian,  $\sigma$ . The values chose for this parameter are 10 ms, 25 ms, 50 ms, 75 ms and 100 ms. Considering an interval around the mean (50% of the signal) of  $\pm 3\sigma$ , the temporal support is spread from a minimum length of 60 ms to a maximum length of 600 ms, covering the most of the sEMG activity of the different muscles.

Finally, the last step is characterized by the summation of the white noise signal and the pure burst of activity both generated at the step 2, obtaining the final sEMG signal that is show in the example in Figure 5.4. In the process just explained the SNR is defined before the application of the modulation function; this allows to obtain a final signal in which the peak to peak amplitude ratio between signal and noise is constant across all the different  $\sigma$  conditions. Another possibility may have been to multiply first for the modulation function, compute the power of the extracted signal and consequently generate the noise using the same formula reported above. The last approach, equally correct, provides a simulate sEMG signal in which the amount of noise is dependent on the different

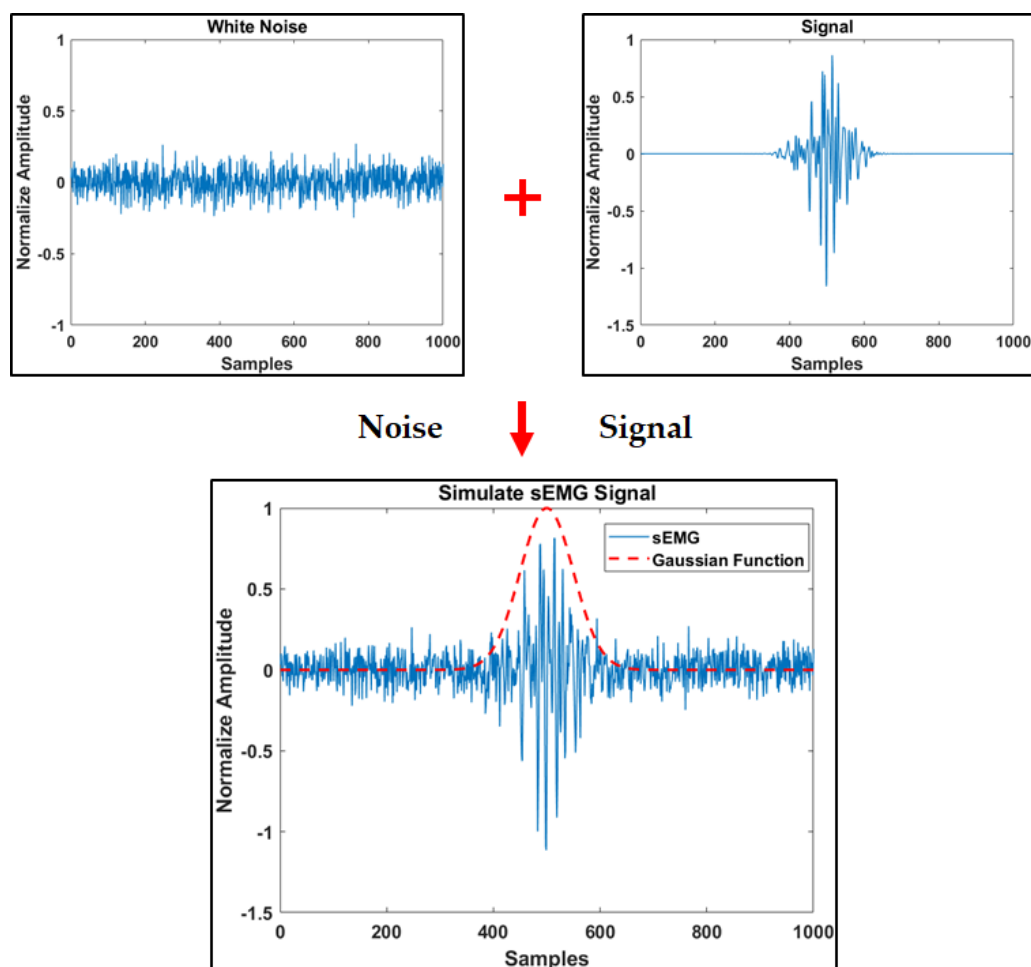


Figure 5.4: Step 3: Example: Final sEMG signal generation, 10dB.

temporal support  $\sigma$  imposed. Since the study aim to find the best threshold and time window for the ATC technique, the first approach has been selected.

### 5.1.2 ATC Parameters

The ATC is characterized by two main parameters:

#### 1) Threshold Level

The values of the threshold is computed channel by channel multiplying the respective ARV value for the particular threshold level selected. In this way the position is dependent on the amplitude of each single channel. The values extend from 1.2 up to 3.2 with an increment of 0.4. The range has been chosen looking at the simulate sEMG signals in order to set the threshold in different positions,

starting lower with respect to the baseline noise and including different levels up to an higher point.

In the Figure 5.5 is reported an example that shows two different conditions of threshold level, i. e. 1.2 and 2.4. It is possible to notice the expected behavior

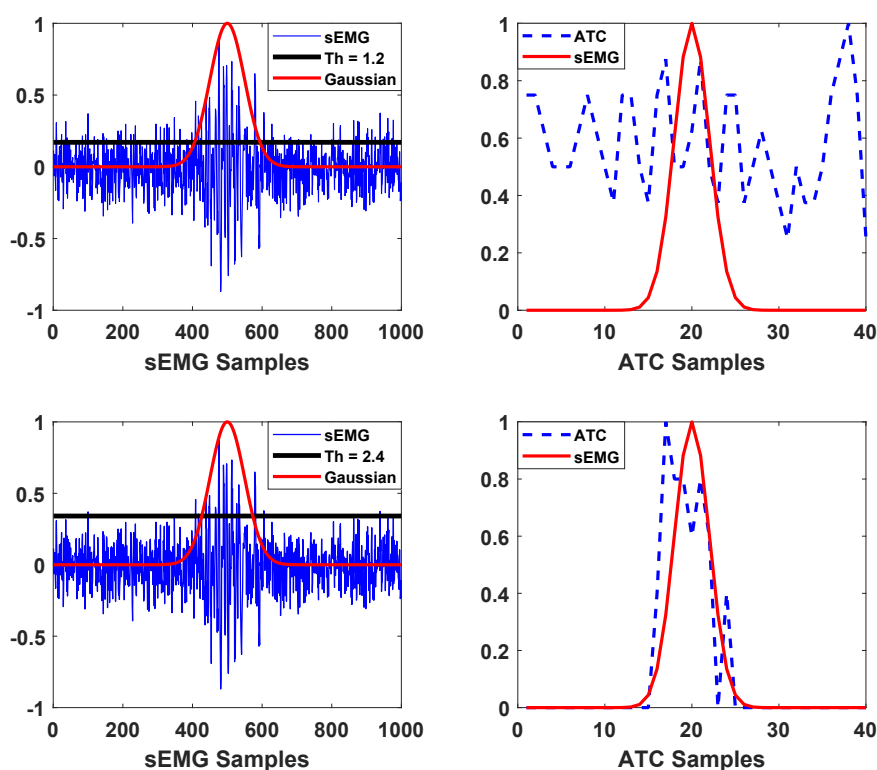


Figure 5.5: Example: Threshold level = 1.2; Threshold level 2.4 on a sEMG signal with SNR = 10dB,  $\sigma = 50\text{ms}$  and Time Window = 50ms.

in which for different heights of the threshold, different noise contributes are accounted for in the ATC signal. The minimum acceptably threshold level is related to the SNR.

## 2) Time Window

The choice of the time window has been done considering several aspects:

- Number of TC events;
- Time Resolution;
- Latency Time;

The number of TC events is related to the number of levels that the ATC signal uses to reproduce the traditional sEMG envelope. Lower is this value, higher is the difficulty in the reconstruction. Therefore, for a low number of TC events there is an amplitude quantization phenomenon.

With latency, it refers to the amount of time that is needed to wait in order to have information about the ATC value of that time window.

The time resolution gives information about the precision of a measurement with respect to time. In this work it is related to the size of the time window that has been chosen to count the number of TC events, through which the ATC signal is generated. The time resolution value is set to 25 ms and the choice is justified from two observations:

1. Assuming a time window of 25 ms the number of TC events is between 1 and 3; it would be useless to consider shorter values respect to 25 ms for the reason why two adjacent time windows could account for the same information.
2. Since in this study the ATC technique will be applied specifically for the gait muscle synergies analysis, assuming an average gait cycle length of 1 s for healthy subjects and known that an acceptable time resolution is generally 5% of that length, 25 ms satisfies this requirement (2.5%).

Starting from this assumption, have been considered the following values of time window: 25 ms, 50 ms, 80 ms, 100 ms, 125 ms and 200 ms with an overlap respectively of 0%, 50%, 69%, 75%, 80% and 88% in order to keep the time resolution fixed at 25 ms.

In the Figure 5.6 is reported an example that shows two different conditions of time window, i. e. 50 ms and 200 ms.

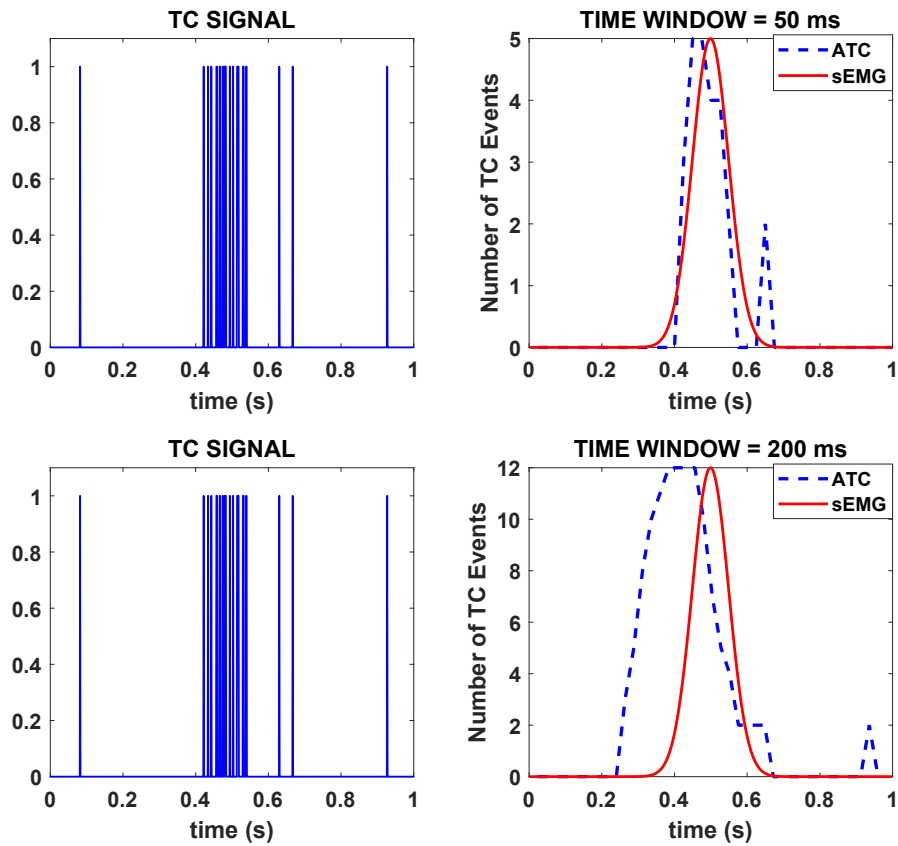


Figure 5.6: Example: Time Window = 50 ms; Time Window = 200 ms on a sEMG signal with SNR = 10dB,  $\sigma = 50\text{ms}$  and Threshold = 2.4

Looking at the example, it is possible to observe that the results are pretty diverse when are considered two different time windows. Taking into consideration a  $\sigma$  of 50ms, the result that comes with a bigger value of time window, like 200 ms, consists of an anticipated and spread over time ATC Signal. With 50 ms instead the result is more similar to the original one.

Briefly summarizing, have been considered two different categories of parameter; the first one regards the simulation of the sEMG signal and includes SNR and Sigma, while the second one refers to the extraction of the ATC signal, in which are included the threshold level and the time window.

## 5.2 Methods

Will be now discussed the way that has been followed to run the simulations and will be also introduced the indicator chose to assess the similarity between the two curves, i.e. the Gaussian function and the corresponding ATC signal.

### 5.2.1 Output Similarity Index

The output of the algorithm is represented by the calculation of the *Determination Coefficient*  $R^2$  between the Gaussian function, which is used to represents the original activation, and the ATC signal, that has been extracted from the same sEMG activation.

$R^2$  is a very stringent criterion because it evaluates both shape and magnitude between the two curves.

Mathematically the  $R^2$  index is defined as  $100 \times \text{Standard Pearson Correlation Coefficient}$ , in which the total sum of squares is taken with respect to the mean value of the original signal  $y$ . The formula is the following:

Where  $y_i$  represents the original activation, i.e. the Gaussian function, and  $\hat{y}_i$

$$R^2 = 1 - \frac{SS_{RES}}{SS_{TOT}} = 1 - \frac{\sum_i (y_i - \hat{y}_i)^2}{\sum_i (y_i - \bar{y})^2}$$

Figure 5.7:  $R^2$  formula [46].

represents the ATC signal.

The meaning of the similarity indicator  $R^2$  is to express how much of the original signal variance is explained in the reconstructed one. In the formula above, the ratio is composed by the nominator  $SS_{res}$ , that stands for "Sum of Squares of Residuals", and by the denominator  $SS_{tot}$ , that means "Total Sum of Squares". The last two expressions account respectively for the sum of the squares of the deviations calculated between the original and the reconstructed signals and for the proportional to the variance of the data [46].

For a good condition of similarity the  $R^2$  must be close to 1.

In this work the threshold value is set at  $R^2 \geq 85\%$ , pretty high because the ATC signals will then be used to model the muscle synergies. Since the target is to get very high similarity between the two output, it is important to start from a very close situation. In order to have the same length in term of number of samples, the Gaussian function has been sub-sampled.

## 5.2.2 Simulation Setup

The simulations have been run exploring all the parameters combinations and computing the  $R^2$  between the two signals in two different ways:

1. **Single Repetition:** From each parameters combination has been simulated one single repetition of the sEMG signal, from which has been extracted the correspondent ATC signal. This approach has been called "Single Repetition".

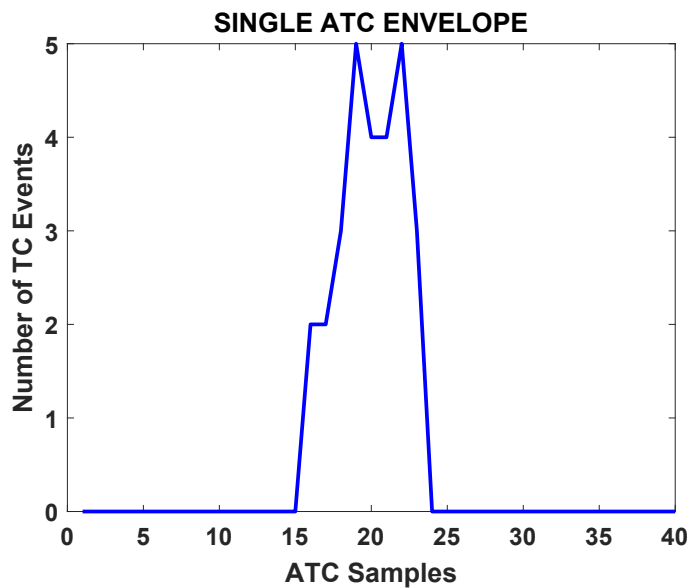


Figure 5.8: Single repetition, ATC signal.

2. **Multiple Repetitions:** From each parameters combination have been simulated multiple repetitions of the sEMG signal and from each of them has been extracted the correspondent ATC signal. The final ATC curve is obtained averaging between the multiple ATC signals extracted from the multiple repetitions of the same sEMG signal. This approach has been called "Multiple Repetitions".

As it is possible to notice watching at the two Figures 5.8 and 5.9, the single repetition approach is characterized by an high component of variability from one repetition to the other. This is justified by the stochastic nature behind both the sEMG signal definition and, as a consequence, the ATC technique. Indeed, the number and the position of the TC events is a function of the sEMG signal behavior.

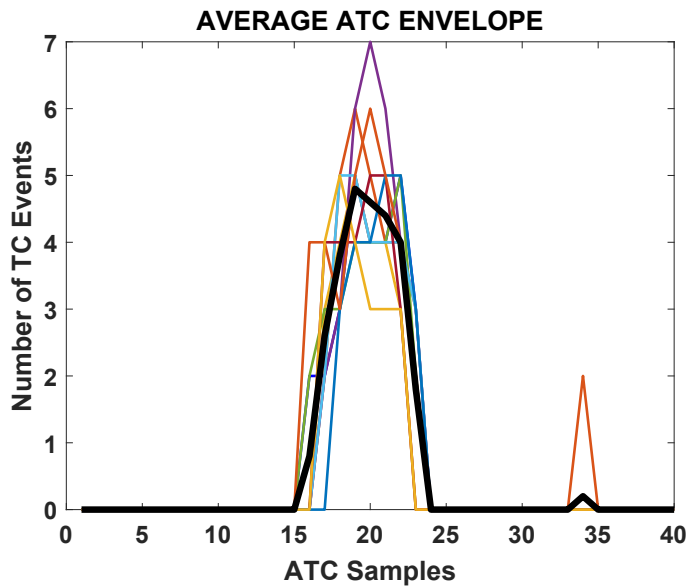


Figure 5.9: Multi repetitions, ATC signals and average ATC curve in black.

Looking at the multiple approach, this effect is reduced thanks to the average operation, that acts as a low pass filtering and allows to return a curve that is smoother and more similar with respect to the original Gaussian function.

Regarding the output index, on the single repetition side, the  $R^2$  has been computed for each parameters combination and it quantitatively assesses the similarity between a single sEMG signal repetition, model by the Gaussian function, and the correspondent ATC extraction.

On the other side, the  $R^2$  allows to evaluate the similarity between the same Gaussian function and an average ATC signal that has been obtained averaging between multiple repetitions.

Since the algorithm has an intrinsic stochastic component, each single simulation has been run multiple times in order to characterize the distribution of  $R^2$ .

The number of iterations is set to 1000. From a statistical point of view, the latter has been considered sufficient basing on the *Central Limit Theorem* [46]. The last mentioned claims that in particular cases it is possible to approximate the mean and the standard deviation of the population through the use of the mean and the standard deviation of the sample.

Since the number of occurrences is higher with respect to 30, even if the sample doesn't have a Gaussian distribution, it is possible to define both for the mean and the standard deviation of the sample a confidence interval with a certain

confidence level [46].

It has been verified that, selecting niter = 1000 and referring to the multiple repetitions approach, the mean of the population is approximated by the mean of the sample (for the parameters combination in which  $R^2_{\mu} \geq 85\%$ ) with a confidence interval  $< 0.6$  and characterized by a confidence level of 95%.

### 5.3 Simulations Results

The results will be now shown separately for the two approaches, i.e. single and multi repetitions, highlighting the differences between them.

The purpose of the simulations has been to allow to find the best combination of the ATC parameters (Time Window and Threshold level), that works well across the most of the sEMG signal characteristics (SNR, Frequency Range, Burst Activity etc.).

Ideally, the perfect results should show, for certain ATC parameters combinations, an high  $R^2_{\mu} \geq 85\%$  value across all the SNR and  $\sigma$  conditions.

Let's start the analysis considering first the average value of  $R^2_{\mu}$  obtained across all the iterations of the algorithm. This first operation allows to skim the results, showing the parameters combinations that are giving better results. In a second moment, the parameters combinations that have given the best results in terms of  $R^2_{\mu} \geq 85\%$ , will be analyzed paying attention to the distribution of the index across the different iterations.

#### Single Repetition

In the Figure 5.10 are reported all the  $R^2_{\mu}$  values that derive from all the parameters combinations. The plots show the behavior of  $R^2_{\mu}$ , whose values are on the y axis, as a function of the two ATC parameters, i.e. time window and threshold. The values of the threshold level are on the x axis, while there are six different subplots corresponding to the six values investigated for the time window.

The Figure 5.10 has been obtained for a SNR of 10 dB and it generally represents the minimum Signal to Noise ratio condition that allows to deal and process with a biological signal like the sEMG. For SNR values of 15 or 20 dB the situation is very similar and their figures have been discarded, while for SNR values of 0 and 5 dB the situation is even worse and has not been reported.

It is possible to notice that, differently from the ideal situation cited previously, none of the subplots is characterized by an ATC parameters combination whose location of  $R^2_{\mu}$  is above the 85% threshold of acceptability.

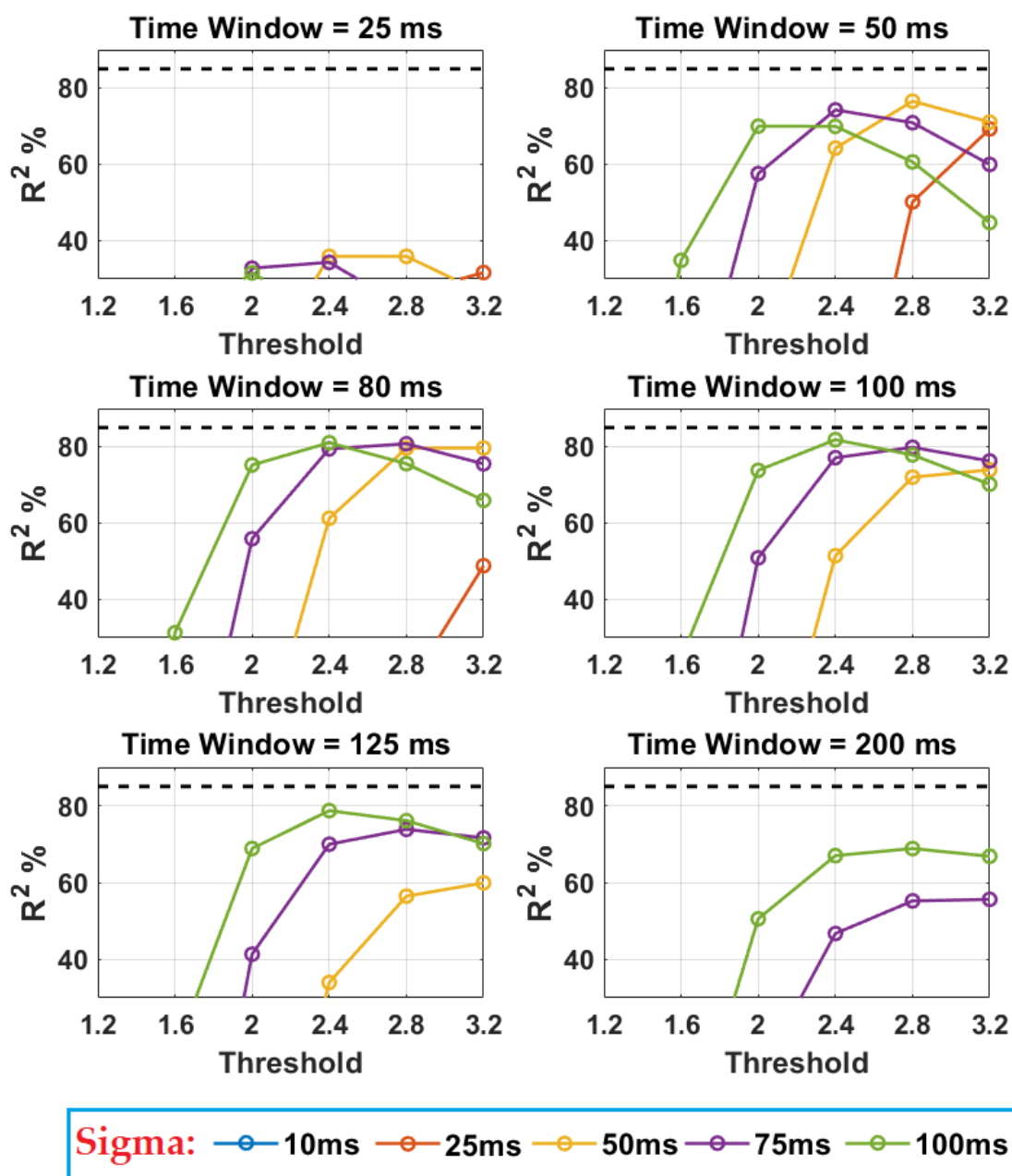


Figura 5.10: Results: Single repetition,  $R^2_{\mu}$ , SNR = 10dB.

The combination that is closest to that condition corresponds to Time Window = 80 ms and Threshold Level = 2.8, in which three curves marked by values of  $\sigma$  50 ms, 75 ms and 100 ms approach to  $R^2_{\mu} = 85\%$ . However this condition is not acceptable and disagree with the desired results. To further support this, it

has also been reported the distribution of  $R^2$  in the figure 5.11.

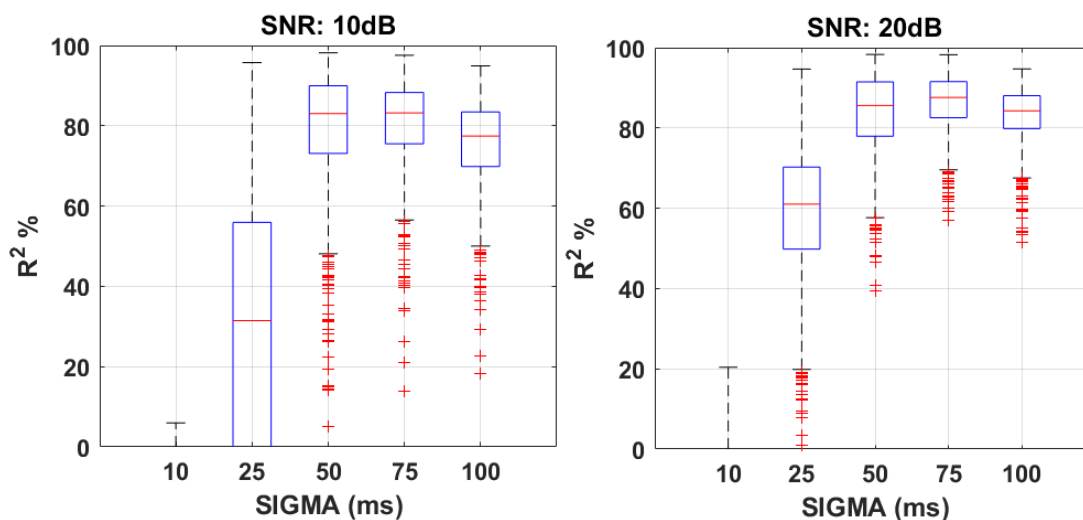


Figure 5.11: Results: Single repetition,  $R^2$  distribution, SNR = 10dB.

Looking at the  $R^2$  distribution for Time Window = 80 ms and Threshold Level = 2.8, SNR of 10 and 20 dB, it is possible to observe that both the boxes are never above the 85% threshold and they are spread over large  $R^2$  intervals, with plenty of outliers, making them not reliable.

### Multiple Repetitions

The situation is much different and pretty better when referring to multiple realizations.

As previously explained, in the Figure 5.12 are reported all the  $R^2_{\mu}$  values that derive from all the parameters combinations. The plots show the behavior of  $R^2_{\mu}$  on the y axis, as a function of the two ATC parameters, i.e. time window and threshold level. The values of the threshold level are respectively on the x axis, while there are six different subplots corresponding to the six values investigated for the time window.

Assuming a SNR of 10 dB, the first notable aspect looking the Figure 5.12 is that there are some curves which exceed the  $R^2$  acceptability level. Since the ideal target is to have all the  $\sigma$  curves that exceed the 85%, focusing on the specific subplots, the attention falls in the one marked with time window = 50 ms. In this particular case, for the most of the  $\sigma$  values, except  $\sigma = 10$  ms, the condition is

satisfied. The latter happens in the precise ATC parameters combination of time window = 50 ms and threshold level = 2.8.

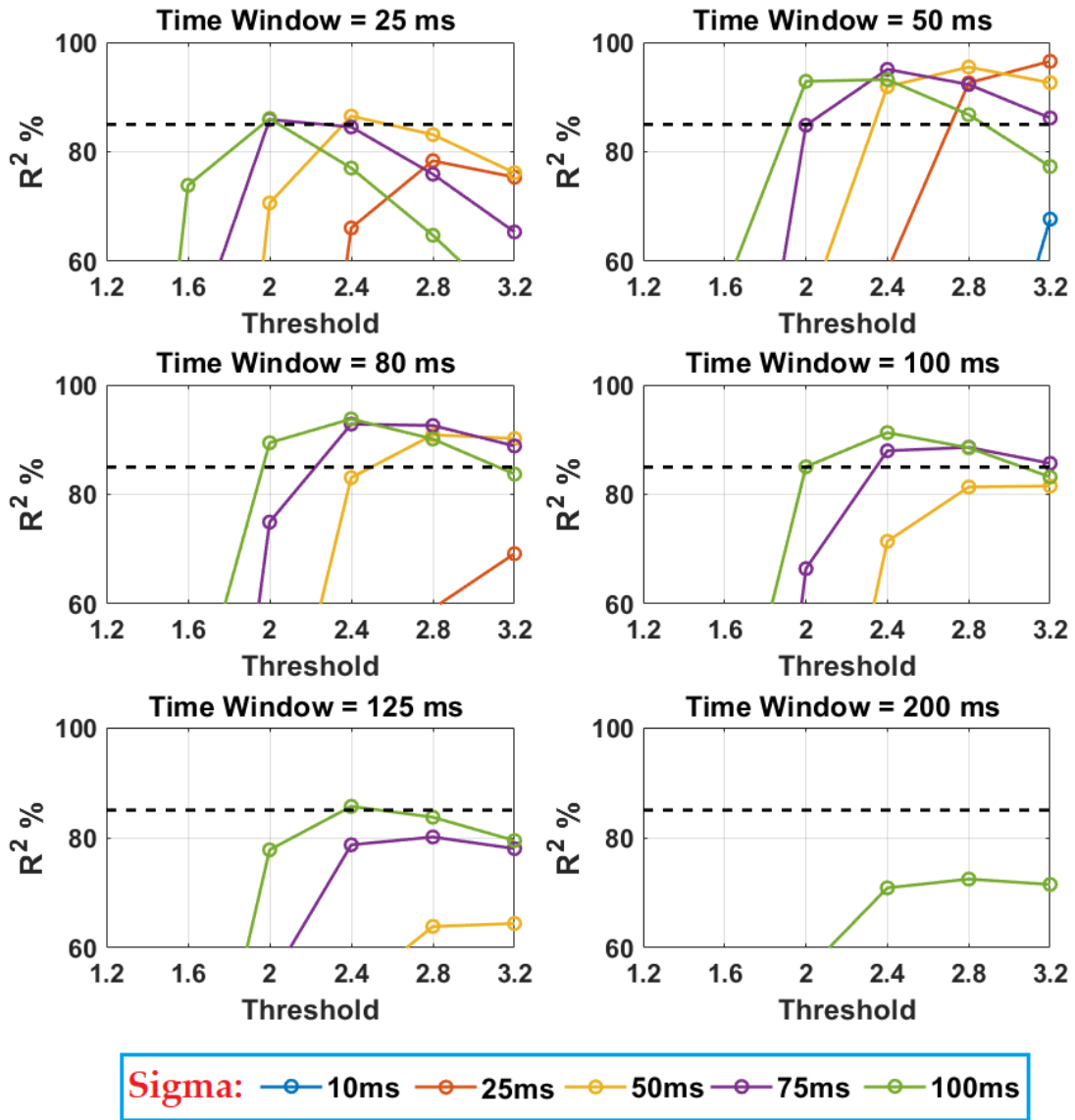


Figura 5.12: Results: Multi repetitions,  $R^2_{\mu}$ , SNR = 10dB.

In order to evaluate the repeatability of the results, let's now consider the  $R^2$  distribution in the specific case of time window = 50 ms and threshold level = 2.8.

In the Figure 5.13 there are four different subplots that represent four condition of SNR with these values: 5, 10, 15 and 20 dB. The distribution of  $R^2$  is shown as a function of  $\sigma$  and in according to the best ATC parameters combination that has been found above, i.e. threshold level = 2.8 and time window = 50 ms.

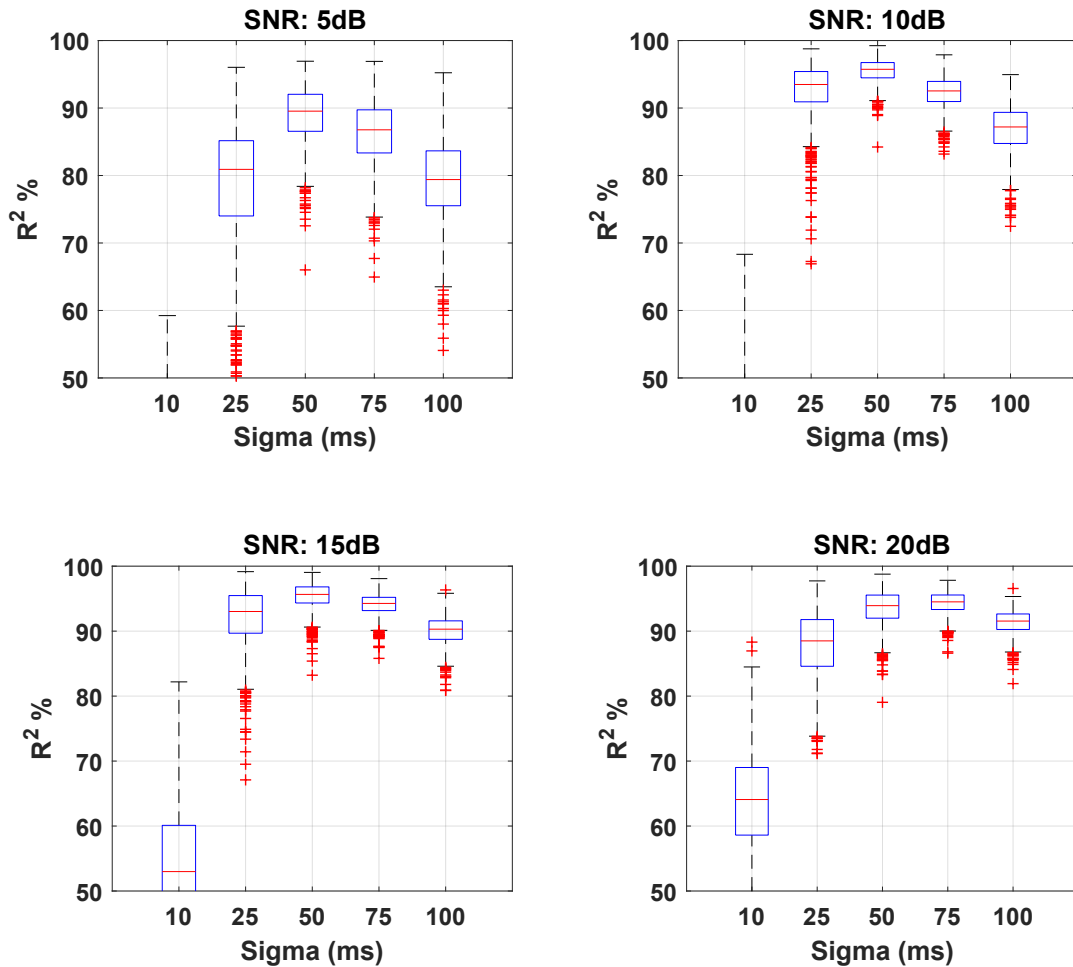


Figure 5.13: Results: Multiple repetitions,  $R^2$  distribution, SNR = 10dB.

The main important aspect to notice is that the  $R^2$  boxes are above the 85% level from SNR = 10 dB up to 20 dB and this happens for all the values of  $\sigma$  except 10 ms. Both the whiskers and the outliers are much more contained than in the case of the single repetition approach.

Merging these considerations, it is possible to conclude that the ATC technique is working well and with a high reliability when it refers to values of  $\sigma$  from 25 ms to 100 ms and starting from a SNR of 10 dB. Differently, for values of SNR that are lower than 10 dB or for  $\sigma$  values that are lower than 25 ms, the boxplots show a behavior that is not acceptable.

## Observation

Thanks to the average across multiple realizations, the performances of the ATC technique are much improved. The average operation has mainly affected the results in two ways:

1. The number of TC events after the sum across multiple realizations is less affected by the amplitude quantization problem.
2. The variability that characterizes each single repetition is pretty reduced.

Concluding, the simulations has allowed to understand that through the ATC approach is possible to obtain a signal which is very similar to the sEMG traditional envelope, here modeled by the Gaussian function, only when it is extracted considering the mean across multiple realizations of the same EMG activation. This reduces the applicability to repetitive movement, like gait, or can be also exploited in rehabilitative protocols to assess the ability of a certain patient to execute a particular motor task multiple times.

## Number of Repetitions Influence

The choice of 10 repetitions, that has been considered to run the simulations, derives from a previous analysis.

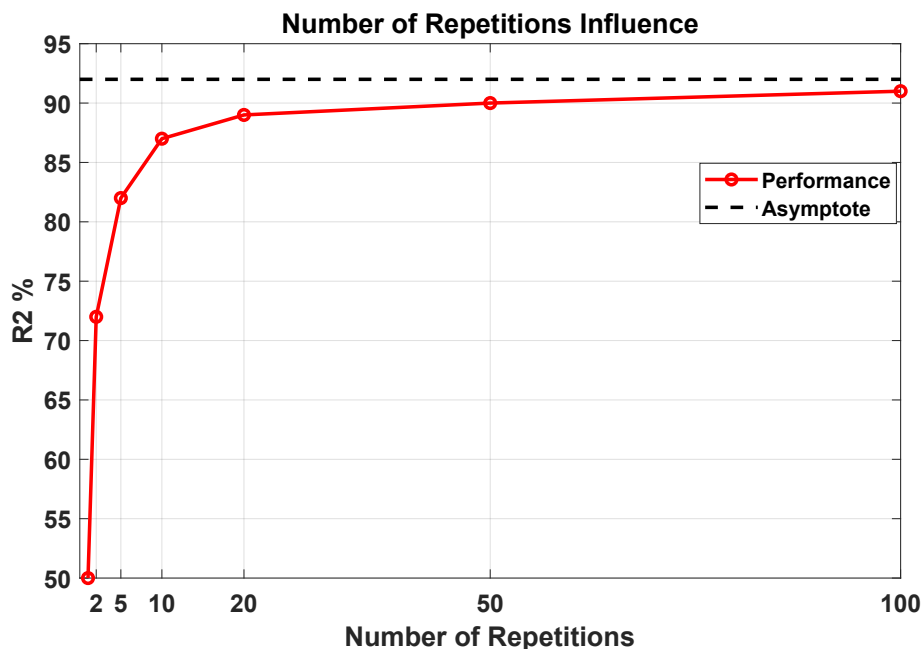


Figure 5.14

In fact, looking at the Figure 5.14, the analysis consisted in comparing the performances of the simulations results obtained changing the number of repetitions and considering the values of: 1, 2, 5, 10, 20, 50 and 100. The  $R^2$  value refers always to the minimum condition of  $\sigma$  curve for the best ATC parameter combination (time window = 50 ms and threshold level = 2.8) that is higher with respect to the  $R^2_{\text{overall}} = 85\%$  threshold.

From the figure it is possible to notice that 10 repetitions represents the first value that satisfies the 85% acceptability criterion when it refers to the  $R^2_{\mu}$  and it also represents the first condition that allows to have the desired condition in term of  $R^2$  distribution previously explained.

In addition, for the number of repetitions choice, has been also considered and kept in mind that it would be great to have a number that is suitable for online applications, where with “online” it means that it should be processed within a short period of time that is consecutive to the data collection and that is compatible with the specific application in which it is used.

## Chapter 6

# ATC-based Muscle Synergies Analysis

The concept of “Muscle Synergies” has been mostly investigated during the last twenty years, as a way to better grasp the approach used by the brain to simplify the control of the body muscles complexity. The hidden strategy behind the synergy idea is founded on the fact that during a particular movement, like the gait, which involves the cooperated activity of an high number of muscles, the CNS does not control separately and directly each single muscle, but these are merged and controlled together in modules, named *muscle synergies*. Therefore, the muscle activation information can be considered as split in two different components, i.e. the synergies weights  $W$  and the temporal coefficients  $H$ . These last provide respectively information about the quantitative contribute of each muscle inside each different muscles module and about how the specific muscles module is activated during a period of time. For a more specific explanation referring to chapter 4.

The usefulness of the muscle synergies analysis is vast and manifold. The main applications regard the neuromuscular motor diagnosis, but it can also be exploited to follow an easier approach to control robotic prosthetic devices. Since clinicians’ tests up to now are mostly concentrated on kinematics and force measures assessment, this approach can offer them information about either neural strategies for movement, previously not considered, and functional outcomes of muscle activity [47].

In this context, the results obtained from the simulations in the previous chapter together with the important advantages offered by the ATC technique in the sEMG signal acquisition and processing, have aroused a strong curiosity and interest on the ATC application in the muscle synergies environment.

In addition to the ATC advantages already introduced in chapter 3, an ATC-based muscle synergies analysis approach could also offer:

- Drastic reduction of the number of samples in the NNMF input matrix.
- Decomposition time much faster.
- Possible real-time/online application.

In this chapter will be analyzed the comparison between the output of the muscle synergies decomposition obtained differently from the Traditional approach and the ATC-based one. The analysis will be done on real sEMG signals and will focus on the similarity assessment between the outputs of the synergies extraction, that are the synergies weights  $W$  and the temporal coefficients  $H$ .

## 6.1 Materials and Methods

The overall process is shown in Figure 6.1.

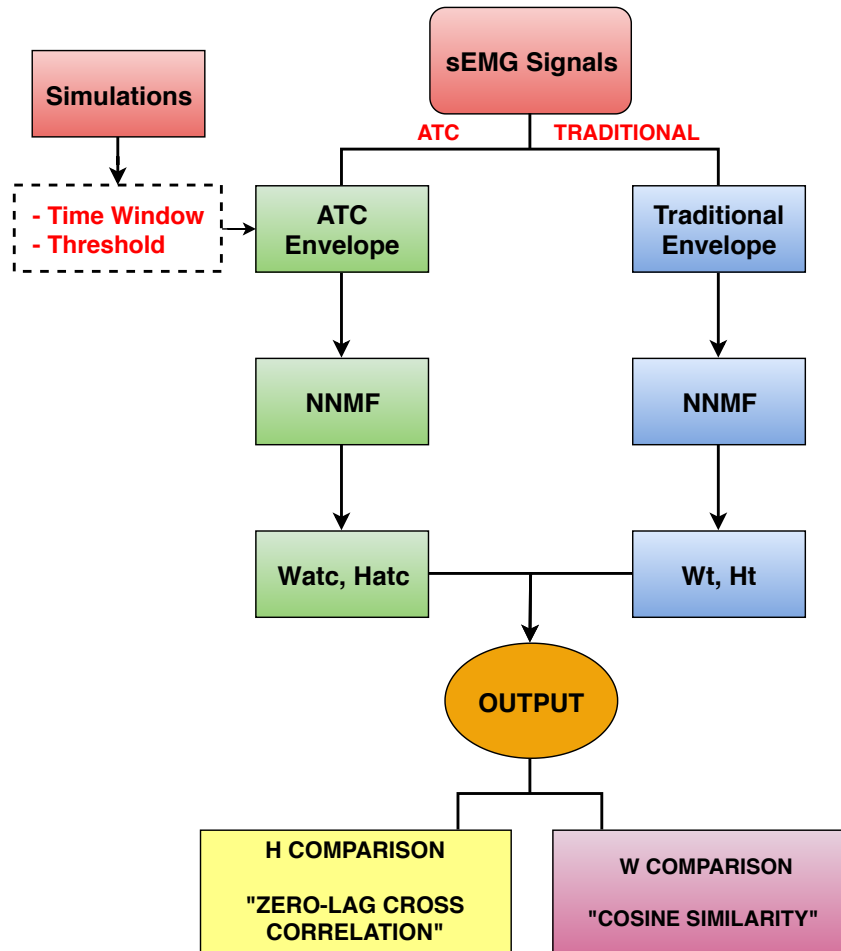


Figure 6.1: Overall high level blocks diagram that shows the comparison process between traditional-based and ATC-based synergies extraction.

Looking at the Figure 6.1, it represents the blocks diagram that explains the general approach followed to compare the two methods. With “Traditional” it refers to the standard method nowadays mostly used to extract the muscle synergies, discussed in the chapter 4. With “ATC” it refers to the muscle synergies analysis based on the sEMG envelopes obtained with the ATC technique.

It is possible to notice that the two approaches differ only for the method used to extract the sEMG envelope, while all the other blocks are the same.

Let's now separately explore each single arm of the overall blocks diagram. In the Figure 6.2 the traditional arm is shown more in details. Starting from the raw sEMG data acquired by a subset of muscles, the traditional envelopes are computed through the use of a low band-pass filter, characterized by  $f_c = 10\text{Hz}$ . The NNMF algorithm receives then in input the number of synergies, which is set previously, and the EMG matrix, made by the different muscles envelopes.

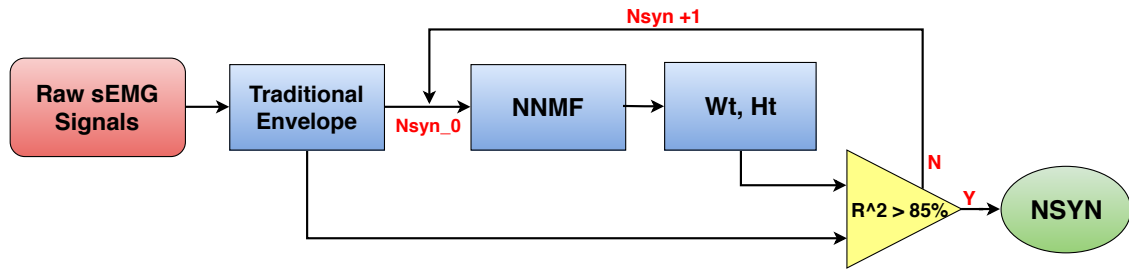


Figure 6.2: Blocks diagram that shows the traditional-based synergies extraction process.

The NNMF decomposition algorithm acts iteratively increasing the number of synergies until the moment in which the quality of the reconstructed sEMG envelopes, with respect to the input ones, satisfies the criterion  $R^2_{\text{overall}} \geq 85\%$  [31]. The  $R^2_{\text{overall}}$  is calculated as the mean between the different  $R^2_{\text{muscle}}$ . In reality, it has been also considered a second threshold in the assessment of the correct number of synergies, verifying that for each single muscle  $R^2_{\text{muscle}} \geq 70\%$ .

In the Figure 6.3 the ATC arm is better analyzed.

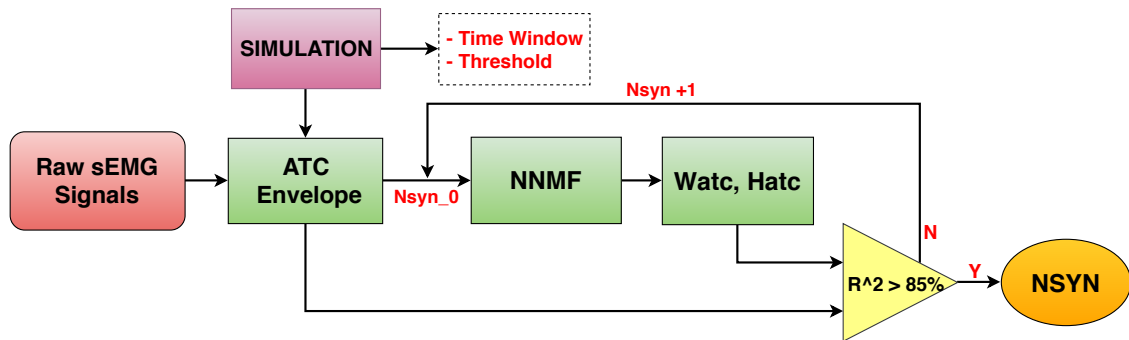


Figure 6.3: Blocks diagram that shows the traditional-based synergies extraction process.

Using a second  $R^2$  threshold on the single muscle allows to avoid situations in which, despite the  $R^2_{\text{overall}} \geq 85\%$ , there are muscle with a  $R^2$  value that is very low.

The ATC-based synergies extraction process starts from the same raw sEMG data, that are now used to compute the ATC envelopes. Considering each single

muscle, on the raw sEMG is defined a threshold that allows to extract the TC signal. Finally, through the sliding of a particular time window on the TC signal, it is possible to count the number of TC events for each of them and define the ATC envelope. In this process have been discarded the time windows in which has been counted just one single event. The latter procedure is graphically shown in the Figure 6.4 for the particular case of the medial hamstring. Once the matrix

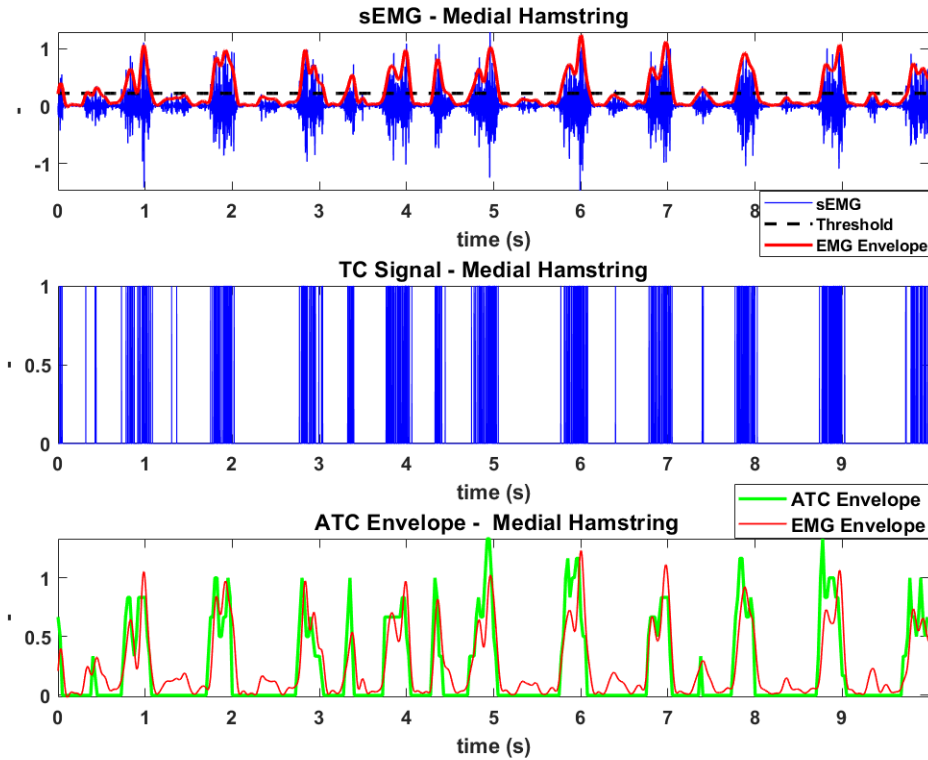


Figure 6.4: Procedure to extract the ATC envelope from the raw sEMG.

made by all the ATC envelope is all set, it is given together with the initial number of synergies as input in the NNMF algorithm. Following the same approach introduced previously, the NNMF decomposition algorithm acts iteratively increasing the number of synergies until the moment in which the quality of the reconstructed ATC envelopes, with respect to the input ones, satisfies the criterion  $R^2_{\text{overall}} \geq 85\%$ . The  $R^2_{\text{overall}}$  is calculated as the mean between the different  $R^2_{\text{muscle}}$ . Also in this case, it has been considered a second threshold in the assessment of the correct number of synergies, verifying that for each single muscle  $R^2_{\text{muscle}} \geq 70\%$ .

Separately, in according to the number of synergies that has been found, both the two methods provide a matrix  $W$  of synergies weights and a matrix  $H$  of

temporal coefficients.

## 6.2 Muscle Synergies Extraction

The simulations have allowed to contextualize the role of the ATC in the muscle synergies topic and the results have clarified the applicability limits and the boarder in which is possible to use it. In according to this, the number of movements that can be considered to test the ATC in a real condition of muscle synergies analysis is reduced. More particularly, it is only possible to consider periodic motor tasks in order to allow the average operation across multiple realization of the same phenomenon.

Note these premises, it has been chosen to consider the gait cycle. Much investigated, a great amount of studies in literature regards gait analysis and muscle synergies during gait.

The analysis has been run on data collected during gait cycle at Politecnico di Torino by the research group of prof. M.Knaflitz.

### 6.2.1 Gait Cycle Bases

The gait cycle represents the shortest repeatable task during human locomotion and it is generally divided in two main phases: stance and swing. The stance represents the phase in which the foot contacts the ground and usually extends from the 0% to the 60%. The swing phase consists in the phase in which the foot is in the air and generally goes from 60% to 100%. These intervals refer to a healthy subject and the phases alternate for each lower limb [48].

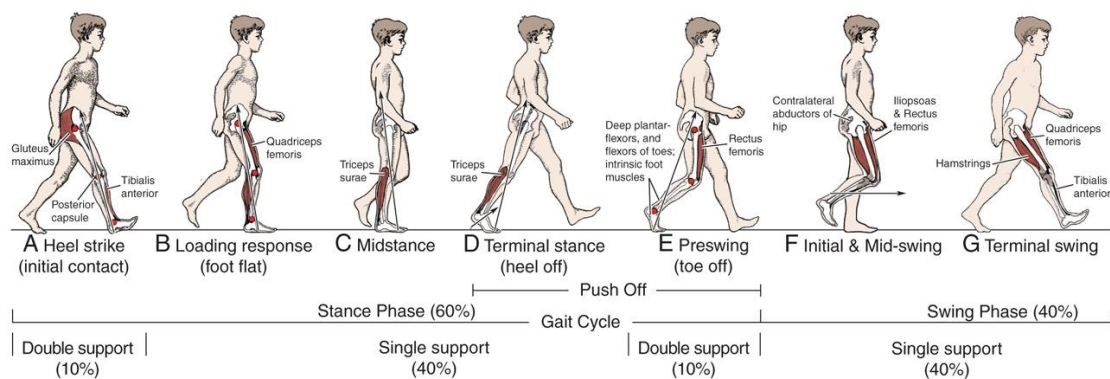


Figure 6.5: Main phases during gait cycle[49].

The Figure 6.5 shows graphically the eight sub-phases in which is possible to divide the gait cycle and the main muscles that act during them. During a cycle the body weight is supported for the 80% from a single limb and the remain 20% by either limbs [48].

The analysis of the gait cycle is important for many reasons, the main are:

- Knowledge of the relationships between the motion control system and the dynamics of the gait;
- Better understanding of the mechanisms that translate the muscular actions of the joints into movements;
- Clinical analysis of pathological situations, in order to identify suitable treatments (therapies, orthoses, surgery, etc.);
- Improvement in sports performance and reduction in the number and severity of injuries.

In order to have a good grasp and to understand the results obtained from the muscle synergies analysis, the interest of this study is more focused on the muscles timing during normal walking. Despite the final goal of the study is to demonstrate the outputs similarity between the ATC and the traditional approach, it is important to know what to expect from the analysis. More details about the gait analysis can be found in [48].

In the Figure 6.6 are qualitatively resumed the main muscles of interest that are recruited during the gait cycle and how they are activated across the cycle length. The analysis will be only focused on the muscles that will be afterward considered in the muscle synergies extraction.

*Tibialis Anterioris*: its activity starts at the toe off extending across all swing duration, characterized by a decrease in middle swing for many subject. It is also activated at heel strike and his activation extends across all the loading response phase, up to the total foot-ground contact.

*Quadriceps*: referring in general to both vastus medialis and rectus femoris, they are qualitatively activated in the first half of the stance phase and in the second half of the swing phase. The rectus femoris is also sometimes active in the second half of the stance phase and initial swing phase.

*Hamstring*: the lateral hamstring starts to be active in the second half of the swing phase. It acts in order to decelerate hip flexion and knee extension, preparing the lower limb to begin the next cycle. Its activity continues during the first half of the stance phase as hip extensor and as antagonist with respect to rectus femoris to stabilize the knee. The activity of the medial hamstring can be approximate to

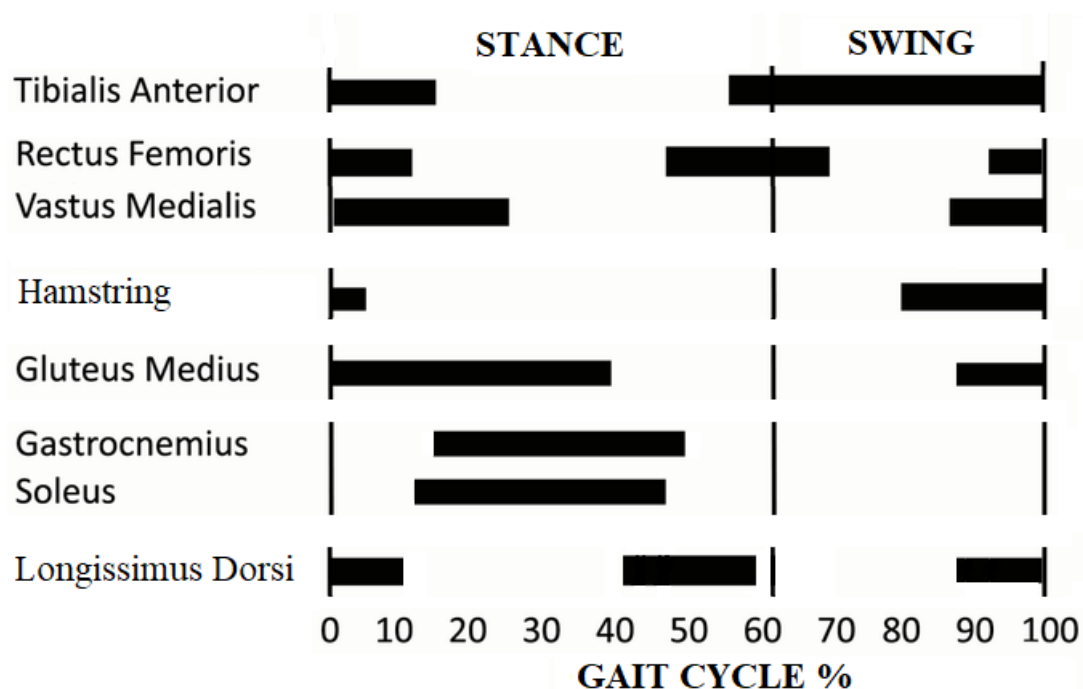


Figure 6.6: Main muscles timing during gait cycle.[50].

the activity of the lateral hamstring.

*Gluteus Medius*: the activity extends from the ending phase of the swing to prepare the heel strike, up to the end of the first stance phase.

*Gastrocnemius*: normally, the muscle begins to contract at the initial stance and maintain that status until the end of the stance. The same pattern for the soleus.

*Longissimus dorsi*: back muscles, they generally are active at initial heel strike and in the transition between terminal stance and pre-swing [51].

## 6.2.2 Muscle Synergies Extraction Setup

Let's now focus on the dataset that has been considered and on the way that has been followed to run the analysis.

### Dataset

The study has been conducted on 8 young healthy females controls subjects, that were kindly provided by prof. M.Knaflitz. More specifically, the eight subjects have been extracted by an original dataset composed by twelve young healthy

females (age:  $24.6 \pm 1.6$  years, height:  $164.1 \pm 6.8$  cm, body mass:  $54.1 \pm 5.7$  kg), that were enlisted for the study among the university student population. None of the subjects were characterized by lower limb injuries or interventions, and all of them were healthy from the perspective of neurological or musculoskeletal disorders, that could have compromised the gait task.

The EMG data, collected with a sampling frequency of 2 KHz, have been collected asking the subjects to walk at a normal self-selected rhythm, going back and forth over a 15m straight walkway, consecutively for 5 minutes. An example of the path is shown in Figure 6.7.

The muscles considered in the muscle synergies analysis are: rectus femoris (RF), vastus medialis (VM), right and left longissimus dorsii (LDR, LDL), tibialis anterior (TA), gluteus medius (GMD), medial hamstring (MH), lateral gastrocnemius (LGS), soleus (SOL) and lateral hamstring (LH). The choice was done in order to consider the main muscles that have a role in each gait cycle phase. In order to segment and timing the different cycles, during the data acquisition have been placed foot-switches [52].

Thanks to the 5 min of recording, in this study, for each control, have been

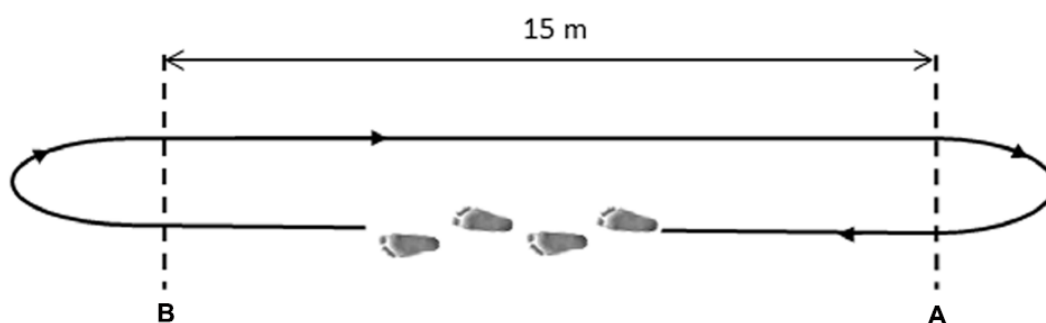


Figure 6.7: Subjects has to walk from point (A) to point (B) at their normal rhythm, then turn back and proceed in the opposite direction [33].

considered 100 consecutive gait cycles, arranged in 10 subgroups each made by 10 consecutive cycles [33]. The latter is very important in order to assess the variability across consecutive cycles that are much distant in time.

### Pre-processing

Since the target is the muscle synergies analysis, in order to extract the linear envelope, the sEMG signals will be treated as explained in the chapter 4.

Firstly, thanks to the foot-switches information, the different gait cycles have been segmented, resampled and concatenated. The latter allows to normalize all the gait cycles at the same number of samples in order to compare them and analyze

them from a statistical perspective.

Subsequently, the sEMG signals have been band-pass filtered between the cutoff frequencies  $f_{\text{low}} = 35$  Hz and  $f_{\text{high}} = 400$  Hz with a fourth order Butterworth filter [52].

The signals have been then rectified and smoothed with a fifth order Butterworth filter at  $f_{\text{smooth}} = 10$  Hz, obtaining the traditional envelopes.

The resampling and the segmentation have been done before the filtering operations as it is necessary to reduce the discontinuities that are created on the sEMG signal following the segmentation and subsequent concatenation of only the typical HFPS steps [53].

On the other side, starting from the same filtered sEMG signals, considering one subgroup at time, have been extracted the ATC envelopes for each single muscle with the approach previously explained.

As a final step, muscle by muscle, one subgroup at time, the sEMG envelopes (either traditional and ATC) have been normalized to the median of the 10 gait cycles peaks. Therefore, the normalization has been made subgroup by subgroup and dividing by the median peak computed between the different peaks of each single gait cycle in that subgroup.

### **Muscle Synergies Extraction**

The data processing has been done with MATLAB (version R2018b, The MathWorks Inc., Natick, MA). The extraction of the muscle synergies has been computed exploiting the function “*nnmf.mat*” available on Matlab, exploiting the multiplicative update version of the algorithm; the number of replicates has been set to 50 and the maximum number of iterations was set to 1000.

The *nnmf.mat* function, as introduced in the chapter 4, factors the initial  $m \times t$  matrix into two non-negative sub-matrices named  $W$  ( $m \times n$ ) and  $H$  ( $n \times t$ ), where “ $n$ ” is the number of synergies. The  $W$  matrix identifies the weight of each muscle within each synergy, and  $H$  defines the correspondent activation timing over the  $t$  time samples. Generally, in the muscle synergies model the weight are constant across time, while the temporal coefficients express how the correspondent synergies is active across the time [54]. The algorithm works minimizing the objective function that is defined as the root mean squared residual between the original EMG matrix and the approximation  $W \cdot H$ .

Since in the literature the number of muscle synergies during gait is generally between 3 and 6 [55, 33], depending on the different muscles considered and the acceptability level of reconstruction criterion, these values represent the number

of synergies that will be considered and iterated in this study.

In order to follow the results of the simulations and in order to repeat the same approach, the muscle synergies have been extracted on the average gait cycle obtained from of each subgroup (10 reps). An example is shown in Figure 6.8. The latter, has been in parallel carried out using both Traditional and ATC approach, obtaining from each of them a particular number of synergies that satisfies the reconstruction  $R^2$  criterion, storing the correspondent  $W$  and  $H$  vectors.

At this point, if the number of synergies would be the same, then would be

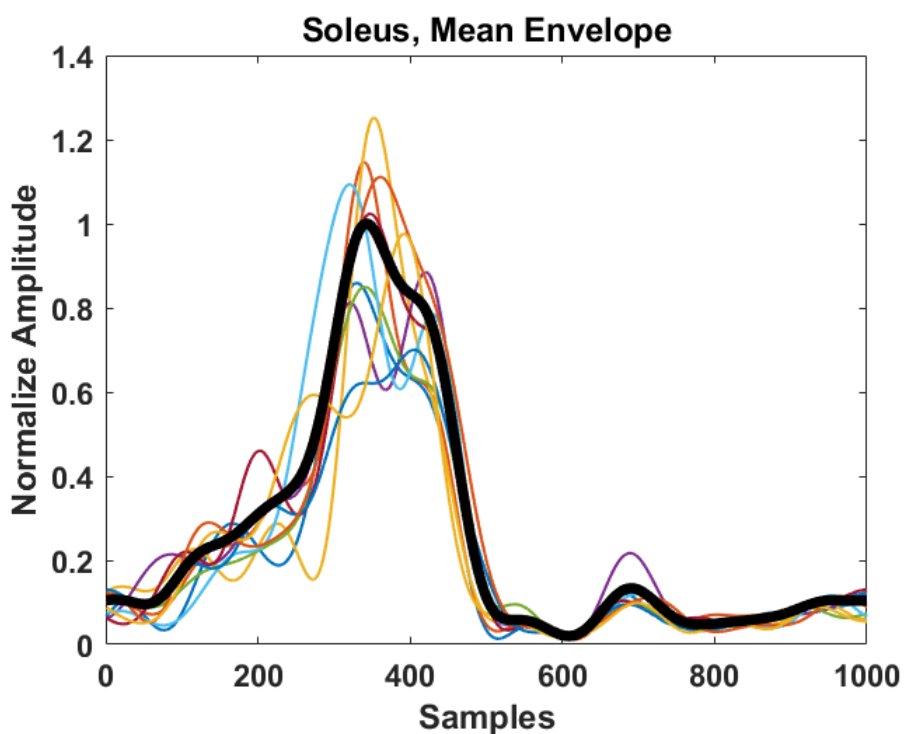


Figure 6.8: Multiple repetitions of the sEMG traditional envelope with the mean in black.

assessed the output comparison between the two synergies weights vectors  $W_{\text{trad}}$  and  $W_{\text{atc}}$  and between the two temporal coefficients vectors  $H_{\text{trad}}$  and  $H_{\text{atc}}$ . Otherwise, if the number of synergies wouldn't correspond, there wouldn't be the possibility to compare the output of the two approaches and, in this case, it would be interesting to understand the reason why it happens.

As explained in chapter 4, the metrics used to evaluate the similarity between the weights  $w$  and the temporal coefficients  $H$  consist respectively in the calculation of Cosine Similarity and the Zero-lag Cross Correlation [32, 33].

### 6.3 Results

For either the two approaches, i.e. ATC and traditional, the number of synergies has been selected in order to respect the  $R^2$  criterion previously explained. It is now natural to ask whether the number of synergies is the same for the two methods considered. In the table 6.1 it is shown the comparison between the number of synergies for each subject.

Table 6.1: The table shows the number of synergies for the two methods.

Subject	N° Syn	
	Traditional	ATC
1	5	5
2	4	5
3	5	5
4	5	5
5	5	6
6	5	5
7	4	4
8	5	5
<b>MEAN</b>	$4.75 \pm 0.46$	$5 \pm 0.53$

More specifically, considering the single subject, the number reported in the table has been calculated picking the maximum value between the 10 different number of synergies that have been extracted singularly from each subgroup (subgroup = 10 gait cycles). This corresponds to the safer condition.

How is it possible to notice, the number of synergies extracted for the traditional method is on average, with a value of  $4.75 \pm 0.46$ , smaller with respect to the one extracted for the ATC, with a value of  $5 \pm 0.53$ . Six subjects present the same number of synergies, while two of them are characterized by a different value, that is always higher in the ATC approach. However, both the average values corresponds to the one reported in literature for healthy young controls, that is our case [33, 56].

#### Observation

Thinking at the possible causes of this difference in the number of synergies, is it possible to observe an important aspect that is due to the intrinsic definition of the two envelopes used to analyze the muscle synergies.

In the Figure 6.9 it is shown an explanatory example of the problem.

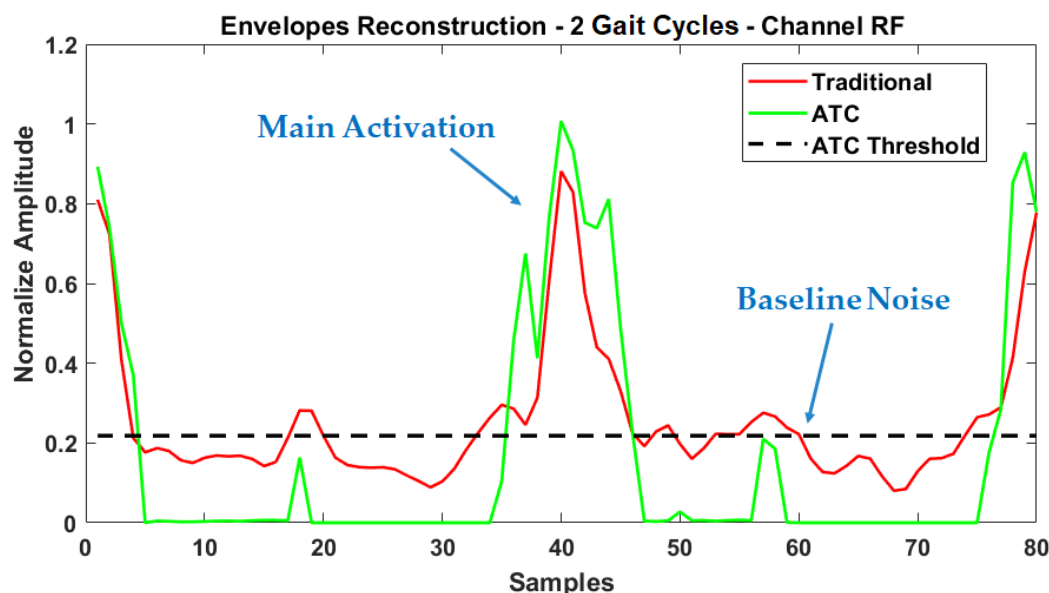


Figure 6.9: The Figure shows the comparison between the sEMG traditional and ATC envelopes.

As it is possible to clearly observe from the Figure, both the envelopes agree in the main activation identification, while they deal differently the contributes that are lower with respect to the ATC threshold level. The reason why it happens is explained by the fact that the ATC technique gets rid of the sEMG raw filtered signal contributes that are lower the threshold level and, distinctively, the traditional envelope represents the smooth behavior of the entire sEMG signal.

Thinking about the consequences that derive from this observation, they lead to understand that a certain percentage of the value of  $R^2$  computed in the number of synergies assessment is due to the baseline noise component reconstruction, which is ideally neglected in the ATC. In other words, one of the reasons that causes the discrepancy in the number of synergies is due to the fact that the two envelopes do not take account for the same contributes in the sEMG signal. In fact, the ATC technique, that was born to reduce the muscle activity events transmission power, is defined on the interest to discard the baseline noise, while the traditional method used to extract the envelope deals, in the same way, either the noise and the activation components.

In addition, since the baseline noise is characterized by a very low frequency content, in extreme terms a constant value, this noise component is easier to reconstruct by the NNMF decomposition method. Although basically it is only an offset contribution in the sEMG signal, it can appreciably affect the value of  $R^2$  in some subjects. The latter, together with the fact that the ATC doesn't ideally account for the baseline noise component, determine that, for the same number of synergies, the  $R^2$  level is generally different and characterized by lower values for the ATC approach.

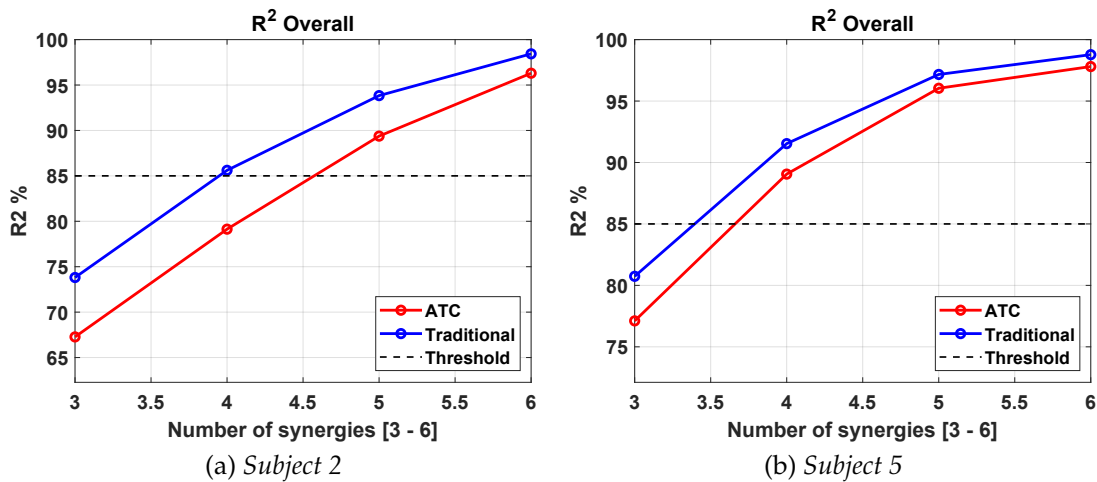


Figura 6.10: The figures show, for both the methods, the  $R^2_{\text{overall}}$  value as a function of the number of synergies. It refers to the specific subjects in which the number of synergies is not the same and it is possible to observe that the ATC curve is lower across all the x axis values. The threshold line refers to the  $R^2_{\text{overall}}$  acceptability criterion.

Considering the two subjects in which the number of synergies is not the same, in the Figure 6.10 there have been reported, for both the methods, the  $R^2_{\text{overall}}$  curves as a function of the number of synergies. It is possible to graphically confirm that the  $R^2_{\text{overall,ATC}}$  values are always lower compared to the traditional one. In all the other subjects this effect is very limited.

Said so, in order to compare the ATC extraction with something more similar in term of information content, has been proposed an alternative way to extract the synergies. The latter is based on considering only the part of the traditional envelopes that is above the correspondent ATC threshold used to compute, for the same muscle, the ATC envelope. An example is reported in Figure 6.11.

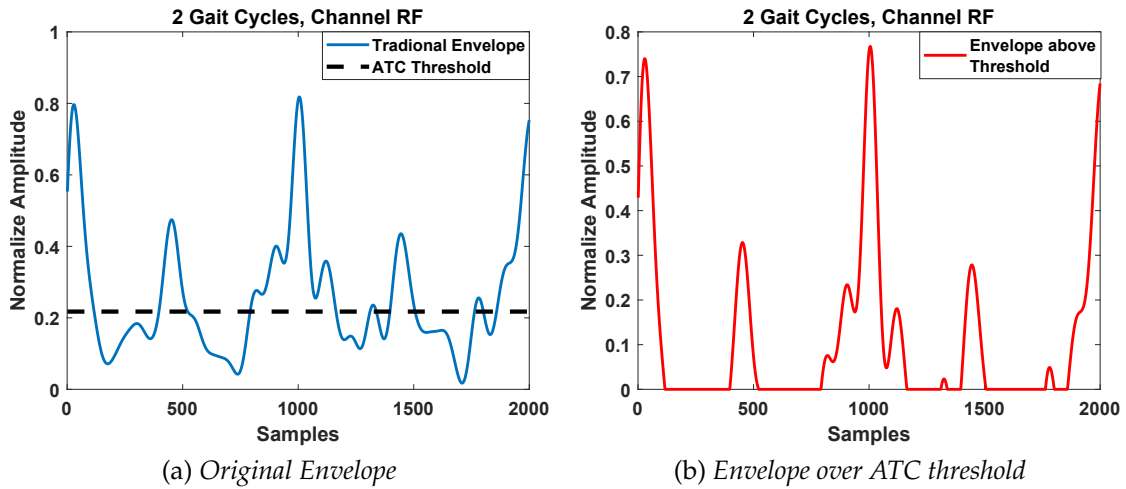


Figure 6.11: The ATC threshold is applied on the original traditional envelope, allowing to extract the version of the envelope that consider only what is over the threshold.

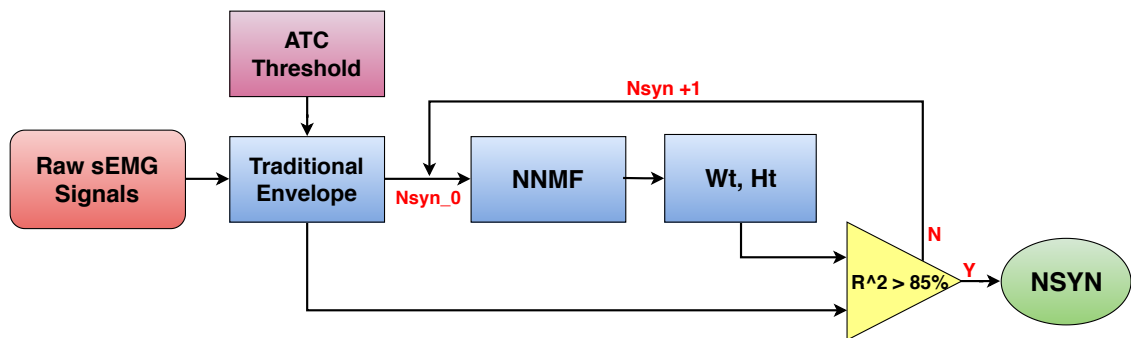


Figure 6.12: Blocks diagram that always shows the traditional-based synergies extraction process, that now also includes the ATC threshold block to allow the calculation of the traditional envelope above that level.

Repeating now the same muscle synergies extraction with the new version of the traditional envelopes, the new results in terms of number of synergies are shown in the table 6.2.

It is possible to comment that, as shown in the table 6.12, through the isolation of the only part of the sEMG traditional envelopes that is above the correspondent ATC threshold level, all the subject present now the same number of synergies. This result confirm the precedent observation validity.

Once verified that the output number of synergies is the same for the two methods, the next step consists in the similarity assessment between the synergies weights  $W$  and the temporal coefficients  $H$ . More particularly, for each single

Table 6.2: The table shows the number of synergies for the two methods in the case in which have been considered only the part of the traditional envelope that are over the correspondent ATC threshold.

Subject	N° Syn	
	Traditional	ATC
1	5	5
2	5	5
3	5	5
4	5	5
5	6	6
6	5	5
7	4	4
8	5	5
<b>MEAN</b>	5 ± 0.53	5 ± 0.53

subject, W and H have been extracted from each subgroup (100 gait cycles = 10 subgroups made by 10 gait cycles) and following the two different methods of muscle synergies analysis, i.e. ATC-based and Traditional-based. The possibility to consider more consecutive subgroups has allowed to characterize the variability of the vectors W and H across an high number of consecutive gait cycles, i.e., as it is defined in the work by Daniele Rimini, Valentina Agostini and Marco Knaflitz, the “Intra-Subject Consistency during Locomotion” [33]. For instance, considering the first subgroup and assuming a number of synergies of 5, both the extraction methods would give 5 synergies weights vectors W and 5 temporal coefficients vectors H that will be compared. This will be repeated for all the 10 subgroups and, finally, from the output similarity indexes obtained from each single subgroup comparison, will be computed the mean and the standard deviation.

In the tables 6.3,6.4 are reported, for each single subject and according to the specific number of synergies, the values of the two similarity indexes used to compare W and H.

Table 6.3: In the table are reported all the cosine similarity values computed between the weights obtained separately with ATC and traditional methods, subject by subject and synergy by synergy (1-1, 2-2 etc.).

Subject	W Similarity (Cosine Similarity)					
	1-1	2-2	3-3	4-4	5-5	6-6
1	98.5 ± 0.7	96.3 ± 1.5	97.4 ± 1.3	98.4 ± 2.7	95.6 ± 4.0	–
2	99.6 ± 0.2	99.9 ± 0.1	99.5 ± 0.4	99.2 ± 0.5	99.7 ± 0.1	–
3	96.3 ± 5.1	99.5 ± 0.2	99.1 ± 0.3	99.1 ± 0.6	98.6 ± 1.1	–
4	99.8 ± 0.1	98.1 ± 1.0	97.3 ± 0.9	99.5 ± 0.4	99.1 ± 0.3	–
5	98.0 ± 1.0	97.0 ± 1.9	99.7 ± 0.2	97.4 ± 1.9	96.8 ± 1.2	99.8 ± 0.1
6	99.4 ± 0.4	99.5 ± 0.2	98.8 ± 0.5	99.7 ± 0.2	99.2 ± 0.2	–
7	97.2 ± 1.6	99.9 ± 0.1	98.4 ± 0.9	97.1 ± 2.8	–	–
8	94.8 ± 3.0	99.4 ± 0.3	99.2 ± 0.9	98.8 ± 1.1	94.6 ± 3.2	–

Table 6.4: In the table are reported all the zero-lag cross correlation values computed between the temporal coefficients obtained separately with ATC and traditional methods, subject by subject and synergy by synergy (1-1, 2-2 etc.).

Subject	H Similarity (Zero-lag Cross Correlation)					
	1-1	2-2	3-3	4-4	5-5	6-6
1	96.5 ± 0.5	97.6 ± 1.2	96.1 ± 1.7	97.0 ± 1.8	95.9 ± 2.2	–
2	96.0 ± 1.0	96.2 ± 1.3	97.4 ± 0.8	98.2 ± 1.1	99.2 ± 0.3	–
3	95.9 ± 2.3	98.2 ± 1.3	98.5 ± 0.7	98.7 ± 0.6	99.3 ± 0.3	–
4	96.2 ± 1.1	98.9 ± 0.6	96.7 ± 1.1	95.0 ± 2.2	97.9 ± 0.6	–
5	97.5 ± 1.2	96.0 ± 2.2	99.3 ± 0.3	98.7 ± 0.5	99.9 ± 0.6	98.6 ± 0.5
6	96.3 ± 1.1	96.9 ± 0.8	98.8 ± 0.6	98.1 ± 0.8	97.7 ± 0.9	–
7	97.5 ± 0.9	96.6 ± 0.7	98.1 ± 0.9	96.4 ± 1.1	–	–
8	96.2 ± 1.7	97.1 ± 0.8	98.6 ± 0.5	97.7 ± 0.8	97.3 ± 1.7	–

Looking at both precedents tables, it is possible to observe for either the indexes an average similarity value across the subgroups that is always higher than 90% and that it is characterized by very low a standard deviation across the subgroups. Specifically, the latter means that both the synergies weights  $W$  and the temporal coefficients  $H$  are very similar between the two extraction methods.

Starting from the overall results, it is now possible to extract and graphically show the comparison of the weights  $W$  and the temporal coefficients  $H$  for a single subject. In the example will be considered the subject 2.

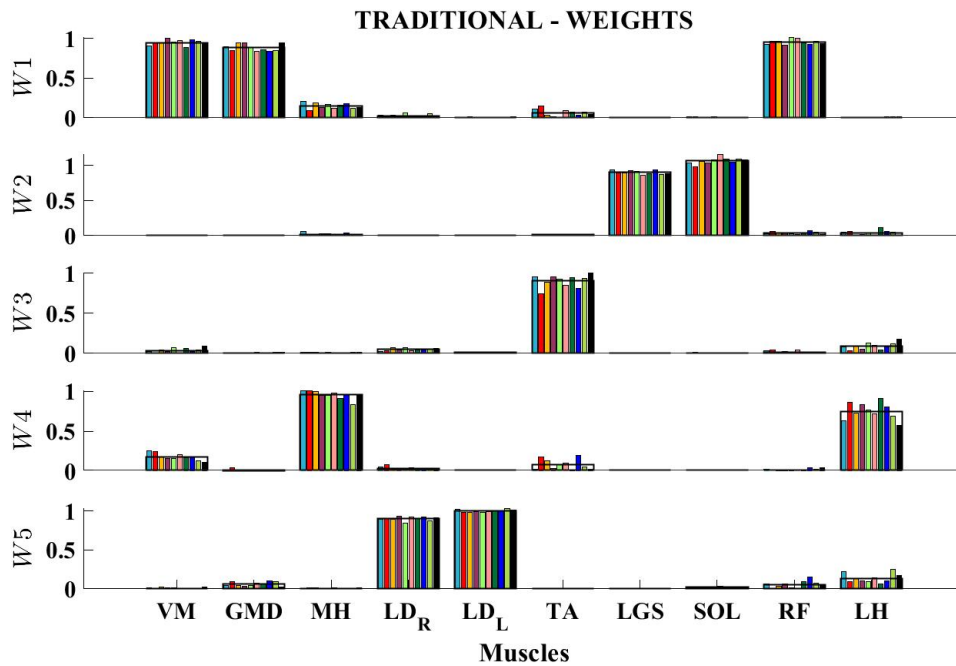


Figure 6.13: It shows the traditional synergies weights  $W$ . Considering a single muscle, there are 10 bars that refers to each single subgroup and an external bar for the average.

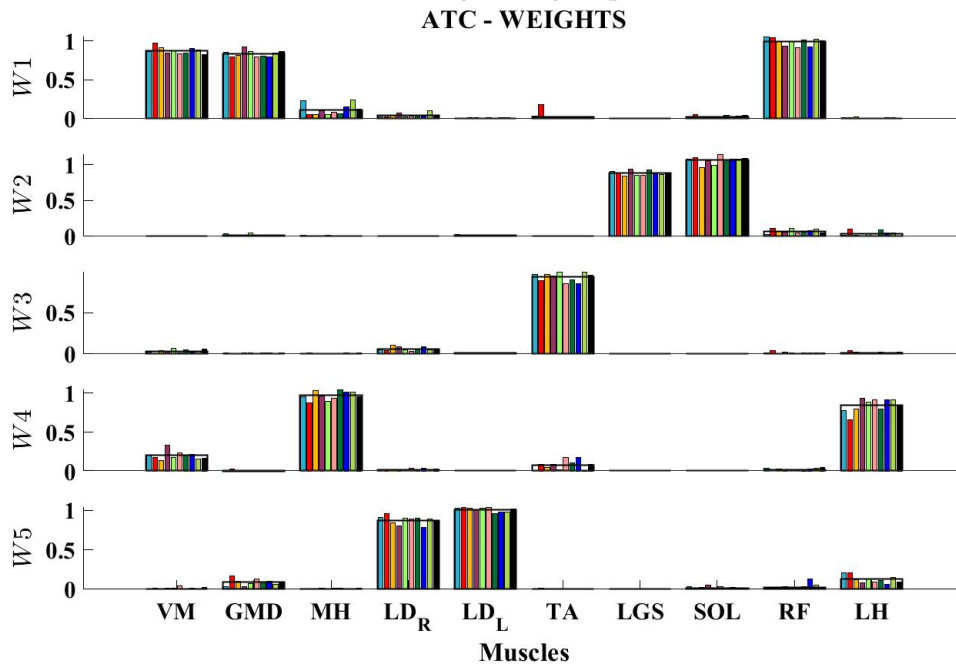


Figure 6.14: It shows the ATC synergies weights  $W$ .

Referring to subject 2, in the Figure 6.17 have been reported the values of the similarity indexes Cosine similarity (CS) and Zero-lag Cross Correlation (CC).

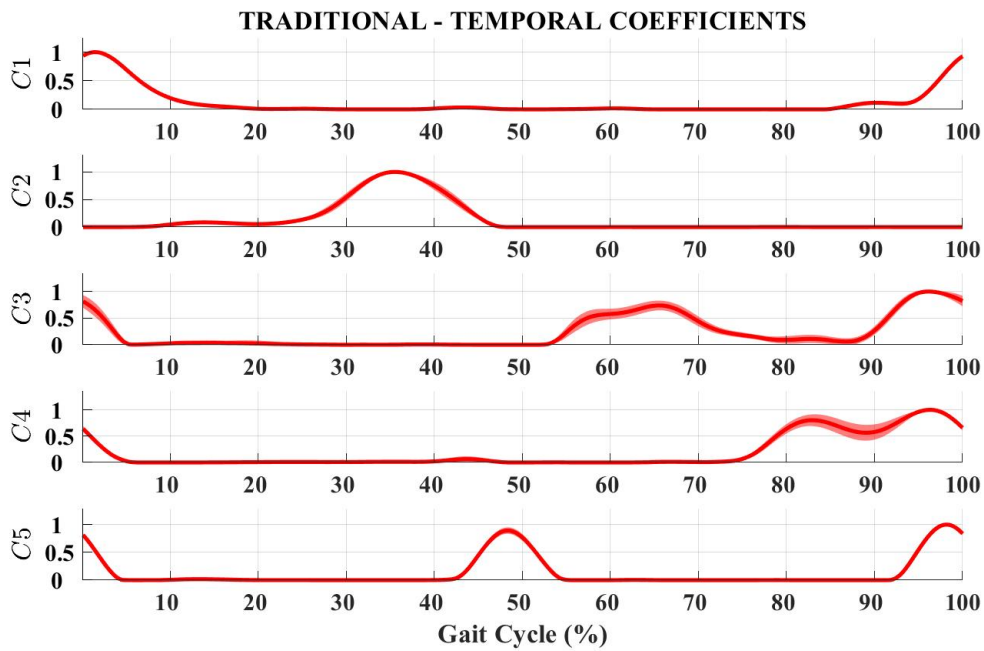


Figure 6.15: It shows the traditional temporal coefficients H. For each synergy is plotted an average curve together with the standard deviation across the subgroups.

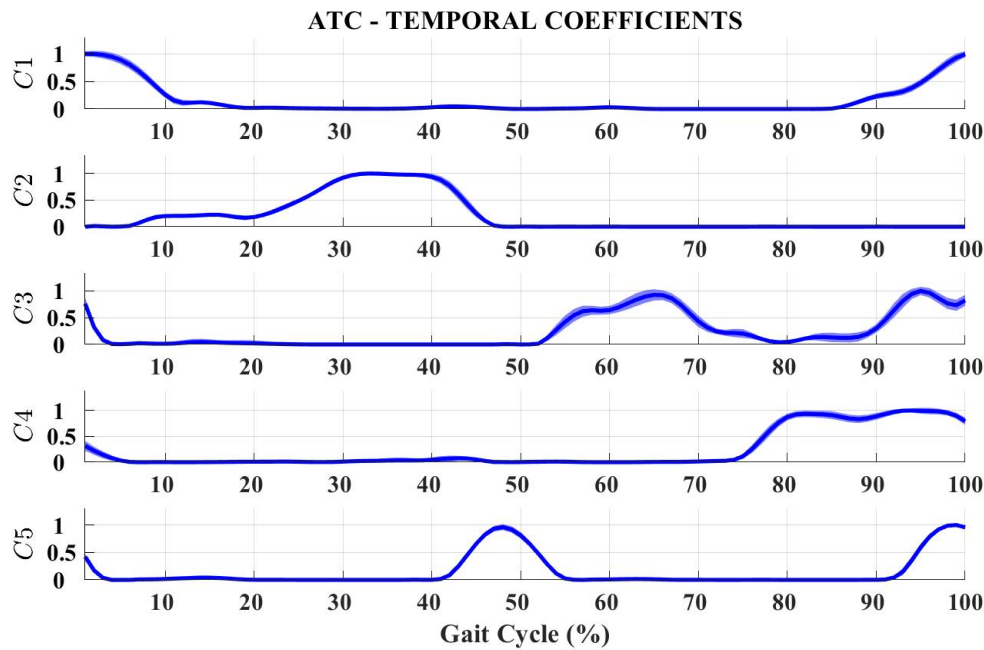


Figure 6.16: It shows the ATC temporal coefficients H. For each synergy is plotted an average curve together with the standard deviation across the subgroups.

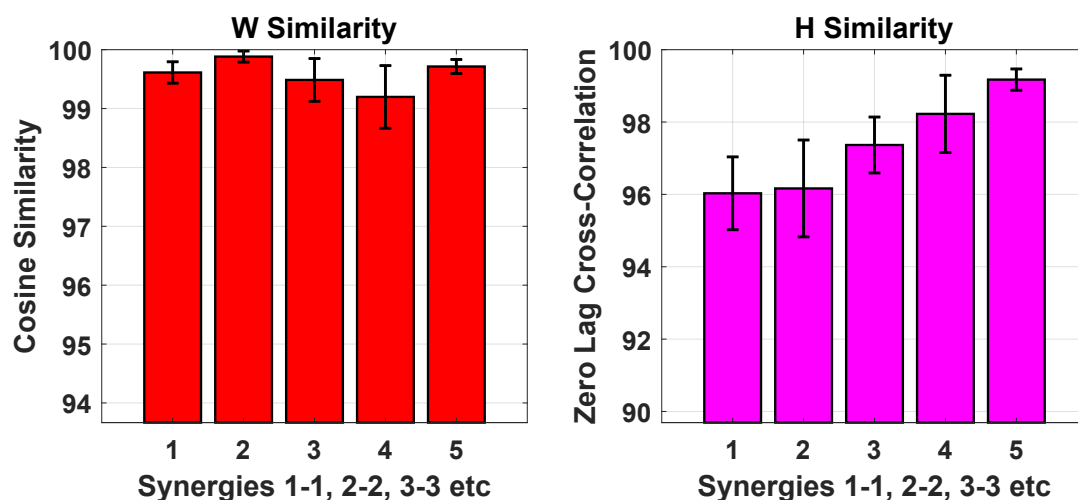


Figure 6.17: Subject 2. Cosine similarity and Zero-lag Cross Correlation for number of synergies = 5.

In this case, for every muscle synergy (1-5), the mean value of CS is higher than 99% and the mean value of CC is always higher than 96%, both characterized by very low confidence intervals. The latter is visually confirmed looking at the plots comparison of the weights  $W$  and the temporal coefficients  $H$  and this is also symbol of reliability and consistency across consecutive subgroups of gait cycles.

In accordance with what has been demonstrated by D.Rimini, V.Agostini and M.Knaflitz in the work [33], the muscle synergies that have been extracted represent the principal biomechanical functions that characterize a healthy subject during locomotion. These are gathered in Figure 6.18.

Synergy	Function	Principal muscles	Biomechanical function
1	F1	TFL – GMD	Stabilize hip joint during heel strike and the load acceptance phase
2	F2	LGS – PL – SOL	Generate propulsion at mid and terminal stance
3	F3	LD <sub>R</sub> – LD <sub>L</sub>	Control the trunk position in the frontal plane at the heel strike of the homolateral and contralateral foot
4	F4	TA	Decelerate the foot during first rocker and control forefoot clearance during swing phase
5	F5	MH – LH	Decelerate the leg at the end of the swing phase

Figure 6.18: Shared muscle synergies across subjects [33].

# Chapter 7

## Conclusions

The study has allowed the ATC event-driven technique to be contextualized through its application within the Muscle Synergies analysis environment.

Through the simulations, it has been possible to show that the ATC envelope cannot be considered as an easy replacement or perfect reproduction of the traditional sEMG envelope when it is computed on a single repetition of a muscle activation. The latter concept, which was expected, is due to the ATC computation inducing a drastic loss in terms of sample numbers, determining an equally large loss of sEMG signal morphological information. Secondly, the ATC envelope is affected by an amplitude quantization problem. This is due to the low number of TC events that appear in a time window of 50ms, and by the high variability from repetition to repetition of the same muscle activation. This variability is due to the stochastic nature of either the ATC approach or the sEMG signal definition. Naturally, starting from these assumptions, the muscle synergy extraction which is derived is not reliable and is not consistent enough when compared to synergies extracted from the traditional method.

At this point, trying to merge the important advantages that characterize the ATC approach, and the main requirements needed to maintain the morphological content of the original muscle activation, it has been decided to resort to the simulation of the mean across multiple repetitions of the same muscle activity. In this way, by the summation of 10 different ATC envelopes representative it is possible to better discretize the amplitude modulation and limit the variability thanks to the low pass filter effect of the average operation. Through the simulation of this approach, it has been found that, for the particular ATC parameters combination of time window = 50ms and threshold level = 2.8, it is possible to extract an ATC envelope characterized by a high similarity level with respect to the traditional one. Specifically, it has been verified that both  $R^2_{\mu}$  and its distribution across the high number of iterations fulfill the similarity criterion previously assumed

( $R^2 \geq 85\%$ ).

These results reduces the applicability only to repetitive movements, like gait.

Finally, exploiting the best combination of ATC parameters that has been found through the simulations results, the outputs of muscle synergies extraction obtained following the two different methods, i.e. ATC and traditional, have been compared and analyzed. Starting from real sEMG signals collected from 10 muscles of the dominant lower limb of 8 healthy young subjects during gait, it is been possible to demonstrate the high correspondence between both synergy weights  $W$  and temporal coefficients  $H$ , the main target of this thesis. The ATC-based extraction agrees on the number of synergies and, for every subject and for every synergy, recognizes correctly the different muscle blocks that correspond to the weights  $W$  and the specific temporal activations that correspond to the temporal coefficients  $H$ .

Repeating the comparison for 10 consecutive subgroups, each of them made by 10 gait cycles, it has permitted to statistically better visualize the results and to assess the intra-variability during the locomotion for the specific subject. Looking at the plots of the weights  $W$  and the temporal coefficients  $H$ , both methods show the same information for all the subjects and the average values of the similarity indexes, i.e. Cosine Similarity (CS) and Zero-lag Cross Correlation (CC), are always higher than 95% and accompanied by a very low standard deviation ( $<5\%$ ) across the subgroups.

Additionally, it is important to note the computational time needed to process and extract the muscle synergies though the NNMF algorithm. In particular, comparing the time that the two methods need to extract  $W$  and  $H$  for 10 subgroups. The traditional approach requires a time of 2 minutes and 37 seconds, while the ATC-based method requires only 15 seconds. A 91% time savings using the latter method.

This study shows the potential in studying and prototyping wearable, low-power, wireless, multi-channel acquisition systems based on ATC techniques that are applicable in muscle synergy analysis that can be exploited to give an online feedback to a clinician or researcher.

In conclusion, it would be interesting to test the technique on different muscle types in order to evaluate its performance with other activation shapes and characteristics, and during other periodic motor tasks in order to assess the robustness of ATC.

# Bibliography

- [1] J. Gordon Betts, Peter DeSaix, Eddie Johnson, Jody E Johnson, Oksana Korol, Dean H Kruse, Brandon Poe, James A Wise, Mark Womble, and Kelly A Young. *Anatomy and physiology*. Openstax, 2013.
- [2] Cindy L Stanfield. *Principles of Human Physiology*. Pearson Education UK, 5 edition, 2013.
- [3] Walter R. Frontera and Julien Ochala. Skeletal muscle: A brief review of structure and function. *Calcified Tissue International*, 96(3):183–195, 2014.
- [4] Arthur C Guyton and John E Hall. *Textbook of medical physiology*. Elsevier Saunders, 2006.
- [5] Suzanne Kasparson. The three muscles actions and the benefits of eccentric training. <https://suzannekasparson.com/2017/06/07/the-three-muscle-actions-and-the-benefits-of-eccentric-training/>, 2018.
- [6] Carlo J. De Luca. The use of surface electromyography in biomechanics. *Journal of Applied Biomechanics*, 13(2):135–163, 1997.
- [7] Wikipedia contributors. Electromyography — Wikipedia, the free encyclopedia. <https://en.wikipedia.org/w/index.php?title=Electromyography&oldid=840557084>, 2018. [Online; accessed 14-May-2018].
- [8] R. Merletti and D. Farina. Analysis of intramuscular electromyogram signals. *Philosophical Transactions of the Royal Society A: Mathematical, Physical and Engineering Sciences*, 367(1887):357–368, 2009.
- [9] Adrian Burden. Surface electromyography. 01 2008.
- [10] Wikipedia contributors. Electromyography — Wikipedia, the free encyclopedia. <https://en.wikipedia.org/w/index.php?title=Electromyography&oldid=840557084>, 2018. [Online; accessed 15-May-2018].

- [11] Marco Antonio Cavalcanti Garcia and Taian Vieira. Surface electromyography: Why, when and how to use it. 4:17–28, 04 2011.
- [12] Carlo J. De Luca. Surface electromyography: Detection and recording. 2002.
- [13] Ulf Lundberg. Muscle tension. <http://www.macses.ucsf.edu/research/allostatic/muscle.php>, 2018.
- [14] Rubana Chowdhury, Mamun Reaz, Mohd Ali, Ashrif Bakar, Kalaivani Chellappan, and Tae Chang. Surface electromyography signal processing and classification techniques. *Sensors*, 13(9):12431–12466, 2013.
- [15] M. Crepaldi, M. Paleari, A. Bonanno, A. Sanginario, P. Ariano, D. H. Tran, and D. Demarchi. A quasi-digital radio system for muscle force transmission based on event-driven IR-UWB. In *2012 IEEE Biomedical Circuits and Systems Conference (BioCAS)*, pages 116–119, Nov 2012.
- [16] S. Sapienza, M. Crepaldi, P. Motto Ros, A. Bonanno, and D. Demarchi. On integration and validation of a very low complexity ATC UWB system for muscle force transmission. *IEEE Transactions on Biomedical Circuits and Systems*, 10(2):497–506, April 2016.
- [17] P. M. Ros, M. Paleari, N. Celadon, A. Sanginario, A. Bonanno, M. Crepaldi, P. Ariano, and D. Demarchi. A wireless address-event representation system for ATC-based multi-channel force wireless transmission. In *5th IEEE International Workshop on Advances in Sensors and Interfaces IWASI*, pages 51–56, June 2013.
- [18] A. Shahshahani, M. Shahshahani, P. M. Ros, A. Bonanno, M. Crepaldi, M. Martina, D. Demarchi, and G. Masera. An all-digital spike-based ultra-low-power IR-UWB dynamic average threshold crossing scheme for muscle force wireless transmission. In *2015 Design, Automation Test in Europe Conference Exhibition (DATE)*, pages 1479–1484, March 2015.
- [19] Ivan Furfaro. Integration and validation of average threshold crossing (ATC) applied to surface electromyography (semg) Politecnico di Torino, DET, 2015.
- [20] Sofia Cecchini. Average threshold crossing validation for functional electrical stimulation applied to surface electromyographic signals. Politecnico di Torino - DET, 2018.
- [21] Elisa Cordedda. Riconoscimento real time di gesti applicato a segnali EMG superficiali basati su ATC. Politecnico di Torino - DET, 2016.
- [22] Bianca Sereni. Design and development of a low-power wearable device for the acquisition of surface electromyography (sEMG) signals with average threshold crossing (ATC). Politecnico di Torino - DET, 2016.

- [23] Fabio Rossi, Paolo Motto Ros, and Danilo Demarchi. Live demonstration: Low power system for event-driven control of functional electrical stimulation. Politecnico di Torino - DET. Institute of Electrical and Electronics Engineers Inc., 2018.
- [24] D. Torricelli, F. Barroso, M. Coscia, C. Alessandro, F. Lunardini, E. Bravo Esteban, and A. d’Avella. *Muscle Synergies in Clinical Practice: Theoretical and Practical Implications*, pages 251–272. Springer International Publishing, Cham, 2016.
- [25] Emilio Bizzi and Vincent CK Cheung. The neural origin of muscle synergies. *Frontiers in Computational Neuroscience*, 7:51, 2013.
- [26] Seyyed Arash Haghpanah, Farzam Farahmand, and Hassan Zohoor. Modular neuromuscular control of human locomotion by central pattern generator. *Journal of Biomechanics*, 53:154 – 162, 2017.
- [27] Dick Stegeman and Hermie Hermens. Standards for surface electromyography: The european project surface EMG for non-invasive assessment of muscles (seniam). 1, 01 2007.
- [28] D. Rimini, V. Agostini, S. Rosati, C. Castagneri, G. Balestra, and M. Knaflitz. Influence of pre-processing in the extraction of muscle synergies during human locomotion. In *2017 39th Annual International Conference of the IEEE Engineering in Medicine and Biology Society (EMBC)*, pages 2502–2505, July 2017.
- [29] Matthew C. Tresch, Vincent C. K. Cheung, and Andrea d’Avella. Matrix factorization algorithms for the identification of muscle synergies: Evaluation on simulated and experimental data sets. *Journal of Neurophysiology*, 95(4):2199–2212, 2006. PMID: 16394079.
- [30] Daniel D. Lee and H. Sebastian Seung. Algorithms for non-negative matrix factorization. In *Proceedings of the 13th International Conference on Neural Information Processing Systems, NIPS’00*, pages 535–541, Cambridge, MA, USA, 2000. MIT Press.
- [31] Vincent CK Cheung, Andrea Turolla, Michela Agostini, Stefano Silvoni, Caoimhe Bennis, Patrick Kasi, Sabrina Paganoni, Paolo Bonato, and Emilio Bizzi. Muscle synergy patterns as physiological markers of motor cortical damage. *Proceedings of the National Academy of Sciences*, 109(36):14652–14656, 2012.
- [32] Andrea d’Avella and Emilio Bizzi. Shared and specific muscle synergies in natural motor behaviors. *Proceedings of the National Academy of Sciences*, 102(8):3076–3081, 2005.

- [33] Daniele Rimini, Valentina Agostini, and Marco Knaflitz. Intra-subject consistency during locomotion: similarity in shared and subject-specific muscle synergies. *Frontiers in human neuroscience*, 11:586, 2017.
- [34] D Rimini, V Agostini, and M Knaflitz. Evaluation of muscle synergies stability in human locomotion: A comparison between normal and fast walking speed. In *2017 IEEE International Instrumentation and Measurement Technology Conference (I2MTC)*, pages 1–5. IEEE, 2017.
- [35] Daniel D Lee and H Sebastian Seung. Learning the parts of objects by non-negative matrix factorization. *Nature*, 401(6755):788, 1999.
- [36] Juri Taborri, Valentina Agostini, Panagiotis K Artemiadis, Marco Ghislieri, Daniel A Jacobs, Jinsook Roh, and Stefano Rossi. Feasibility of muscle synergy outcomes in clinics, robotics, and sports: a systematic review. *Applied bionics and biomechanics*, 2018, 2018.
- [37] Samanta Rosati, Valentina Agostini, Marco Knaflitz, and Gabriella Balestra. Muscle activation patterns during gait: A hierarchical clustering analysis. *Biomedical Signal Processing and Control*, 31:463–469, 2017.
- [38] Paulina Kieliba, Peppino Tropea, Elvira Pirondini, Martina Coscia, Silvestro Micera, and Fiorenzo Artoni. How are muscle synergies affected by electromyography pre-processing? *IEEE Transactions on Neural Systems and Rehabilitation Engineering*, 26(4):882–893, 2018.
- [39] Gelsy Torres-Oviedo and Lena H Ting. Muscle synergies characterizing human postural responses. *Journal of neurophysiology*, 2007.
- [40] Vincent CK Cheung, Andrea d’Avella, Matthew C Tresch, and Emilio Bizzi. Central and sensory contributions to the activation and organization of muscle synergies during natural motor behaviors. *Journal of Neuroscience*, 25(27):6419–6434, 2005.
- [41] Yuri P Ivanenko, Richard E Poppele, and Francesco Lacquaniti. Five basic muscle activation patterns account for muscle activity during human locomotion. *The Journal of physiology*, 556(1):267–282, 2004.
- [42] Evelyn Morin. Lower limb muscle synergies during gait in humans. In *2006 International Conference of the IEEE Engineering in Medicine and Biology Society*, pages 6667–6669. IEEE, 2006.
- [43] Paolo Bonato, Tommaso D’Alessio, and Marco Knaflitz. A statistical method for the measurement of muscle activation intervals from surface myoelectric signal during gait. *IEEE Transactions on biomedical engineering*, 45(3):287–299, 1998.

- [44] Gianluca De Luca. Fundamental concepts in EMG signal acquisition. 02 2019.
- [45] J-JJ Chen, Richard G Shiavi, and Li-Qun Zhang. A quantitative and qualitative description of electromyographic linear envelopes for synergy analysis. *IEEE transactions on biomedical engineering*, 39(1):9–18, 1992.
- [46] Anthony J Wheeler and Ahmad Reza Ganji. *Introduction to engineering experimentation*. Prentice Hall New Jersey, 1996.
- [47] Seyed Safavynia, Gelsy Torres-Oviedo, and Lena Ting. Muscle synergies: implications for clinical evaluation and rehabilitation of movement. *Topics in spinal cord injury rehabilitation*, 17(1):16–24, 2011.
- [48] Jacquelin Perry and Judith Burnfield. *Gait Analysis: Normal and Pathological Function*. 02 2010.
- [49] Gait Cycle. Charschan Chiropractic in North Brunswick, NJ and Scotch Plains, NJ. <https://www.backfixer1.com/plantar-fasciitis/gait-cycle/>, 2019.
- [50] Zhimei Tan, Huihua Liu, Tiebin Yan, Dongmei Jin, Xiaokuo He, Xiuyuan Zheng, Shuwei Xu, and Chunmei Tan. The effectiveness of functional electrical stimulation based on a normal gait pattern on subjects with early stroke: A randomized controlled trial. *BioMed research international*, 2014:545408, 07 2014.
- [51] Maria Grazia Benedetti, Valentina Agostini, Marco Knaflitz, and Paolo Bonato. Muscle activation patterns during level walking and stair ambulation. In *Applications of EMG in clinical and sports medicine*. IntechOpen, 2012.
- [52] Daniele Rimini, Valentina Agostini, Samanta Rosati, Cristina Castagneri, Gabriella Balestra, and Marco Knaflitz. Influence of pre-processing in the extraction of muscle synergies during human locomotion. In *2017 39th Annual International Conference of the IEEE Engineering in Medicine and Biology Society (EMBC)*, pages 2502–2505. IEEE, 2017.
- [53] Valentina Agostini, Gabriella Balestra, and Marco Knaflitz. Segmentation and classification of gait cycles. *IEEE transactions on neural systems and rehabilitation engineering : a publication of the IEEE Engineering in Medicine and Biology Society*, 22, 11 2013.
- [54] I. PITTELOUD. Effect of robotic assisted gait training on the organization of muscular activity in children with cerebral palsy. 2015.

- [55] F. Artoni, V. Monaco, and S. Micera. Selecting the best number of synergies in gait: Preliminary results on young and elderly people. In *2013 IEEE 13th International Conference on Rehabilitation Robotics (ICORR)*, pages 1–5, June 2013.
- [56] Richard R Neptune, David J Clark, and Steven A Kautz. Modular control of human walking: a simulation study. *Journal of biomechanics*, 42(9):1282–1287, 2009.

# Acknowledgements

Firstly, I would like to thank Danilo Demarchi and Paolo Bonato for giving me the chance to work on this project and for addressing me during all the period. The experience has represented a moment of personal growth both from a professional and human perspective.

At the same way, I would also like to thank Paolo Motto Ros and, in particular, Stefano Sapienza for their kind support, help, suggestions and motivation that accompanied and stimulated me throughout the whole thesis.

I thank Federico Parisi for all the advices and the nice friendship that has born during the months in Boston, Greg Shiurring for his thesis editing advices and all the other members of the Motion Analysis Lab.

Another thank goes to Fabio Rossi and to the Civera Lab for guiding me during the first period of the thesis and for all the fun coffee breaks spent together.

I thank Marco Ghislieri for his decisive contribution and pleasant comparisons during the all work.

I would also thank Margherita and all the friends, colleagues and anyone that has contributed to support me during the entire university path, that has been a very rich and priceless experience.

Finally, a big and heartfelt thank to my family that, with a sweet and untiring support, both moral and economic, allowed me to arrive here today, contributing to my personal growth.

*Innanzi tutto, vorrei ringraziare Danilo Demarchi e Paolo Bonato per avermi dato la possibilità di lavorare su questo progetto e di avermi indirizzato durante tutto il periodo. L'esperienza ha rappresentato un momento di crescita personale sia dal punto di vista professionale che umano.*

*Allo stesso modo, vorrei anche ringraziare Paolo Motto Ros e, in particolare, Stefano Sapienza per il loro gentile supporto, aiuto, suggerimenti e motivazione che mi hanno accompagnato e stimolato per tutta la tesi.*

*Ringrazio Federico Parisi per tutti i consigli e la bella amicizia che è nata durante i mesi a Boston e tutti gli altri membri del Motion Analysis Lab.*

## Acknowledgements

---

*Un altro ringraziamento va a Fabio Rossi e al Civera lab per avermi guidato e accompagnato durante il primo periodo e per tutte le divertenti pause caffè trascorse insieme. Ringrazio Marco Ghislieri per il suo contributo decisivo e per i piacevoli confronti durante tutto il lavoro.*

*Vorrei poi ringraziare Margherita e tutti gli amici, i colleghi e chiunque abbia contribuito a sostenermi durante l'intero percorso universitario, contribuendo a renderlo un'esperienza ricca e impagabile.*

*Infine, un grande e sentito ringraziamento alla mia famiglia che, con un supporto dolce e instancabile, sia morale che economico, mi ha permesso di arrivare fin qui oggi.*